

Khaleel N. Abu Shgair

**New Possibilities for Building High-Vacuum
Chambers Using Glued Aluminum Plates and
Application to Sputtered Nanocomposite Coatings**

New Possibilities for Building High-Vacuum Chambers Using Glued Aluminum Plates and Application to Sputtered Nanocomposite Coatings

Vom Fachbereich Maschinenbau und Verfahrenstechnik
der Universität Kaiserslautern
zur Verleihung des akademischen Grades

Doktor-Ingenieur (Dr.-Ing.)

Genehmigte Dissertation

Vorgelegt von

M. Sc. Khaleel Abu Shgair

aus Kufer Elma (Jordan)

D386

Prüfungsvorsitz:	Prof. Dr. rer. nat. C. W. Dankwort
Referent:	Prof. Dr.-Ing. R. Haberland
Koreferent:	Prof. Dr.-Ing. W. Brockmann
Dekan	Prof. Dr. tech. Hans-Jörg Bart

Tag der mündlichen Prüfung: 25.11.2002

Preface

This thesis has been written between 1999 and 2002 during my work period as research assistance at the Department of Precision Engineering (Lehrstuhl für Feinwerktechnik) at the University of Kaiserlautern, Germany.

First of all, I would like to express my sincere gratitude to my supervisor Prof. Dr.-Ing. R. Haberland, without his assistance, insights, fruitful advice, generous support and persistence this work would not be complete. I also thank Prof. Dr.-Ing. W. Brockmann for his responsibility as reviewer. I also thank Prof. Dr. rer. nat. C. W. Dankwort for his chairmanship of the board of the examiners.

Furthermore, I would like to thank all my colleagues at the University of Kaiserlautern who contributed to this work. Especially A. Maier and R. Gausmann for their time and help.

Finally, I would like to express my deep gratitude and great respect to my parents, family and friends who encouraged and supported me.

Kaiserlautern, November 2002

Khaleel Abu Shgair

CONTENTS

CONTENTS..... I

ZUSAMMENFASSUNG..... V

SYMBOLS VII

1. INTRODUCTION..... 1

1.1. Study Objects 1

1.2. Vacuum Technology..... 2

1.2.1. Kinetic Picture of a Gas..... 2

1.2.2. Mean Free Path 3

1.2.3. Outgassing 4

1.2.3.1. Adsorbed Gas 4

1.2.3.2. Dissolved Gas..... 5

1.2.3.3. Vaporization of Materials 5

1.2.3.4. Permeability of Gas Through Walls 6

1.2.4. Chamber Evacuation and Pumping Speed..... 6

1.3. Thin Film Coating Technology..... 7

1.3.1. Basic Aspects of Sputtering 7

1.3.2. Thin Film Formation 8

1.3.3. Coating Structure and Characterization..... 10

1.3.4. Coatings Analysis..... 12

1.3.4.1. Secondary neutral particle mass spectrometry (SNMS) 13

1.3.4.2. X-Ray-diffraction (XRD)..... 14

1.4. Bonding Technology..... 14

1.4.1. Fundamentals of Bonding Technology 15

1.4.2. Types of Bonding Materials..... 16

1.4.2.1.	Epoxy adhesives	16
1.4.2.2.	Polyurethane Adhesives.....	16
1.4.2.3.	Acrylate Adhesives.....	17
1.4.2.4.	Phenolic Resins	17
1.4.2.5.	Modified Silane Polymers.....	17
2.	OUTGASSING TEST	18
2.1.	<i>Introduction to Outgassing</i>	18
2.2.	<i>Vacuum Materials</i>	18
2.3.	<i>Literature</i>	19
2.4.	<i>Outgassing Test Stand</i>	21
2.5.	<i>Experimental Procedure</i>	22
2.6.	<i>Outgassing Results</i>	22
2.7.	<i>Discussion and Conclusion</i>	33
3.	VACUUM CHAMBER DESIGN.....	37
3.1.	<i>Introduction to Vacuum Chamber Design</i>	37
3.2.	<i>Design and Mechanical Load Of The Chamber</i>	37
3.2.1.	Design Constraints	37
3.2.2.	Mechanical Properties of the Vacuum Chamber	38
3.3.	<i>Glue Selection and Tests</i>	39
3.4.	<i>Workpiece Transportation System</i>	47
3.5.	<i>Assembly of the Chamber</i>	48
3.6.	<i>Pumping System</i>	51
3.7.	<i>DC-Sputtering Magnetron</i>	51
4.	DEPOSITION OF NANOCOMPOSITE (Ti, Si, Al)N COATINGS	53
4.1.	<i>Introduction to Sputtering Process</i>	53

4.2.	<i>Sputtering Process</i>	53
4.2.1.	Sputtering Mechanisms	53
4.2.2.	Interactions of Ion Approached the Surface of a Target	54
4.2.3.	Sputtering Advantages.....	55
4.2.4.	Sputtering Techniques	56
4.2.4.1.	Non-Reactive Sputtering Processes.....	56
4.2.4.2.	Reactive Sputtering Processes.....	57
4.2.4.3.	Diode Sputtering.....	57
4.2.4.4.	RF Sputtering	57
4.2.4.5.	Triode Sputtering.....	58
4.2.4.6.	Magnetron Sputtering	58
4.2.4.7.	Unbalanced Magnetron Sputtering.....	59
4.3.	<i>Deposition of Hard Coatings</i>	60
4.3.1.	Types of Hard Coatings.....	61
4.3.1.1.	Multicomponent Coatings.....	61
4.3.1.2.	Multilayer Coatings	61
4.3.1.3.	Nanocomposite Hard Coatings.....	62
4.4.	<i>Characteristics and Properties of Hard Coatings</i>	64
4.4.1.	Hardness	64
4.4.2.	High Temperature Oxidation	65
4.4.3.	Friction and Wear.....	66
4.4.4.	Other Selected Properties of Coatings.....	66
4.5.	<i>Deposition of Nanocomposite (Ti, Si, Al)N Coatings</i>	67
4.5.1.	Experiment.....	68
4.5.2.	Results and Discussion	69
4.5.2.1.	Chemical and Structural Analysis	69
4.5.2.2.	Mechanical Properties Analysis	79
4.5.3.	Conclusions.....	86
5.	CONCLUSION.....	88
5.1.	<i>Outgassing Rate Test</i>	88
5.2.	<i>The Vacuum Chamber Construction</i>	88

5.3. Deposition of Nanocomposite (Ti, Si, Al)N Coatings	89
6. SUMMARY	91
7. REFERENCES	93

ZUSAMMENFASSUNG

In dieser Arbeit wurde ein (Ti, Al, Si) N System untersucht. Ein wesentliches Ziel der Untersuchung sollte die Möglichkeit der Herstellung von Nanocomposite-Beschichtungen mit Multilayer-Filmen aus TiN und AlSiN Schichten sein. Durch diese Untersuchungen soll der Zusammenhang zwischen den mechanischen Eigenschaften (Härte, Elastizitätsmodul) und denen der Mikrostruktur verstanden werden. Ein Teilpunkt der Arbeit befasst sich mit dem Einfluss der Temperatur auf die Änderungen des Mikrogefüges der Beschichtungen bei Glühtemperaturen von 600°C. Die Oberflächenhärte, der Elastizitätsmodul und die Diffusion der Schichten wurden als Beurteilungskriterien für den Vergleich zwischen den beschichteten Proben mit und ohne dem Glühenprozeß benutzt.

Zum Erreichen der Aufgaben wurde eine Vakuumkammer mit drei Sputter-Magnetrons für das Beschichten mit Dünnschichtfilmen für verschiedene Materialien konstruiert. Die Vakuumkammer besteht im wesentlichen aus zwei Kammern: Der Vorvakuumkammer um das Werkstück zu laden und der Hauptvakuumkammer, in der das Sputtern der Dünnschichtfilme stattfindet. Das Werkstück ist auf einem Wagen befestigt und kann auf einem Gleis zwischen den Kammern mit Hilfe von Schrittmotoren zu den entsprechenden Positionen der Magnetrons bewegt werden. Die Kammern sind durch eine Verbindungstür getrennt, die von außen manuell betätigt werden kann. Die Kammern wurden zum Erreichen der Vakuumdichtheit verklebt und verschraubt. Daher wurden verschiedene Kleber im Hinblick auf die Vakuumdichtheit und die Ausgasungsraten getestet. Als geeignet hat sich ein Epoxidharz für den Einsatz im Vakuum herausgestellt.

Die Evakuierungseigenschaften der Kammer wurden durch Minimieren der Ausgasungsraten der verwendeten Materialien verbessert. Die Ausgasungsrate verschiedener Aluminiumwerkstoffe (A2017 und A5353) wurde in einem einstündigem Ausgasungsversuch bestimmt. Dabei wurden verschiedene Bearbeitungsverfahren und Oberflächenbehandlungen der Werkstoffe getestet. Die Bearbeitung des Werkstoffes Aluminium A2017 mit Ethanol als Kühlflüssigkeit bei der Bearbeitung zeigte eine Verringerung der Ausgasungsrate um den Faktor 6 im Vergleich zu dem unbehandeltem Werkstoff des gleichen Materials.

Die Reduzierung der porösen Aluminiumoxidschicht auf der Oberfläche des Materials konnte durch Beizen mit Salpetersäure und anschließendem Konservieren durch Aufbringen einer porenfreien Oxidschicht mit Hilfe eines Eloxalverfahren erreicht werden. Dadurch wird die Oberfläche geschützt und die Ausgasungsrate minimiert, auch nach Lagerung in feuchter

Umgebung. Mit Hilfe eines Gasanalysator wurde gezeigt, dass 85% der Gase innerhalb der Vakuumkammer Wasserdampf und die restlichen N_2 , H_2 , und CO waren. Durch eine Flüssigstickstoffkryofalle konnte der Wasserdampfanteil gesenkt und die Evakuierungseigenschaften der Kammer verbessert werden. Dadurch wurde es möglich eine Vakuumkammer zu bauen, die innerhalb einer Stunde auf einen Druck von 1×10^{-6} mbar mit einer Turbomolekularpumpe (450 l/s) evakuiert werden kann, bei einem Vakuumvolumen von 160 Litern und einer inneren Oberfläche von $1,4 \text{ m}^2$. Dieses niedrige Ausgangsdruckniveau wird zum Sputtern von guten Dünnschichtfilmen benötigt.

Vielschicht-Dünnschichtfilme wurden in Stickstoff reaktiv gesputtert, um zu zeigen, dass nanostrukturierte Dünnschichten im (Ti, Al, Si) N System durch reaktives Magnetron Sputtern der Vielschichtfilme (TiN, AlSiN) produziert werden können. Die SNMS Spektroskopie der Testobjekte zeigt, dass eine vollständige Diffusion zwischen den Schichten auch bei niedrigen Substrattemperaturen stattfindet. Das starke Magnetfeld der Magnetrons und die hohe Sputterleistung sind in der Lage ein großes Verhältnis „Ionen zu Atom“ zu erzeugen, welches den Beschichtungsatomen eine große Mobilität verleiht und somit die Diffusion erzeugt.

Anhand des XRD Musters für dieses System wurde gezeigt, dass die Struktur der Mischung aus zwei Phasen besteht. Eine Phase ist als TiN bekannt, wohingegen die andere amorphe Phase nicht bestimmt werden konnte. Möglicherweise handelt es sich dabei um SiN_x , AlN oder eine Kombination Ti-Al-Si-N der Verbindungen.

Zusammenfassend konnte gezeigt werden, dass mit der konstruierten Vakuumkammer Nanocomposite-Beschichtungen mit Multilayer-Schichten aus TiN und AlSiN produziert werden können.

SYMBOLS

Symbols	Units	Description
λ	m	Mean free path
n	molecules/m ³	Gas density
P	Pa	Pressure
N'	molecule	Number of molecules in the volume
N	molecule	Number of molecules that traverse the distance x before suffering a collision
S	L/s	Pumping speed
Q	mbar L/cm ² s	Outgassing rate
V	m ³	Volume
C	L/s	Orifice conductance
A	m ²	Surface area
ΔP	mbar	Pressure difference between both sides of the orifice

1. INTRODUCTION

The deposition of hard coating materials using the physical vapor deposition (PVD) magnetron sputtering process has reached a high share within the coating techniques due to its wide mechanical applications, specially in the deposition of hard cutting tools coatings and the high oxidation resistance coatings. Different methods and materials are used to produce this hard coatings nowadays, such as, single layer coating, multilayers coating, and the two phase nanocrystal amorphous coating like the (Ti, Al, Si)N system. The investigation of the nanocrystal structure of the (Ti, Al, Si)N system by the deposition of multilayers is studied. The hardness and the chemical composition of the coated samples were tested before and after annealing at 600 °C.

In this chapter the vacuum technology, thin film coating technology and the bonding technology are topics of discussion.

1.1. Study Objects

The nanocomposite coating materials, for example, the (Ti, Al, si)N system have recently attracted increasing interest due to the possibility to combine high hardness, high oxidation resistance, stiffness, and low friction coefficient properties. Therefore, it is used in many industrial applications, like the cutting tools, wear resistance, high oxidation resistance and high friction contact surfaces.

In this work a (Ti, Al, Si) N system was investigated. The main point of investigation was to study the possibility of producing the nanocomposite coating structures by deposition of multilayer films from TiN, AlSiN. This also tries to understand the relation between the mechanical properties (hardness, Young's modulus), and the microstructure (nanocrystalline with individual phases). Particularly special attention was given to the temperature effects on microstructural changes in annealing at 600 °C for the coatings. The surface hardness, elastic modulus, and the multilayers diffusion and compositions will be the test tools for the comparison between the different coated samples with and without annealing at 600 °C.

To reach this goal the following tests and work were done:

- A rectangular aluminum vacuum chamber with three unbalanced sputtering magnetrons for the deposition of thin film coatings from different materials was constructed

- The chamber consists mainly of two chambers, the pre-vacuum chamber to load the workpiece, and the main vacuum chamber where the sputtering deposition of the thin film coatings take place. The workpiece is moving on a car traveling on a railway between the two chambers through a self constructed rectangular gate controlled manually from outside the chamber, and between the different sputtering magnetrons inside the main chamber.
- The chamber was sealed for vacuum use using glue. Therefore, different types of glue were tested not only for its ability to seal the chamber for vacuum use, but also whether it can be used in vacuum (low outgassing rates).
- The evacuation characteristics of the constructed chamber was improved by minimizing the inner surface outgassing rate. Therefore, different machining methods for the treatment of the inner surface of the vacuum chamber were tested. As a result it was possible to construct a chamber that can be pumped down to the range of 1×10^{-6} mbar within one hour of evacuations. This is a good base pressure for the process of sputtering deposition of hard thin film coating.

1.2. Vacuum Technology

1.2.1. Kinetic Picture of a Gas

The kinetic picture of a gas is based on several assumptions[1]:

- The volume of gas under consideration contains a large number of molecules. A cubic meter of gas at a pressure of one bar and a temperature of 22 °C contains 2.48×10^{25} molecules, while at a pressure of 10^{-7} Pa, a very high vacuum, it contains 2.5×10^{13} molecules.
- Adjacent molecules are separated by distances that are large compared with their individual diameters. If we could stop all molecules instantaneously and place them on the coordinates of a grid, the average spacing between them would be about 3.4×10^{-9} m at atmospheric pressure. The diameter of most molecules is in the 2×10^{-10} to 6×10^{-10} m range, and they are separated by distance of about 6 to 15 times their diameter at atmospheric pressures.
- Molecules are in a constant state of motion. All directions of motion are equally likely and all velocities are possible, although not equally probable.

- Molecules exert no force on one another except when they collide. If this is true, then the molecules will be uniformly distributed throughout the volume and travel in straight lines until they collide with a wall or with one another.

Many interesting properties of ideal gases have been derived by using these assumptions, the main property is the mean free path.

1.2.2. Mean Free Path

The fact that molecules are randomly distributed and move with different velocities implies that each travels a different straight-line distance (a free path) before colliding with another [2]. While not all free paths are the same length. The average, or mean, of the free paths λ , according to kinetic theory is:

$$\lambda = \frac{1}{\sqrt{2} * \pi * d_o^2 * n} \quad [1.1]$$

Where:

d_o : The molecular diameter [m]

n : Gas density [molecules/m³]

The mean free is clearly gas density dependent. If the temperature is constant, it is also pressure dependent. For air at room temperature the mean free path is easily calculated by:

$$\lambda = \frac{6.6}{P} \quad [1.2]$$

Where:

λ : The mean free path [mm]

P : Pressure [Pa]

Kinetic theory also describes the distributions of free paths:

$$N = N' * e^{\frac{-x}{\lambda}} \quad [1.3]$$

Where:

N' : The number of molecules in the volume

N : The number of molecules that traverse the distance x before suffering a collision

For the case of two gases, a and b, the mean free path of a in b is:

$$\lambda_a = \frac{1}{\sqrt{2} * \pi * d_a^2 + \sqrt{\left(1 + \frac{v_b^2}{v_a^2}\right) * n_b * \pi * \frac{(d_a * d_b)^2}{4}}} \quad [1.4]$$

1.2.3. Outgassing

The gas load in vacuum fixturing and chamber walls adsorbed on and dissolved in metals. This gas load will affect the performance of high and ultrahigh vacuum systems if its not removed. Gas is dissolved in a metal during its initial melting and casting. It consists mainly of hydrogen, oxygen, nitrogen and carbon oxides. Gas is also physi- and chemi- sorbed on the interior surfaces from exposure to ambient atmosphere. It consists of a large quantity of water vapor, with carbon oxides, oxygen and some nitrogen. The nature and quantity of the adsorbed layer is also a function of the metal, the gas used to release the system to atmosphere and the time and extent to which it was exposed to the surrounding air. Fig.1.1 shows the different mechanisms in which materials are producing outgassing.

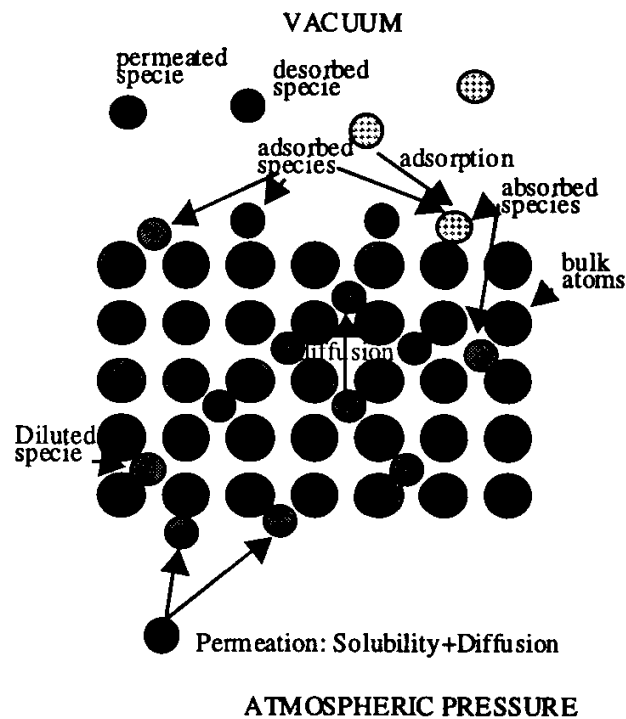


Fig. 1.1 Surface and bulk phenomena in vacuum [3]

1.2.3.1. Adsorbed Gas

Adsorption takes place by physical adsorption or chemical adsorption. In physical adsorption gas molecules are attracted weakly by Van der Waals forces with binding energy of less than

40 kJ/mol, in chemical adsorption actual chemical bonding occurs between the gas molecules and the molecules atoms on the surface of the vacuum chamber material. This binding energies vary between 80 kJ/mol and 800 kJ/mol. The quantity of gas adsorbed at constant temperature on a given surface increased with the pressure of gas in the gas phase, the relationship between the quantity adsorbed and the pressure is called the adsorption isotherm. There exist several models to describe these isotherms [4], the three most important can be attributed to:

- Langmair-Isotherm. This assumes that the adsorption energy is independent of surface converge.
- Freundlich-Isotherm. This assumes that the adsorption energy decreases exponentially with surface converge.
- Temkin-Isotherm. This assumes that the adsorption energy decreases linearly with surface converge.

Adsorbed gas may be removed from the metal surface by thermal desorption as the vacuum baking process, chemical cleaning or the energetic particle bombardment (glow discharge cleaning).

1.2.3.2. Dissolved Gas

Efflux of dissolved gas from within the metal fixuring and walls can be eliminated by rendering it immobile, reducing its initial concentration, or erecting a barrier of its passage. Dissolved gas can be rendered immobile by different methods. The initial concentration can be substantially reduced by vacuum melting, by first degassing parts in a vacuum furnace, or by in-situ baking of the complete system, also the vacuum firing of components and subassemblies will effectively remove the dissolved gas load in cleaned and degreased parts.

1.2.3.3. Vaporization of Materials

The vapor pressure of most materials is low enough to allow their use in vacuum systems. A few metals should not be used in vacuum constructions because of their vapor pressures are high enough to interfere with normal vacuum baking procedures. Alloys containing zinc, lead, cadmium, fore example have unsuitably high vapor pressures for vacuum applications, on the other hand aluminum and stainless steel has low vapor pressure that made them suitable for the vacuum applications use.

1.2.3.4. Permeability of Gas Through Walls

Gases permeate through most materials, also gases present in the ambient air can permeate to vacuum chambers through the system walls and sealed parts. Permeation of gases is a combination of two physical processes, dissolution and diffusion, where first the gas dissolved in the solid and then it diffuses to the inner wall of the system, where the gas arrives at the inner surface it desorbs to the vacuum volume.

1.2.4. Chamber Evacuation and Pumping Speed

The pumping rate and base pressure of high vacuum systems are limited by the surface (water) desorption rate (see fig. 2.15). The pumping time is not only dependent on the pump size, chamber volumes, and internal surface area but also on the state of surface treatments, cleanliness. This is especially true when the interior surfaces become covered with deposition residues, some of which are hygroscopic [1]. The equation that describes the time dependence of pressure in the evacuation of a vacuum chamber is:

$$S * A - Q = -V \frac{dP}{dt} \quad [1.5]$$

Where:

- S: Pumping speed [L/s]
- P: Pressure [Pa]
- Q: Outgassing flow rate [Pa.m³/s]
- V: Volume [m³]

The first term on the left is the quantity of gas exiting to the pump per unit time, the second term is the amount of gas per unit time entering the chamber from outgassing, permeation, and leaks. The $-V \frac{dP}{dt}$ is the net rate at which gas is removed from the system. If Q is constant or at least changes much more slowly with time than the system constant [V/S], as it does for outgassing, the approximate solution can be written:

$$P = P_0 * e^{\frac{-St}{V}} + \frac{Q}{S} \quad [1.6]$$

The first term in the solution represents the time dependence of the pressure that is due to the initial gas concentrations; the second term represents the contribution of the other gas sources. After some time of evacuation the pressure is given by the equation:

$$P = \frac{Q_1}{S} * t^\alpha \quad [1.7]$$

where:

Q1: the value of Q at some initial time (1h)

α : constant ≈ 1

The most important uncertainty associated with pump performance, pressure and flow measurements and external leakage is due to outgassing. The outgassing rates can easily vary by many orders of magnitude depending on history and the material of a surface, its treatment, humidity, temperature, and the period of exposure to vacuum. Since one usually approaches the ultimate pressure of a system asymptotically, even small changes in gas loads results in large differences of evacuation times and the chamber base pressure.

1.3. Thin Film Coating Technology

1.3.1. Basic Aspects of Sputtering

Sputtering is an atomic process that uses a glow discharge to generate a flux of ions incident on the target surface. These ions cause atoms, and occasionally clusters of atoms, to be knocked free from the target surface by momentum transfer. Illustrated in figure 1.2 is the classical architecture of a DC-diode glow discharge [5]. Several distinct regions within the plasma are shown. Directly adjacent to the cathode is the cathode glow region, which is luminous due to ion, both positive and negative, neutralization at the cathode surface. Next is the cathode dark space or sheath, and it is across the region that most of the voltage is dropped, providing the accelerating force driving the ions into the target. When an ion strikes the cathode, along with the generation of heat and the removal of neutral sputtered atoms there is a 5-10% probability of secondary electron emission. Emitted secondary electrons are then accelerated back across the dark space into the negative glow region. In this region the electrons expend most of their energy creating additional ions and generating a cold cathode discharge. It is these secondary electrons that are responsible for sustaining the discharge.

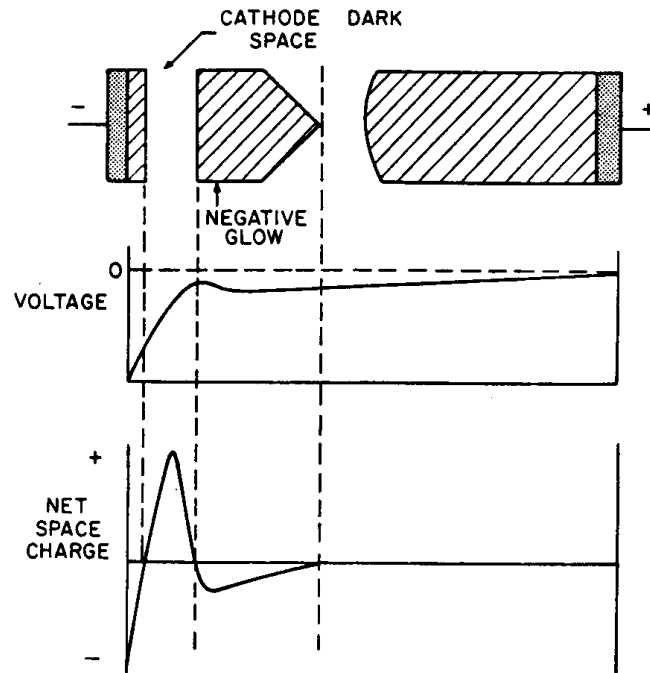


Fig.1.2 Schematic illustration of the primary regions, voltage characteristics, and net space charge for a DC-glow discharge [5]

Under appropriate pressure conditions, beyond the negative glow region is another dark space (Faraday dark space), the positive column, an anode dark space, and the anode; however, for sputtering plasmas the negative glow usually fills the chamber, and the other regions are therefore not considered further.

1.3.2. Thin Film Formation

In sputtering deposition, as well with the other standard vacuum deposition process of evaporation, material arrives at the substrate mostly in an atomic or molecular form (see figure 1.3) [6]. The atom diffuses around the substrate with a motion determined by its binding energy to the substrate and is influenced by the nature as well as the temperature of the substrate. Energetically, the surface of the substrate is like an egg carton, with each of the depressions constituting a temporary resting point or adsorption site for the deposition and diffusing atoms. At each hop. The atom will either jump over the barrier into an adjacent site, or might even hop right out (re-evaporate). After a certain time, the atom will either evaporate from the surface or will join with another diffusing single atom to form a double, which is less mobile but more stable than the single atom, so their mobility is severely limited, as is the chance of their (re-evaporation). The chance of forming the atomic pair will depend on the single atom density and hence on the arrival or deposition rate. In time, the

doublets will be joined by another single atoms to form triplets, quadruplets and so on. This is the nucleation stage of the thin film growth, leading to the formation of quasi-stable islands, each containing tens or hundreds of atoms. During the next, island growth stage, the islands grow in size rather than in number. Eventually they grow large enough to touch; this is the agglomeration or coalescence stage. From observations of the stage, it appears that the islands often display liquid-like behavior during coalescence, and there are often crystallographic reorientations as a result of competition between the structures of the coalescing islands. Coalescence proceeds until the film reaches continuity. During the coalescence stages, the film therefore typically consists of hills and valleys. During the island stage, each island is usually single crystal or contains just a few crystals. On a polycrystalline substrate, the orientation of each island will be random, so that the resulting film is polycrystalline. On a single crystal substrate, the island orientations may be determined by the substrate structure so that growth and coalescence leads to a single crystal film. This is the phenomenon of epitaxy [7]. If surface atoms are mobile, they have a greater opportunity of finding low energy positions, consistent with crystal growth, in the growing film. Mobility is enhanced by increased substrate temperature, crystal growth is also encouraged by low deposition rates. Hence, on single crystal substrates, for each deposition rate there will be a temperature, the epitaxial temperature, above which single crystal films can grown. During the island stage, each island will contain one or a few crystallites. The same mechanisms obtain as in single crystal growth take place.

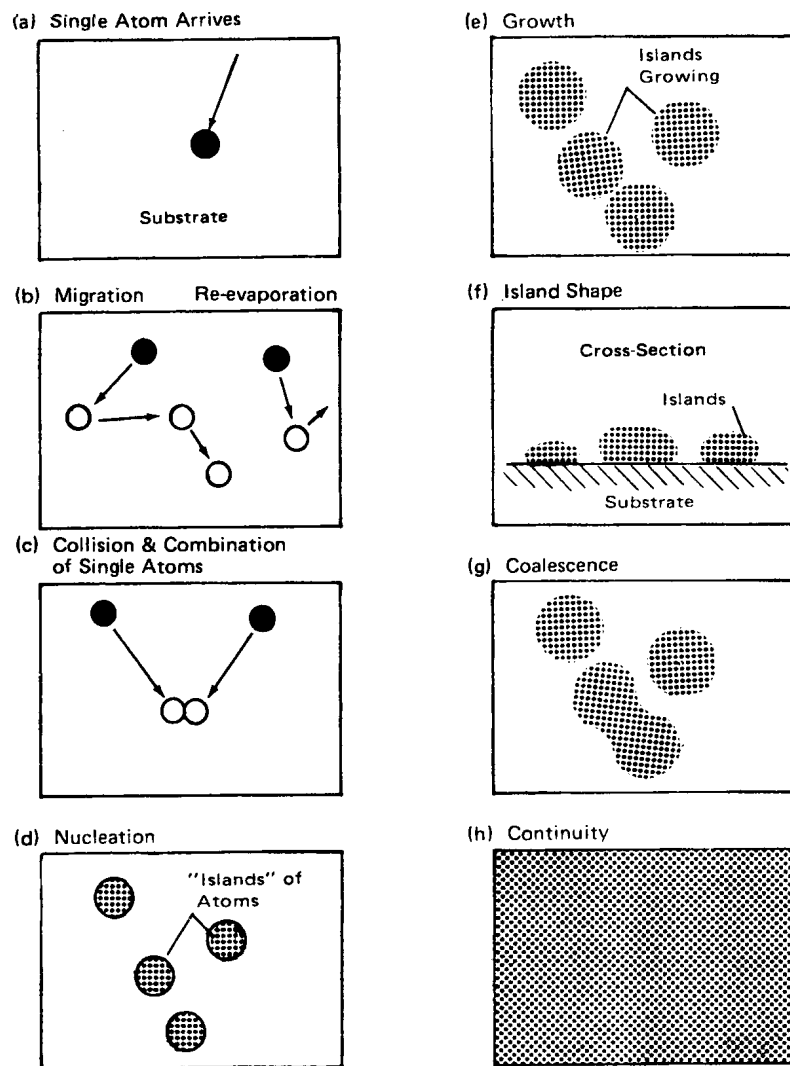


Fig. 1.3 Formation of a thin film [6]

All of the relationships above were found for the comparatively simple case of deposition by vacuum evaporation. The structure of the growing films was found to be extremely sensitive to deposition conditions. Electron bombardment either prior to or during deposition was found to encourage film continuity and reduce epitaxial temperatures. Ion bombardment and increased arrival energy of the depositing atoms, also reduced the epitaxial temperature.

1.3.3. Coating Structure and Characterization

In common with bulk materials, the properties of a coating are closely allied to its microstructure, there exist six structural levels of matter down to the final element particles (see figure 1.4) [8], and it is the interactions which occur between these different levels of structure which dictate the properties of engineering materials, these interactions may start just above one atomic spacing and extend over many grain diameters. The structure property

relationships derived for the generic coating types reflect this complex situation which is further compounded by the realization that, in general, coatings are not deposited at equilibrium in many deposition processes and contain a variety of defects (dislocations, gross porosity, vacancies, cracks). Clearly the correct choice of deposition technology does not stop at the laying down of the coating; the end-user has to be aware of the vast range of techniques, both chemical and physical, which can be used to characterize the coating substrate composite system. For this reason those methods which are most appropriate to the chemical and physical characterization of advanced engineering coatings are mentioned in the next section.

		Engineering structure	Integrated circuits Chinese wall
Γ	6	Microstructure	Diameter of grain or phase boundary Large grain size
ϕ	5	Phase	Small Large elementary cells
M	4	Molecule	Monomers High polymer
A	3	Atom	
N	2	Nucleus	
E	1	Elementary particle	
		Level of structure	Size of structural objects (m)
			10^{-15} 10^{-12} 10^{-9} 10^{-6} 10^{-3} 10^0 10^3

Fig. 1.4 The six structural levels [8]

One feature common to many of the gaseous (vapor) state coatings is that the solid materials is distributed in an array of fairly closed packed columns that run perpendicular to the substrate, and it is the columnar microstructure that has considerable influence over the physical and chemical behavior of the film. The microstructure is anisotropic and so are most thin film properties (see fig. 1.5). Many attempts have been made to model film morphology, ranging from a consideration of adatom mobility on the growing surface to computer simulation and evolutionary growth models [9], but as yet it has been impossible to predict fully the properties of vapor deposition coatings from a knowledge of their deposition conditions.

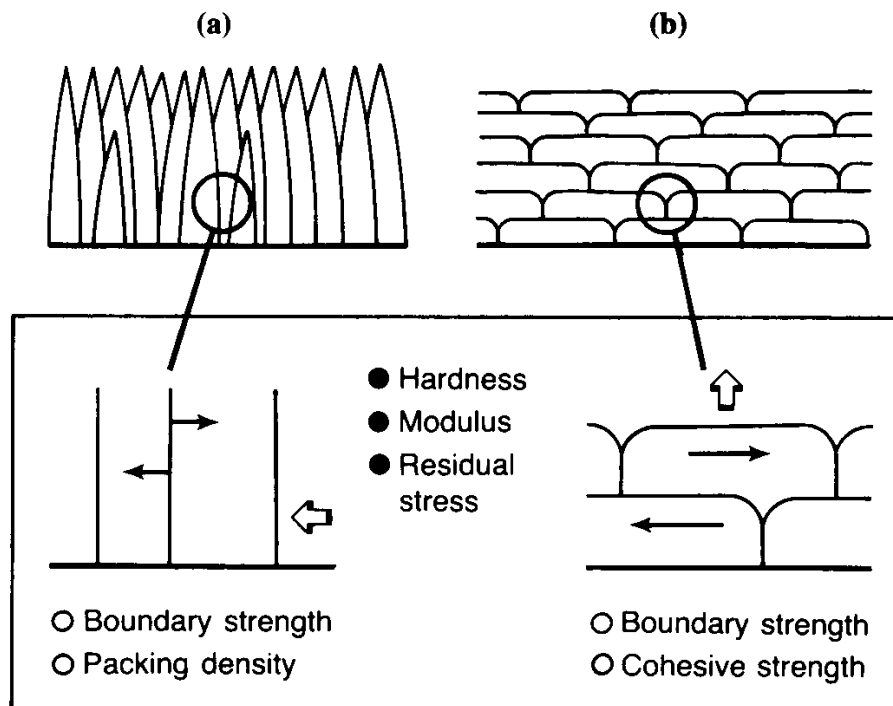


Fig. 1.5 Schematic diagrams of the structure property relationships for coatings deposited from (a) the vapor state and (b) the molten-semi-molten state [6]

In contrast to the coating deposited from the vapor state, those processes which make use of the semi-molten state typically give rise to coatings which consist of lenticular splats whose boundaries run parallel to the substrate surface (see fig. 1.5).

Understanding the structure property relationships which exist for the coating substrate composite system is important, since the successful application of advanced surface coatings is often dependent on such knowledge. Equally important is the requirement for improved process control and the introduction of expert systems to enhance the selection procedures currently employed when deciding on the correct process for a given application.

1.3.4. Coatings Analysis

The physico-chemical characterization of materials and, in particular coatings, raises a number of questions concerning the type of information being sought; whether it is elemental composition, the identification of chemical phases and their distributions within the coating or the nature of interfaces between different phases. Unfortunately no single analytical method provides all this information and a wide array of techniques has been developed, each of which may contribute more or less to the overall picture. The analytical techniques available may be rationalized in terms of the source of excitation, whether its photons, energetic ions or

electrons which interacts with the surface to produce a range of secondary emissions which carry information concerning the composition and structure of the probed material. In addition, it is important to establish the difference between the volume of material probed and the sampled volume since the analytical probe may pass through the specimen, but the entity being analyzed may originate from the coating, coating substrate interface or substrate material. The characteristic depth from which information originates varies greatly with the source of excitation and therefore the chosen technique. The depth resolution of these techniques may be orders of magnitude smaller than the sampling depth and will depend upon the material being investigated and the particular acquisition geometry or sampling mode. Another important parameter is the characterization process is the sensitivity of the analytical technique which often depends on the coating substrate materials and again the type of instrumentation used.

The Secondary neutral particle mass spectrometry (SNMS) and the X-ray diffraction were used to study the composition and structure of our deposited nanocomposite coating. The operating principle of both systems are described below.

1.3.4.1. Secondary neutral particle mass spectrometry (SNMS)

Secondary neutral particle mass spectrometry (SNMS) is characterized by simple and good quantifiability, as well as low detection limits, connected with very good dissolution of depth. (SNMS) is used e.g. frequently to the quantitative depth profile analysis at multi-component layers and multi-layer systems. For the analysis of dielectric samples and electrically isolating layer systems the SNMS procedure is particularly attractive in the electron gas version. The so-called high frequency method (HFM) offers a simple and reliable possibility to avoid the often disturbing charging which is induced by primary or secondary. The emitted atoms and molecules – mainly neutral – that are emitted from the surface of a solid body under the bombardment with a high energy (0.5. 25 keV) primary-ion-beam are detected in the SNMS approach by mass spectroscopy. To make these sputtered –but neutral- particles accessible to mass spectroscopic analysis it is required to ionize them as efficiently as possible. This mostly happens by means of electron collision or photo ionization. due to the thereby reached uncoupling of emission and ionization process the probability of proof of different atoms or molecules is almost independent of the sample composition, from which the good quantifiability of the measured SNMS intensities is derived.

1.3.4.2. X-Ray-diffraction (XRD)

The XRD is a procedure, which supplies information about the crystal structure, crystalline defects, substrate orientations or mechanical stresses in the microscopic range. An important operational area is the x-Ray graphic phase analysis from solids to the determination of the components in crystal quantities. The investigations can be accomplished without destruction. The x-Ray quanta of primary radiation used with the XRD meet the sample atoms and energize their electrons to harmonious oscillations. These atoms send a secondarily radiation with the frequency of the energizing radiation. In crystals the strew centers (sample atoms) possess a regular periodic arrangement with atomic spacings, which is about just as large as the wavelength of the incident x-ray. It comes therefore to the overlay (interference) with the radiation outgoing from neighboring atoms. In certain directions reinforcement of the emitted wave fronts lies forwards (diffraction maxima), in other extinction (diffraction minima). From the measured picture the crystal structure of the examined sample range can be determined.

1.4. Bonding Technology

Adhesives serve the purpose of fastening thing together, either temporarily or permanently. Adhesive and bonding materials have been used successfully in the last few years in every branches of the industry for the banding structures, because of their good properties and characteristics. Bonding materials has some advantages compared with the other traditional joining methods [10]. Some of these advantages are the followings:

- No adverse effect on the material characteristics of the joined parts.
- Bonding of different materials.
- Bonding of heat-sensitive materials.
- Bonding of thin materials over large area.
- Uniform distribution of tension in bonded areas.
- Low-heat joining processes.
- Prevention of crevice corrosion.

The bonding joining method also possess certain well disadvantages and used limitations, such as:

- Low temperature resistance.
- Low resistance to peel stress.
- Necessity for surface pre-treatment.

- Critical ageing behavior under the effect of certain liquid and gaseous media.

1.4.1. Fundamentals of Bonding Technology

Bonding is the joining of identical or different types of materials by means of an adhesive, creating a positive-substance bond throughout the entire surface of the joint. In order to be able to transmit forces the adhesive must not only wet and adhere to the respective materials, but must also possess an adequate degree of internal strength. The ability of an adhesive to adhere to the surface of the material is referred to as adhesion, while the force of attraction between the molecules is known as cohesion (see fig.1.6). In every case, the forces of adhesion are formed initially during manufacturing process. The first prerequisite for good adhesion lies in the optimum wetting of the respective parts by the adhesive. Adhesion which can successfully be used only occurs if physical forces such as dipole, dispersion or Van der Waals forces take effect between the wetted surface and the adhesive, and/or chemical bonds arise such as covalent or ionic or complex linkages. The aim should be to achieve chemical bonds, since these are stronger by their very nature. It is, however, essential that impurities and absorbent layers on the surface of the materials are removed by appropriate pre-treatment. On surfaces treated in the right way, the adherent reactions to the adhesive can then take place. Cohesion is of decisive importance in addition to adhesion for the effectiveness of the bonded fastening. The cured adhesive, a polymer materials should possess a sufficient degree of inner strength over a wide temperatures range. For example, it should be cross-linked and/or possess a high molecular weight. Cohesion, therefore, is a factor which develops as a function of material characteristics in particular the resistance to creep or deformation of the adhesive under physical stress. The relationship between the faces of adhesion and those of cohesion is decisive for the strength of a bonded joint. Irrespective of how high the cohesion forces in an adhesive layers are, if there are no adhesion forces in effect (and vice versa), the adhesive will be incapable of fastening two parts together securely.

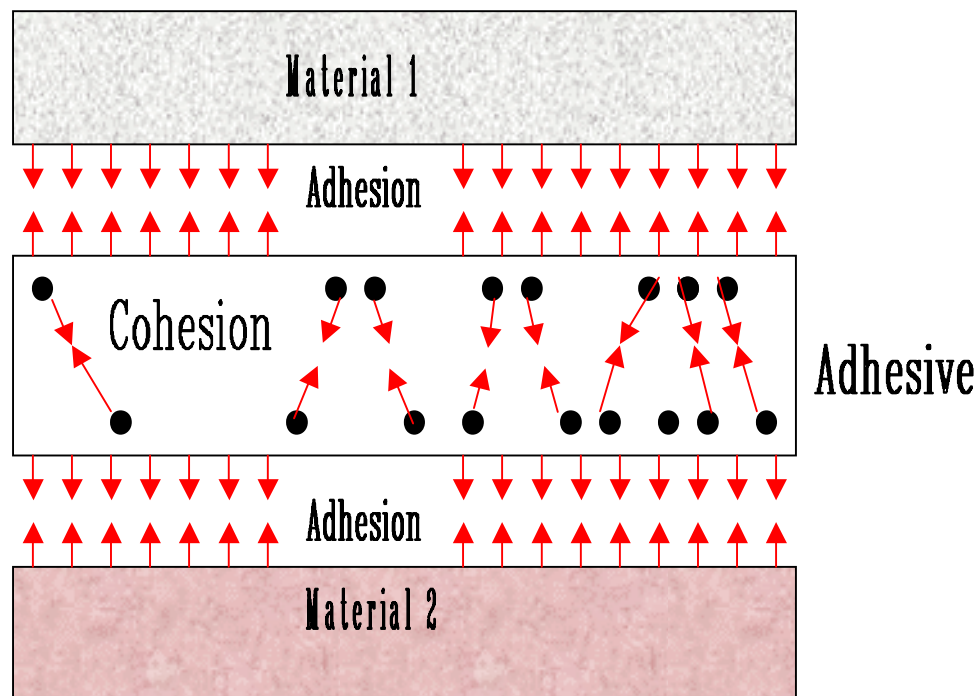


Fig. 1.6 Fundamentals of adhesives: adhesion and cohesion [10]

1.4.2. Types of Bonding Materials

1.4.2.1. Epoxy adhesives

Epoxy adhesives are based on epoxy resins, which cure either with amines at room temperature or with organic acids or specially harden at higher temperatures. In principle, epoxy adhesives can be formed both in one and two component forms. Epoxy adhesives are predominantly used for the construction of metal assemblies, where they represent typical metal adhesives. Provided the metals have been suitably pre-treated, no other adhesive systems exhibit such outstanding adhesion and similarly impressive resistance to ageing.

1.4.2.2. Polyurethane Adhesives

Polyurethane Adhesives are based on isocyanates, a group of molecules of high reactivity. They are available in one or two component form depending on what characteristics are required or under what conditions they should cure. One component consist of prepolymers composed of diisocyanates and high molecular polyether or polyester-polyols. In the case of two component, one component consists of high molecular diisocyanates. Polyether or polyester-polyols are used as resins in combination with suitable catalysts. The advantages of these adhesives lies in their adaptable curing time, which can vary from a few minutes to a

few hours, and they permit the construction of elastic assemblies which are able to withstand high dynamic loads.

1.4.2.3. Acrylate Adhesives

The group of acrylate adhesive includes cyanoacrylate adhesive, anaerobically curing adhesives and two component acrylate adhesives. The cyanoacrylates are of the one component type and cure on countless materials under the effect of atmospheric humidity. They cure faster without any additive and auxiliary devices, than any other adhesive system. cyanoacrylate adhesives are suitable for bonding small parts. Anaerobically curing adhesives based on special dimethacrylate esters, which contain suitable accelerators, are also one component adhesives but cure only on metals and subject to the exclusion of air. These adhesives are traditionally used to secure screws and nuts, to bond shafts and hubs and seal mating parts and flanges. Two component acrylate adhesives are known by a variety of names (A/B systems), the excellent reactivity of acrylates is utilized in the formulation of adhesives. Acrylates cure rapidly on numerous substrates with the addition of special hardeners (peroxides) and exhibit a high degree of adhesion.

1.4.2.4. Phenolic Resins

Phenolic resins consist of phenols and aldehydes which cure under the effects of pressure and heat (5 bar and 250 °C). The vinyl phenolic resins were used in the industry because of their outstanding strength and resistance to ageing.

1.4.2.5. Modified Silane Polymers

Modified silane polymers consist of a polymer base with silane groups which cross-link under the influence of moisture. These adhesives are available in one and two-component form. Since they possess an average degree of tensile strength, bonded joints made with them exhibit outstanding elasticity. The principal advantage of this adhesive is that they contain no silicon. As a result, no problem arises with the painting of bonded parts during their further processing, moreover they require less surface pre-treatment compared with other adhesive materials.

2. OUTGASSING TEST

2.1. Introduction to Outgassing

In the design of ultrahigh vacuum deposition systems, the stringent base pressure and pump down requirements cannot be met only by increasing the available pumping speed. The primary solution to this design problem is a choice of vessel material and surface treatment which minimizes its outgassing. For that in the vacuum science literature different series of stainless steel and aluminum material under different machining and surface treatments can be found [11-14].

In this study we have made a systematic comparison of outgassing measurements from two different types of aluminum alloy materials, after various standard and advanced surface treatments. The examined treatments included normal surface machining, machining under different types of alcohol, temperature vacuum bake out, pickling and anodizing under different conditions and voltages. Base line comparisons were made to samples given standard alkaline detergent wash/deionized water rinses, treatments in ultrasonic bath.

2.2. Vacuum Materials

The outgassing rate of a metal depends on the physical and chemical state of the surface and the previous history of the material. Therefore, it's not surprising that outgassing measurement in the literature for nominally similar materials show a large variation. Nevertheless some generalizations are possible for outgassing of the vessel material under consideration. Generally, two materials are considered for fabrication of the ultra vacuum systems: type 304 stainless steel and aluminum (usually type 6061 or 6063). This materials are chosen for vacuum application because of their

1. low outgassing rate
2. corrosion resistance
3. machinability
4. weldability

For stainless steel and aluminum the outgassing for unbaked vessels is dominated by H₂O. The sources of the outgassing of H₂O are:

1. H₂O molecules are adsorbed on or absorbed within the passivation oxide layer that is present on these metals.

2. H₂O can be released from the surface by the reduction of iron oxides in steel surface and Al(OH)_x in the aluminum surfaces.

In this work aluminum was selected for the construction of the vacuum chamber, two different available types of aluminum alloys were mainly tested under different conditions: A2017 T4 and A 5353. This selection was done because of the following considerations

1. The material available in the university workshop in the shape and dimension that fit with the required chamber design.
2. It showed good cryogenics properties, since the chamber is cooled by liquid nitrogen to trap the vapor of water from inside the chamber to improve its evacuation rates.
3. Studying and comparison of the outgassing rates between different series of aluminum alloys
4. These two alloys showed a high strength which is comparable to that of stainless steel.

2.3. Literature

Aluminum has vacuum characteristics approximately equal to stainless steel if treated properly. An additional advantage is the lower material and machining cost, and good thermal conductivity. Furthermore it has high allowance for localized high heat flux and the fact that aluminum is completely non magnetic. For that aluminum alloy vacuum systems have recently received considerable attention in the pursuit of high and ultra-high vacuum.

Della [11] studies the correlation of outgassing of stainless steel and aluminum with various surface treatments such as compound electro polishing, high vacuum temperature, vacuum bake out, vacuum re-melting and glow discharge cleaning. From his work the absolute outgassing rate varied by only a factor of 2.8 for stainless steel and a factor of 1.4 for aluminum alloys, even though the surface roughness differed by more than two order of magnitude.

Ishimaru [12] constructed a vacuum chamber from aluminum alloy (A6063-T6-EX). The inner surface of the chamber was machined under different conditions to minimize the porous aluminum oxide / hydroxide layer. Special extrusion techniques were used, like machining in a chamber filled with mixed oxygen-argon atmosphere, machining using ethanol as coolant, both processes showed low outgassing rates.

Suemistu [13] studied the outgassing rate measurement of aluminum alloy surfaces milled with various alcohols. All the alcohols tested in the study showed equivalent thin oxide layer

2. Outgassing Test

on the treated surface; and the surface carbon contents, also based on the measurement done together with other practical factors, isopropanol was chosen as an alternative to ethanol.

The influence of surface roughness on outgassing rate was studied by Tokai [14] by ultrahigh vacuum compatible mirror polishing of the aluminum alloy surface (electrochemical buffing treatment). The study showed good correlation between the surface roughness factor and the outgassing rate.

Chen [15] tested the thermal outgassing from aluminum alloy (A6063 and A1050) vacuum chambers. The chamber was treated with special extrusion methods then the outgassing rate were measured for several cases like: exposure to air for 1.5 year, after partially filling with water for 1 week. The study showed that baking the chamber at 150 C° for 24 hour (in air) can lower the outgassing rate even for the case where the chamber was filled with water for 1 week.

Ota [16] measured the outgassing from aluminum surface layer induced by the synchrotron radiation. The relation between the photon stimulated gas desorption from aluminum and the amount of carbon on the surface were investigated experimentally. He found that, the photo adsorption yield during the first stage of irradiation is reduced 3 orders of magnitudes by removing carbon on the surface using argon etching. Also he showed that the amount of desorbed CH₄, CO, CO₂ decreases almost linearly as the carbon is removed.

Suemitsu [17] constructed an other aluminum alloy chamber and its vacuum properties were tested by. He showed that the ultimate outgassing rate was observed to be less than 1×10^{-13} Torr l/s. cm² after a 100 C°, 45 hour bake out. The chamber also can be pumped down to the order of 10^{-10} Torr within 23 hours without bake out but within 6 hours with bake out. This low outgassing property was achieved by an ethanol milling technique applied to the inner surface of the chamber.

Tajiri [18] studied minimizing of the outgassing of an aluminum surface by developing an electro polishing method to obtain a mirror finish and pit-free, smooth surface by controlling the flow of the electrolytic fluid during polishing. The ultimate vacuum pressure and the characteristics of sputtered coatings where also investigated. Different cleaning procedures where studied and other factors that's can effect the outgassing of the aluminum sputtering chamber.

2.4. Outgassing Test Stand

Fig. 2.1 shows a schematic diagram of the apparatus for the outgassing measurements presented in this test. The test workpieces of the different aluminum alloys have a surface area of 58 cm^2 [$50 \times 50 \times 4$]mm, treated according to one of the surface treatments listed in Table I and Table II. The test chamber is fabricated from stainless steel with an inner surface area of 950 cm^2 . The system is pumped down by a UHV compatible 53 l/s turbo molecular pump. An appendage vacuum system is attached to the test chamber which contains a differentially pumped residual gas analyzer (RGA). The pressure was measured by a compact cold cathode ionization gauge (PKR).

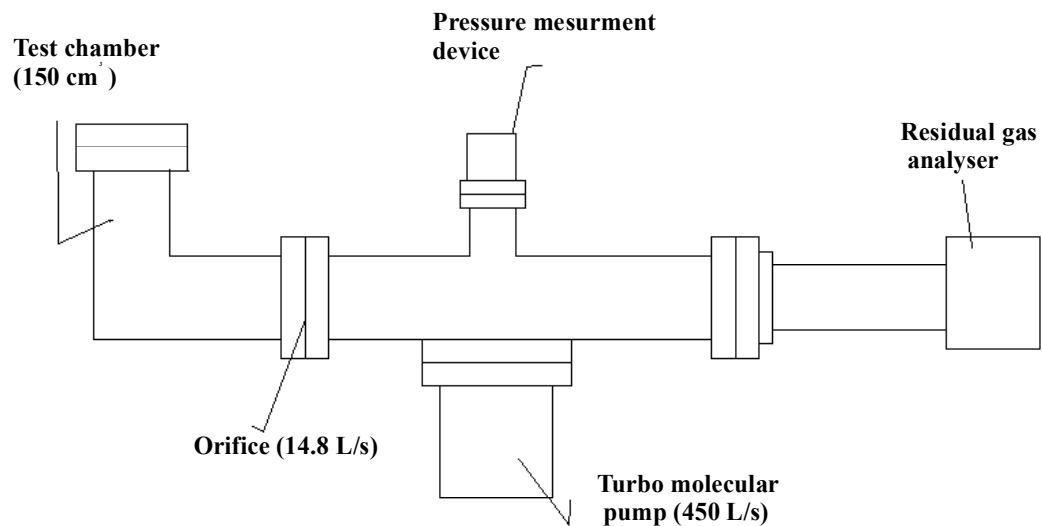


Fig.2.1 Schematic diagram of experiment apparatus

The measurement was carried out by a throughput outgassing test method [19],[20], in which a pressure difference of the test chamber is measured through a conductance orifice. Very often it is assumed that the down stream pressure is negligible. In our study a special test was made to measure the relation between the pressure measurement before and after the orifice. Fig. 2.2 shows the pressure measured in the test chamber before and after an orifice with (14,8 l/s) conductance. From this figure we can note that the pressure before the orifice is approximately a factor of 2 higher than the pressure after the orifice. For that this factor will be used in our calculation of the outgassing rates.

2.5. Experimental Procedure

Comparison of outgassing data in the literature is often difficult because of unspecified procedures from which the data were obtained. Variation in materials formulation, storages, and handling histories are some of the reasons that make it hard to compare the results of experiments done by different working groups. In our study the following measurement procedures were employed:

The test chamber was evacuated for approximately 24 h. Afterwards it was vent to 1 atm. room relative humidity ($65\% \pm 5\%$) and ambient temperature (20 ± 2 °C) for 10 minutes.

The chamber was pump down again for 1 hr. Pressure versus time was saved as empty chamber.

The chamber was vented again to 1 atm. room air after each outgassing test, the test workpiece was stored in the chamber and then it were pumped down for the required time.

In each test pressure versus time was measured by the cold cathode pressure measurement gauge (PKR) which is connected to the computer directly.

In some samples test the residual gas analyzer were used to analyze the gas percentage inside the test chamber.

2.6. Outgassing Results

In Fig. 2.3 a typical curve of the outgassing rate versus time is shown between the two different aluminum material samples without machining compared to the outgassing rate of the empty chamber.

From that curves it could be noted that two materials show low outgassing rate compared to the one of the empty chamber.

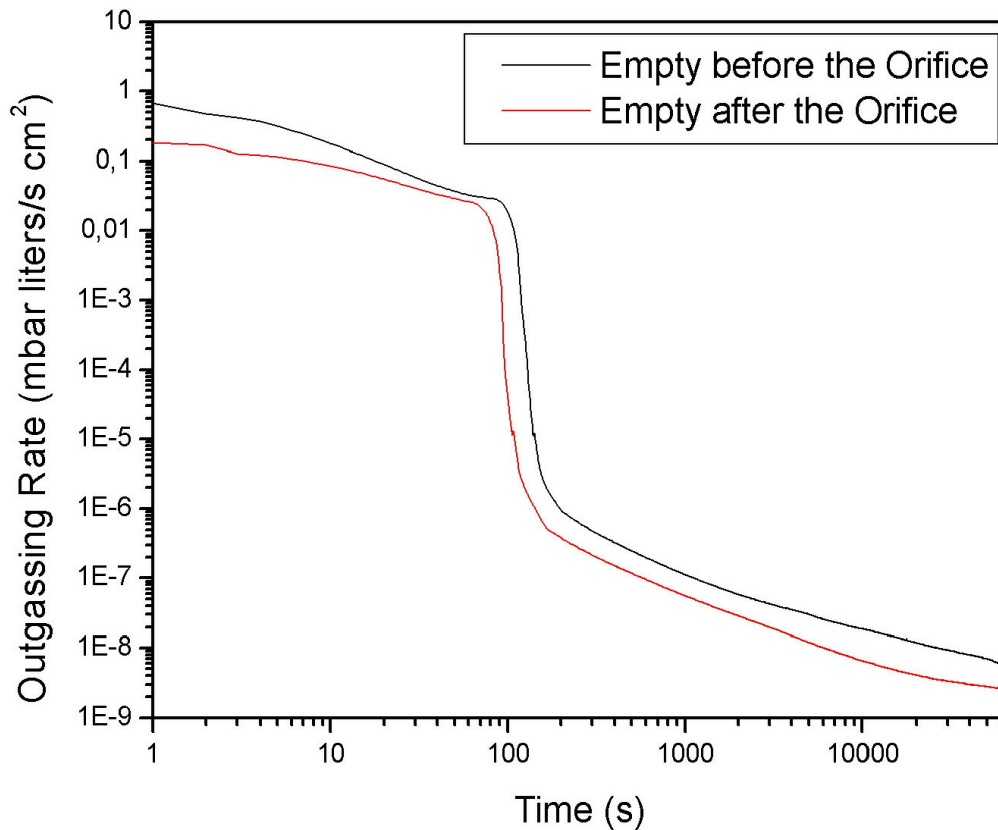


Fig.2.2 Outgassing Rate of empty chamber before and after the orifice

Therefore, further tests and surface treatment were done to the surface of these samples. Fig. 2.4 shows the results of tests done with material A (A2017-T4) as described in Table I. Fig.2.5 shows the results of the same tests done with samples of material B (A5353) as described in Table II. Material A shows a low outgassing rate under the different surface treatment conditions compared to the results of the sample without machining. It can be noted that all the test procedures show good results while some of them show a result a proximately equal to the outgassing of the empty chamber. More or less the same results can be drawn from Fig. 2.5 for the test of material B. The material shows a low outgassing rate under the different procedures used in cleaning and surface treatment.

Table I. Surface treatments to samples of material A (A 2017-T4)

Sample Name	Surface treatment description of material A (A 2017 T4)
Sa0_1	Sample without machining
Sa1_1	Machined surface without cleaning
Sa2_1	Machined surface and cleaned in ultrasonic bath with water and RBS (5 %) under 81 C° for 1 hr. After that put in another ultrasonic bath containing deionized water for 12 min. Then dried with argon gas.
Sa3_1	Machined surface and cleaned in ultrasonic bath with water and RBS (5 %) under 81 C° for 1 hr. Then put in another ultrasonic bath containing deionized water for 12 min. After that baked in 100 C° for 1 hr. Then dried with argon gas.
Sa4_1	Machined surface and cleaned in ultrasonic bath with water and RBS (5 %) under 81 C° for 1 hr. Then put in another ultrasonic bath containing deionized water for 12 min. After that baked in 100 C° for 12 hr. Afterwards dried with argon gas.
Sa5_1	Machined surface with fine glass papers (1000) under ethanol as cooling fluid. Then cleaned in ultrasonic bath with water and RBS (5 %) under 81 C° for 1 hr. Then put in another ultrasonic bath containing deionized water for 12 min. After that dried with argon gas.
Sa6_1	Machined surface with fine glass papers (1000) under isopropanol as cooling fluid. Then cleaned in ultrasonic bath with water and RBS (5 %) under 81 C° for 1 hr. After that put in another ultrasonic bath containing deionized water for 12 min. Then dried with argon gas.

From the comparison of the two material results we can note that the two materials show low outgassing rates under the test conditions. It could be noted also that the results of material A in the short time outgassing are better than the one of material B (see Fig. 2.4). Therefore, material A was selected for further tests and comparisons with other aluminum alloy materials.

Table III summarizes some of the machining conditions in which material A was tested. Surface machining was done with ethanol as coolant fluid and isopropanol as coolant fluid. The test was repeated with the same samples after one week. Fig. 2.6 shows the outgassing rates of the different machining conditions. It can be noted that some of the test procedures show better outgassing rates like machining under ethanol, and some show worse results like the sample machined with water as coolant fluid.

Table II. Surface treatments to samples of material B (A 5353)

Sample Name	Surface treatment description of material B (A 5353)
Sb0_1	Sample without machining
Sb1_1	Machined surface without cleaning
Sb2_1	Machined surface and cleaned in ultrasonic bath with water and RBS (5 %) under 81 C° for 1 hr. Put in another ultrasonic bath containing deionized water for 12 min. then dried with argon gas.
Sb3_1	Machined surface and cleaned in ultrasonic bath with water and RBS (5 %) under 81 C° for 1 hr. Then put in another ultrasonic bath containing deionized water for 12 min. After that baked in 100 C° for 1 hr. Then dried with argon gas.
Sb4_1	Machined surface and cleaned in ultrasonic bath with water and RBS (5 %) under 81 C° for 1 hr. Then put in another ultrasonic bath containing deionized water for 12 min. After that baked in 100 C° for 12 hr. And as a last step dried with argon gas.
Sb5_1	Machined surface with fine glass papers (1000) under ethanol as cooling fluid. then cleaned in ultrasonic bath with water and RBS (5 %) under 81 C° for 1 hr. Then put in another ultrasonic bath containing deionized water for 12 min. And dried with argon gas.
Sb6_1	Machined surface with fine glass papers (1000) under isopropanol as cooling fluid. Afterwards cleaned in ultrasonic bath with water and RBS (5 %) under 81 C° for 1 hr. Then put in another ultrasonic bath containing deionized water for 12 min. Then dried with argon gas.

Fig.2.7 shows the outgassing rates of two samples from material C [A6083] which is usually used in the fabrication of commercial vacuum chambers [11]. The first sample was machined with ethanol as coolant fluid, the second was machined under isopropanol as coolant fluid. From the comparison of Fig.2.7 with Fig 2.6 it can be simply seen that the two materials show similar outgassing results under the same surface machining treatment.

Table III. More surface treatments for samples of material A (A 2017-T4)

Sample Name	Surface treatment description
Sa7_1	Retest of sample Sa4_1 after one week
Sa8_1	Machined sample with fine glass paper (1000) and Ethanol as coolant fluid. Afterwards cleaned and dried by argon gas
Sa9_1	Machined sample with glass paper (1000) and water as coolant fluid. Afterwards cleaned and dried by argon gas

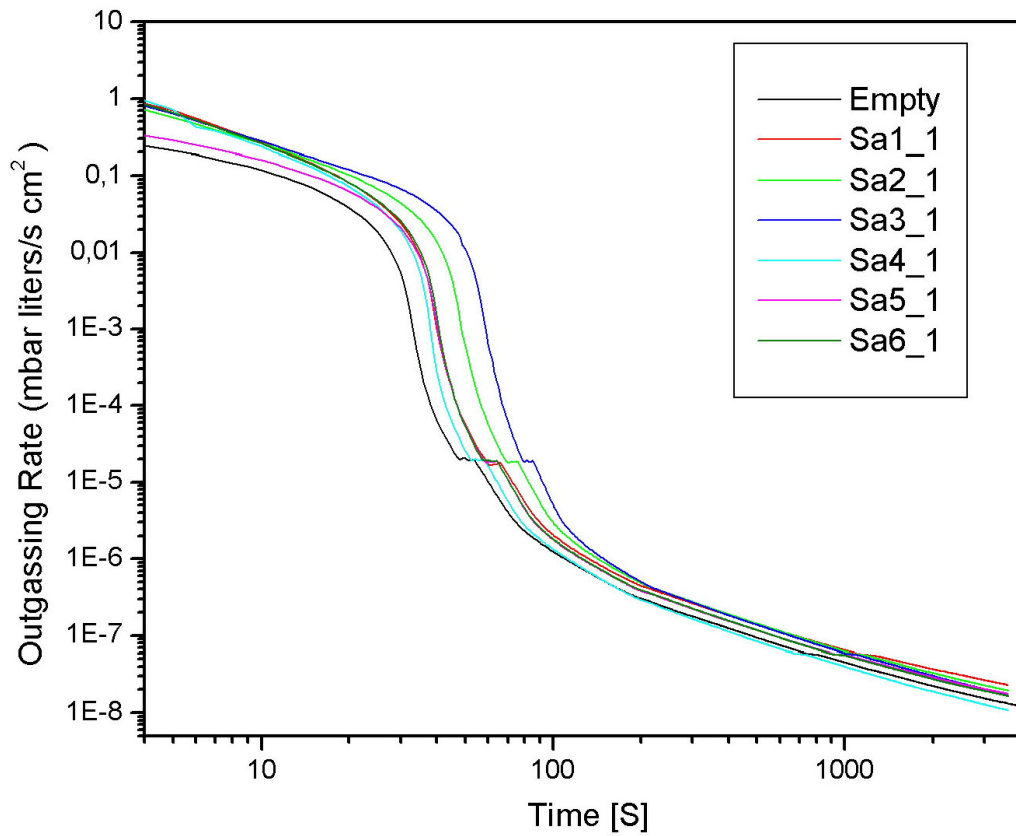


Fig. 2.4 Outgassing Rate of material A [A2017-T4]

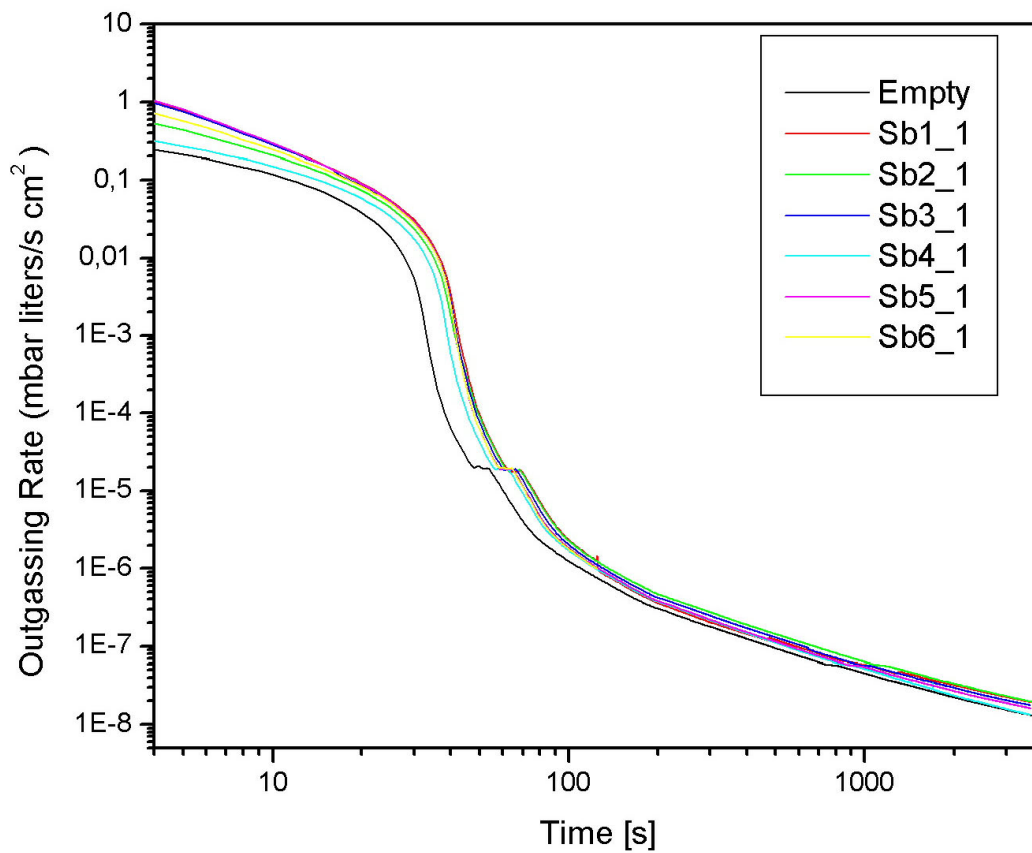


Fig. 2.5 Outgassing Rate of material B (A5353)

From the above results we can conclude that the different machining processes improve the outgassing rate of the material within a small range. Therefore further tests were used to improve the outgassing rate depending on the reduction of the passive porous oxide layer on the top surface of the workpiece. Therefore, alkaline pickling process was used in some samples to remove this passive porous oxide layer by immersing the workpiece in a solution of NaOH (1 mol) concentration for 30 minutes.

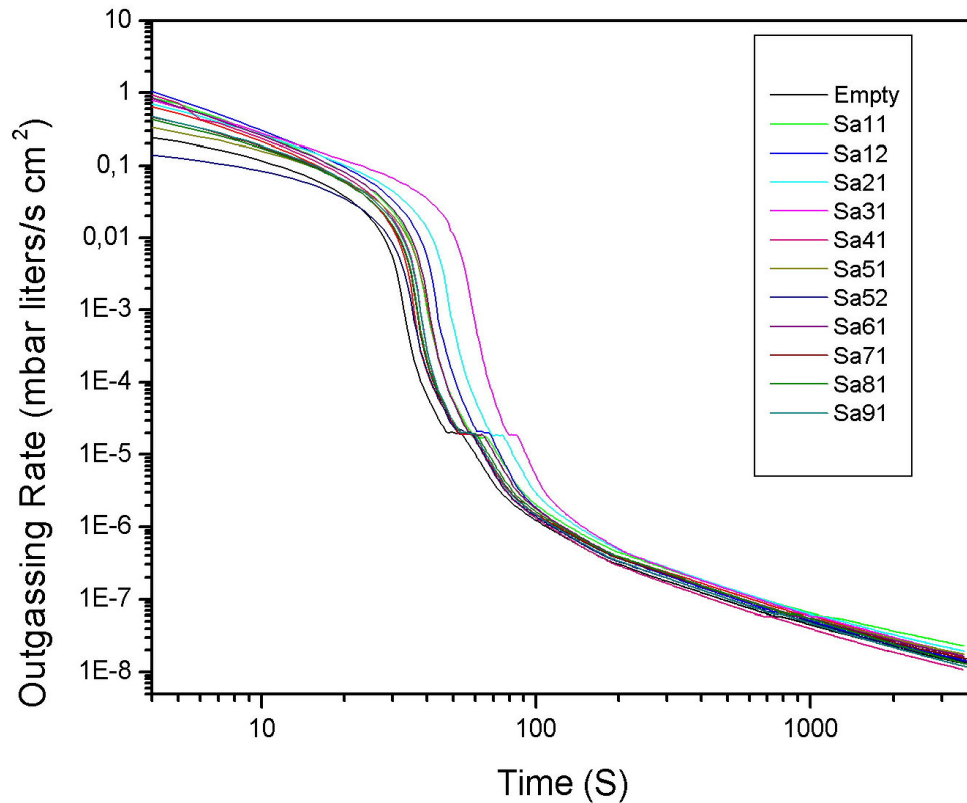


Fig. 2.6 Outgassing Rate of material A as described in Table III

The sample was cleaned with water and immersed in a solution with 38% concentration HNO₃. Fig.2.8 shows the current (indication of the passive porous oxide layer thickness) versus time for a sample treated by the alkaline pickling.

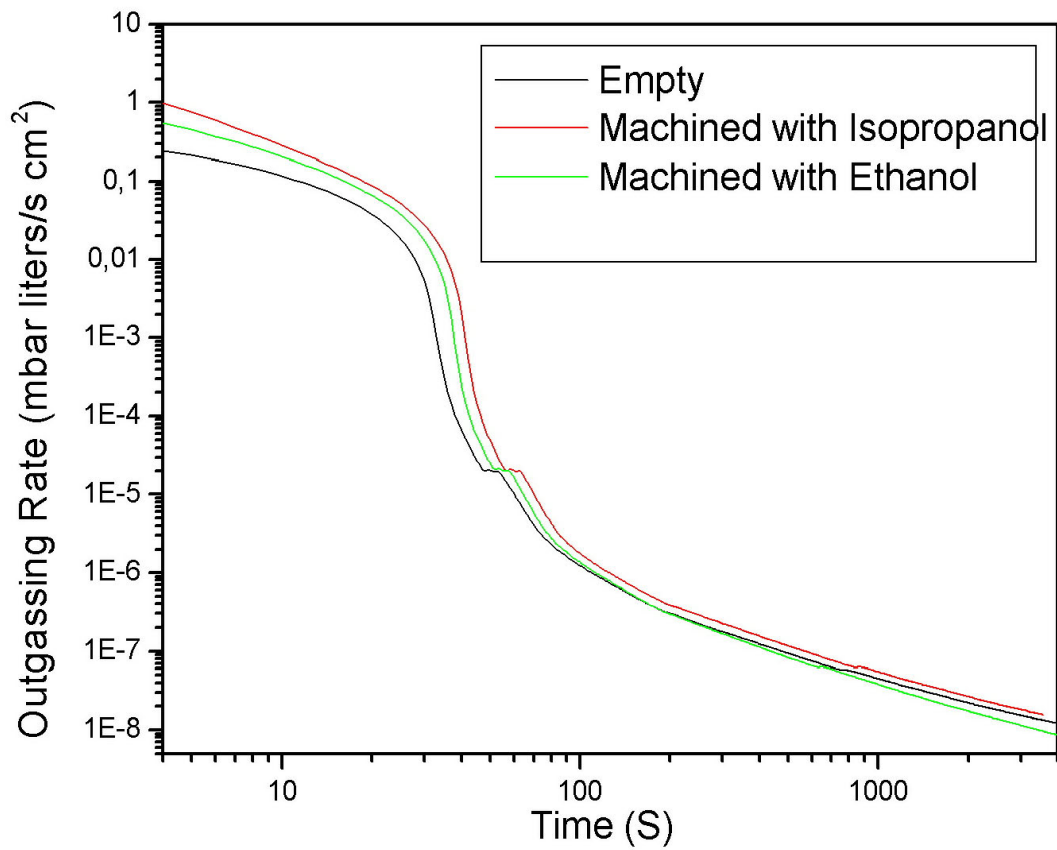


Fig. 2.7 Outgassing Rate of material C [A 6083]

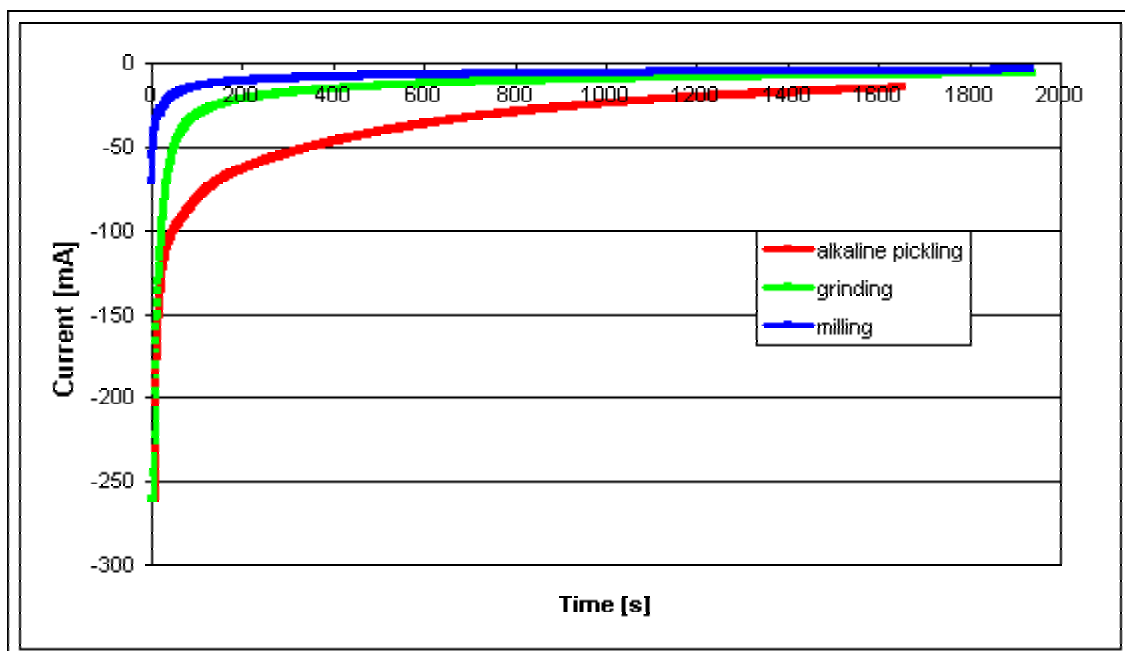


Fig.2.8 Porous oxide layer thickness for various machined samples as indicated by current versus time

One sample was grinded under ethanol as coolant fluid, and the second sample was normally milled.

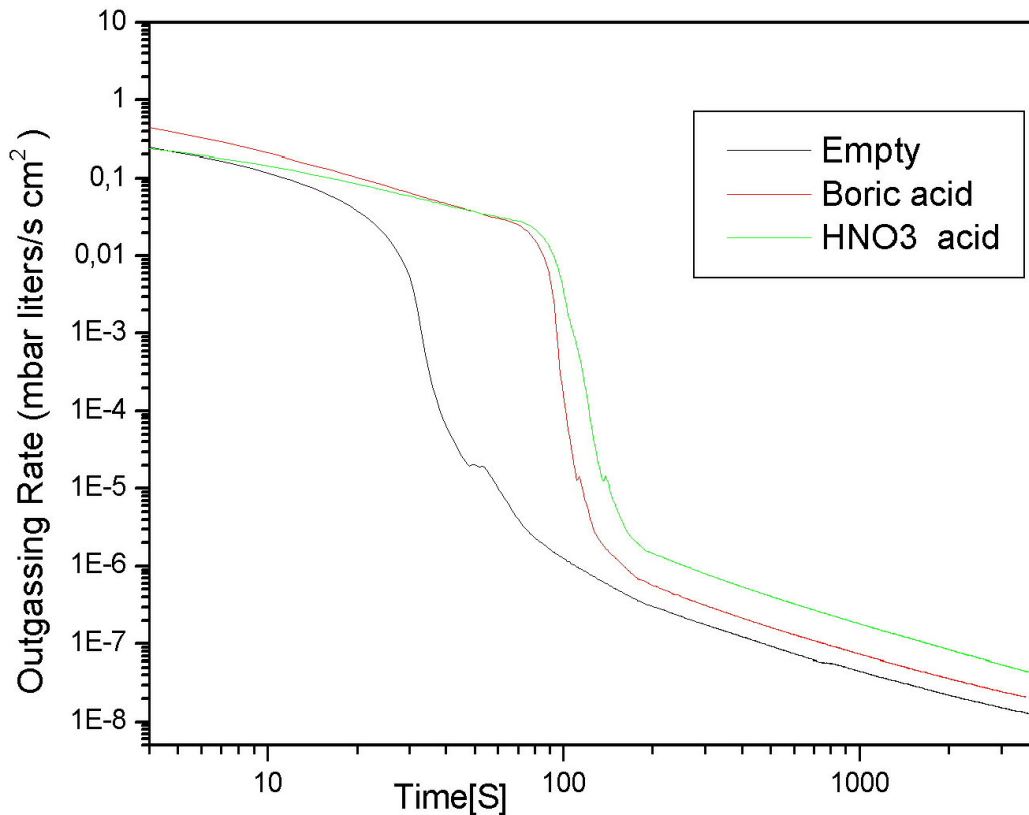


Fig. 2.9 Outgassing Rate comparison between anodizing acids with HNO₃ acid and Boric acid

As described above the pickling processes show a minimum oxide layer which means a low outgassing rate [11],[12],[14]. As a matter of fact another oxide layer could be developed on the fresh surface and influence again the outgassing rate of that surface. Therefore, the idea was to construct a thin non-porous oxide layer on the top of the pickled surface to protect it by an anodizing process. For the optimization of the anodizing process several tests were carried out. The influence of the anodizing acid, anodizing voltage, humidity effect on the outgassing of the anodized surfaces was investigated.

Fig. 2.9 shows the outgassing rate of two samples. One was anodized with HNO₃ acid 10% and the other with Boric acid 10%. It could be noted that the Boric acid shows better results. Another test was carried out to find the best voltage values which can be used in the anodizing process. Fig. 2.10 shows the outgassing rate of three different voltage values where the sample was tested after pickling and after anodizing with the required voltage as shown in Table IV. It could be noted that the voltage values of 100V and 30V have the lowest outgassing rates. (seen fig.2.11). The third anodizing test was the examination of the samples

2. Outgassing Test

under humid atmosphere to check if the anodizing of the surface produces a porous oxide layer. The samples from anodizing with 100V and 30V were tested in full humid atmosphere for 24 h. Fig. 2.12 shows the results compared with the results of the pickled sample.

The final conclusion from the above tests can be seen in Fig. 2.13. It is shown that the pickling process and the anodizing process with 30 V show the lowest outgassing rate. Consequently the surface of the required chamber will be pickled to remove the passive oxide layer. Afterwards a thin non-porous layer will be grown by anodizing with 30V using Boric acid.

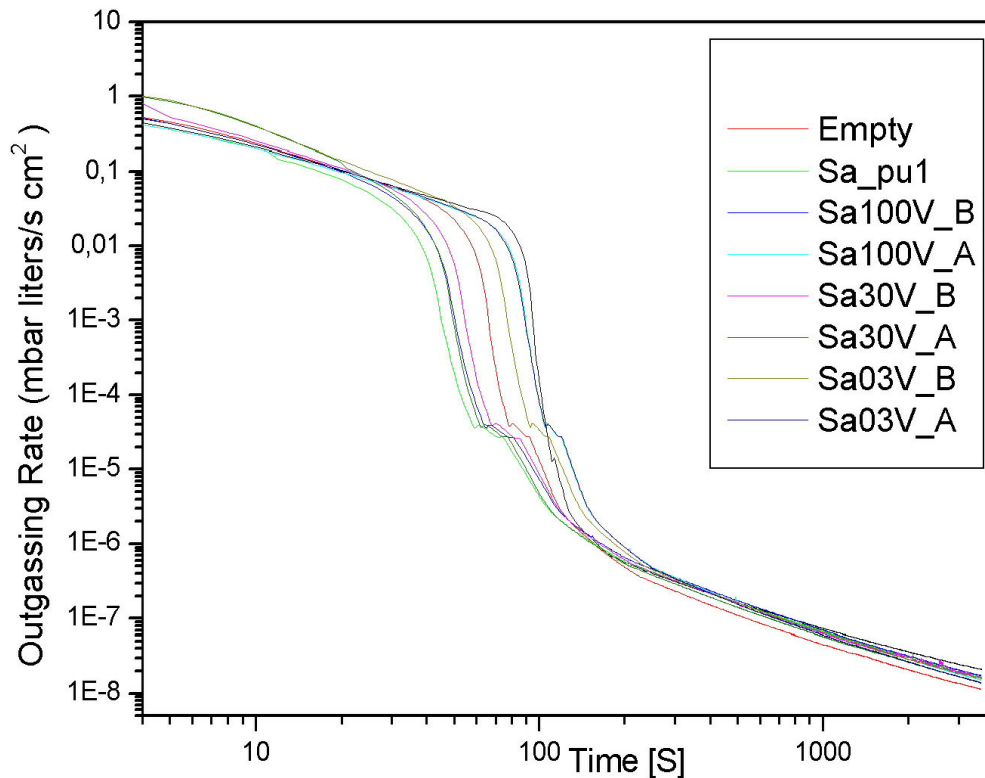


Fig. 2.10 Outgassing rate of material A pickled and anodized in Boric acid with various voltages

Table IV. Pickling and anodizing process for samples from material A

Sample Name	Surface treatment description
Sa_pu1	Sample pickled in NaOH (1 mol) concentration. Immersed in water, then in a HNO ₃ solution. Afterwards cleaned and dried by argon gas
Sa100V_B	Sample pickled in HNO ₃ acid 10% concentration, after that cleaned with water. Then cleaned and dried with argon gas
Sa100V_A	Same sample Sa100V_B was then anodized with 10% Boric acid and 100 Volts, after that cleaned with water. Then dried with argon gas
Sa30V_B	Sample pickled in HNO ₃ acid 10% concentration. Cleaned with water. Afterwards cleaned and dried with argon gas
Sa30V_A	Same sample Sa30V_B was then anodized with 10% Boric acid and 30 Volts. Cleaned with water. then dried with argon gas
Sa03V_B	Sample pickled in HNO ₃ acid 10% concentration. After that cleaned with water. then cleaned and dried with argon gas
Sa03V_A	Same sample Sa03V_B was then anodized with 10% Boric acid and 3 Volts. Then cleaned with water. Afterwards dried with argon gas

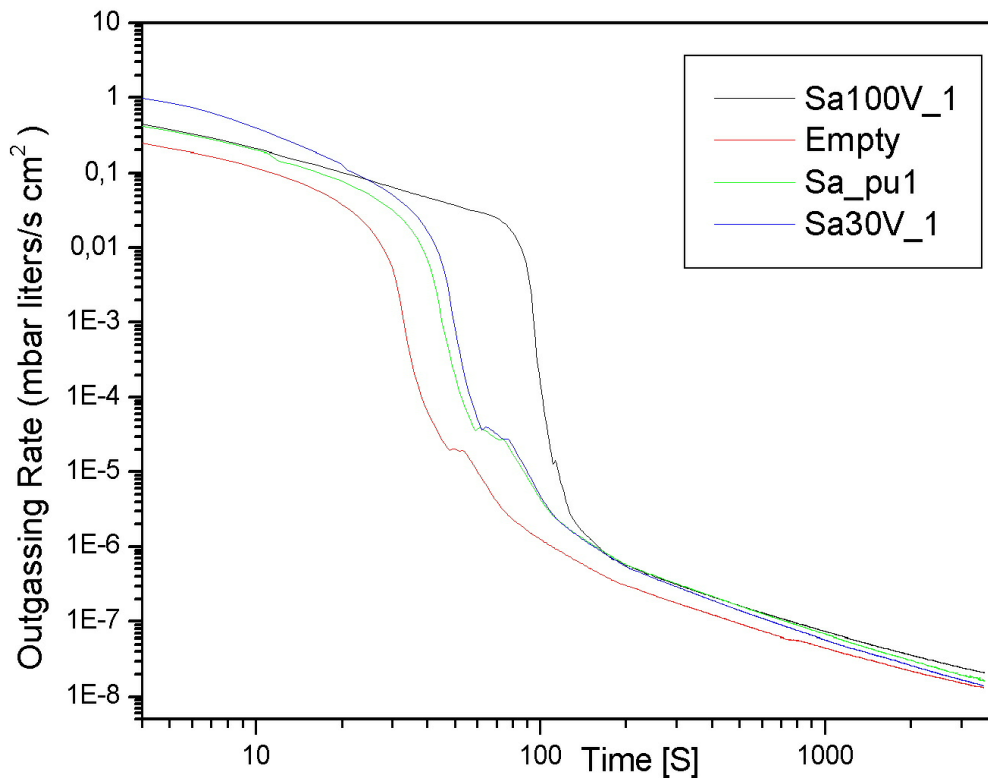


Fig. 2.11 Final comparison between the Outgassing Rates for the different tests of material A

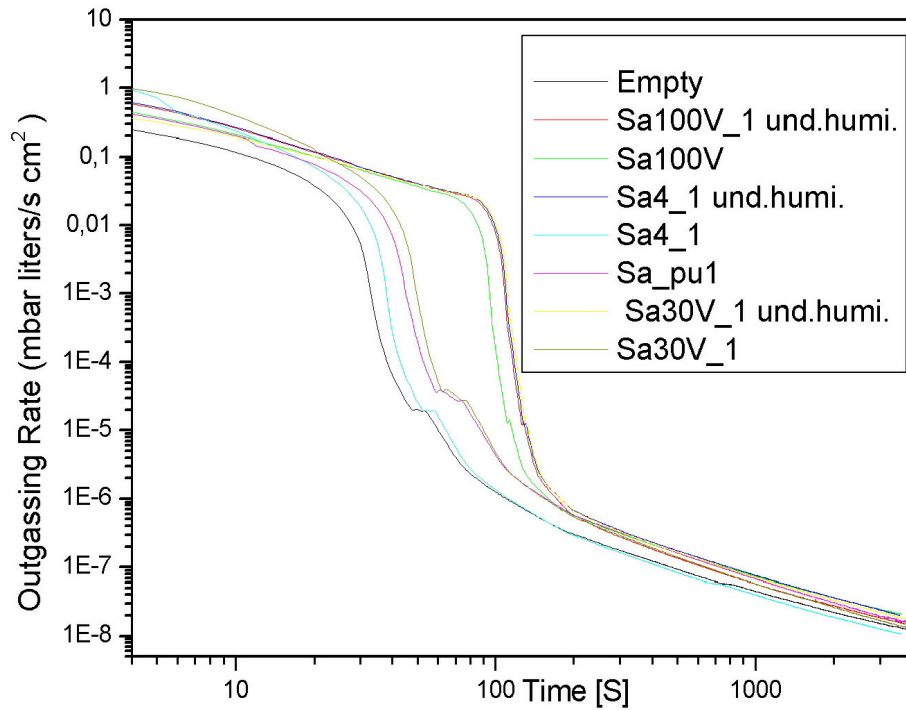


Fig. 2.12 Comparison of the lowest Outgassing Rate of material A under humid conditions

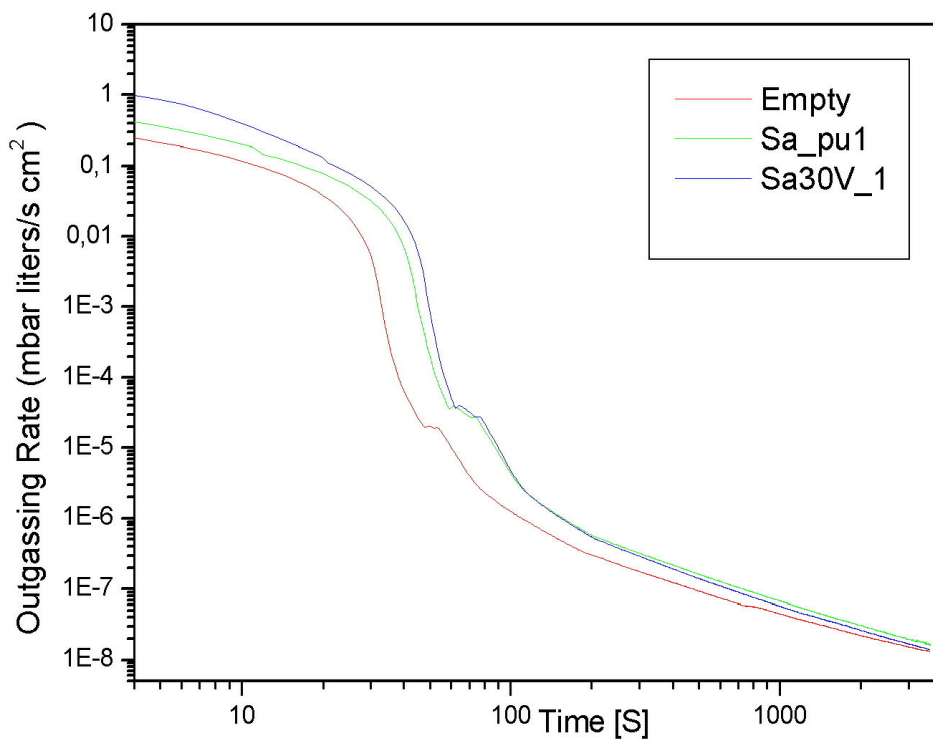


Fig. 3.13 Final comparison between the Outgassing Rate for the material A

2.7. Discussion and Conclusion

In this chapter the focus was on testing the short term (~ 1 hr.) outgassing rate of the selected aluminum alloy samples. The throughput method was used in the calculation of the outgassing rates of the samples, which can be described by equation [2.1]

$$Q = C * \Delta P / A \quad [2.1]$$

where A: Surface area [cm²]

C: Orifice conductance [l/s]

ΔP : Pressure difference between both sides of the orifice [mbar]

Q: Outgassing rate [mbar l/cm² s]

This method was used by [11],[12],[13] in the comparison between the different procedures used to optimize the outgassing rate of stainless steel and aluminum. It should be considered here that the focus of their tests has been on long test time (t >10 h.). Therefore its difficult to compare their results with ours. In Fig.2.3 we can see that both of the non machined samples show a 6 time higher rate of outgassing than the empty chamber. This is typical due to the contaminations of the surface with different components like oil, and because of the porous oxide layer on the top of the surface which acts as bulk reservoir for the absorbed materials. The indentation was to study the reduction of these effects by different treatments of the surface. Fig. 2.4 and Fig. 2.5 show the results of this surfaces as described in Table I and Table II. It can be seen that all these treatments were able to reduce the outgassing rate. A reduction of the outgassing rate of the sample which was machined under ethanol and baked in 100 C° for 1 hr. to nearly one order of magnitude was achieved. The improvement of the outgassing rate gives an indication about the influence of the top porous oxide layer on the outgassing rates that are measured. The comparison of the two figures shows that the outgassing rates in both materials are influenced by the surface treatment. It can be concluded that material A shows a lower outgassing rate in the short period of time, for that, it was selected for further testes. As shown in Fig. 2.6. some of the surface treatments which were carried out to the samples surface, increase the surface outgassing rate, while other treatments reduce the outgassing rate. Fig. 2.6 shows the results for the repetition test after one week. The samples have been stored in usual room conditions. Fig. 2.7 shows an outgassing test with samples from aluminum (A 6083) which is used commercially in the construction of

2. Outgassing Test

aluminum vacuum chambers. The samples showed low outgassing rates a factor of 2 worse than the empty chamber. This is a factor less than the best sample of material A.

As mentioned above all of the surface treatments done before have been done to improve the cleanliness of the surface, and to reduce the thickness of the porous oxide layers. Therefore, pickling process was done to some samples. This process was applied to remove the oxide layer as it can be seen in Fig. 2.8. A comparison between the thickness of the oxide layers of material machined under ethanol as cooling fluid is shown. The thickness of the oxide layer is indicated in the current. From this curves it can be seen that pickling process was the best way for the reduction and removing of the porous oxide layer. As a matter of fact another problem arises after removal of oxide layer. The surface is exposed to the atmosphere. The aluminum surface will react with oxygen and water to produce another porous oxide layer. Another test was carried out to produce a non-porous oxide layer on the top of the fresh surface by an anodizing process. Fig. 2.9 and fig. 2.10 show the outgassing rates of samples anodized under different voltages and with different acids. The conclusion from Fig. 2.10 is that the curves of anodizing with 30 volt shows lowest outgassing rates. The other curves show more or less similar results. Another test was selected to compare this anodized surfaces after exposure 1 week to full humid atmosphere (see Fig. 2.12) . Fig. 2.13 shows the final comparisons of the results of the samples that were pickled and anodized with Boric acid and anodizes at 30 volts.

Fig. 2.14 shows the residual gas analyzer (RGA) results of the empty chamber. Its obvious that the content of vapor water inside the chamber is more than 90%,. The remaining gases of the atmosphere in the chamber are (N_2 , H_2 , O_2 , CO). More or less the same results can be seen in Fig.2.15 which shows the RGA of the chamber, while the outgassing rate of the sample Sa30V_1 was measured. As a result, the same composition of gases were inside the chamber.

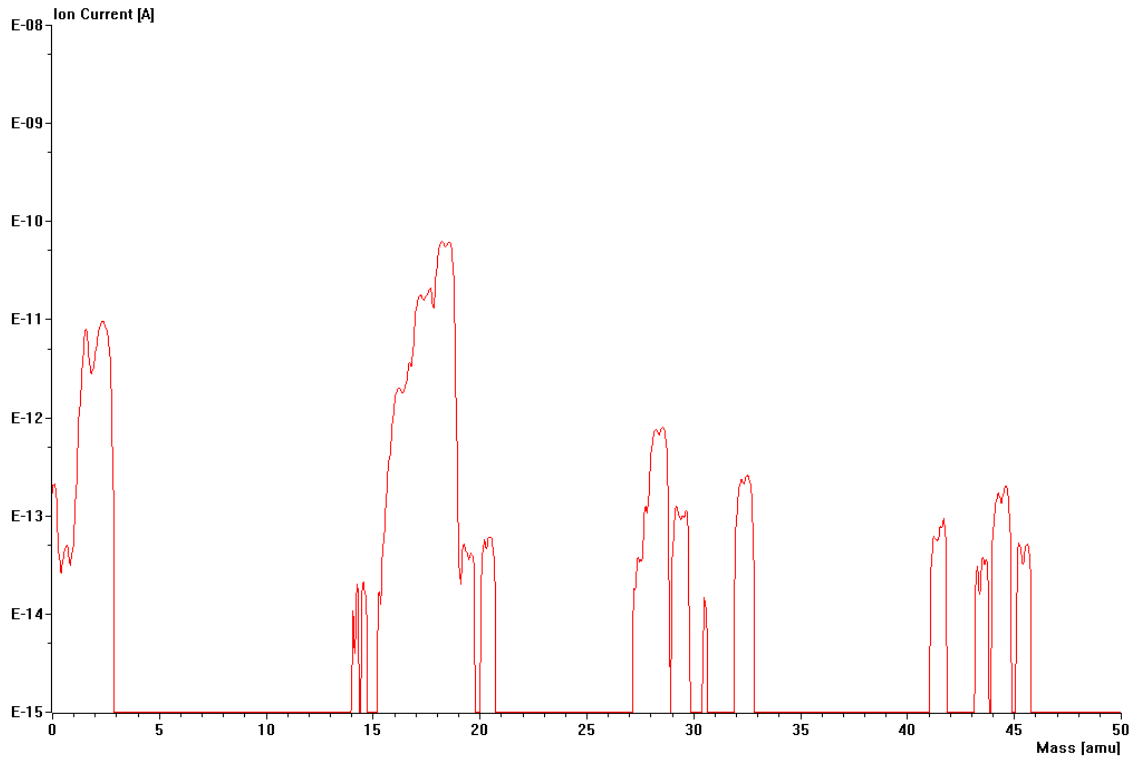


Fig. 2.14 Residual gas analyses (RGA) of an empty chamber

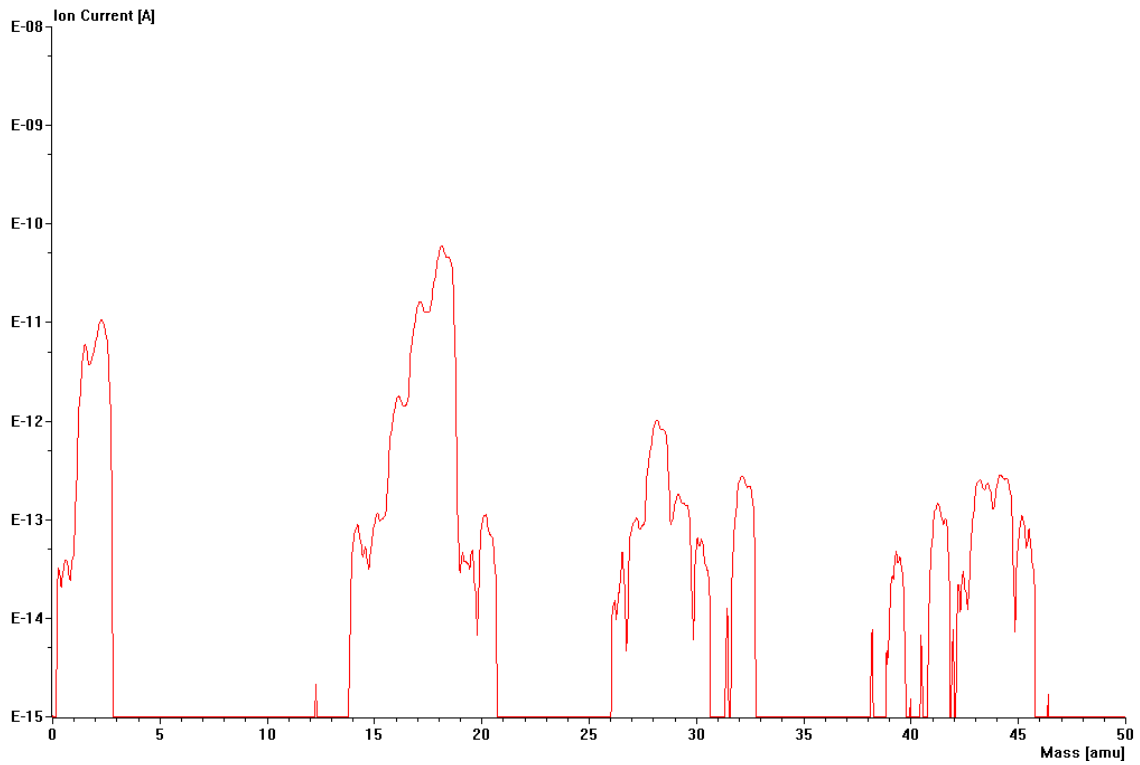


Fig. 2.15 Residual gas analyses (RGA) of sample Sa30V_1

2. Outgassing Test

As a result of the above it is clear that the reduction of the surface porous layer on top of the surface and the protection of it by producing another passive non-porous oxide layer using anodizing process (30 V, Boric acid) will protect the surface for longer time and will minimize the outgassing rate also if stored under humid atmosphere.

A basic comparison between the outgassing rates of the aluminum samples tested here and the results of tests done on aluminum and stainless steel [11-15] shows that the procedure was used here to treat the surface of the samples was able to minimize the outgassing rates to the same magnitude or even lower in short time test. This gives more push for the implementation of aluminum in the construction of vacuum systems.

3. VACUUM CHAMBER DESIGN

3.1. Introduction to Vacuum Chamber Design

In the last few years intense development in the thin film technology took place, not only in the development of new coating materials, but also in the optimization and construction of vacuum systems.[21-23]. The main focus in the department of precision engineering in the University of Kaiserslautern is the development of hard coating for mechanical applications. Therefore the construction of a new vacuum chamber that can fulfill the needs of depositing different hard coatings will be discussed in this chapter.

The vacuum chamber consist mainly of two aluminum rectangular chambers, where the aluminum plates are fixed together by aluminum screws and sealed together for vacuum tightness by epoxy glue. One of them as the pre-vacuum chamber to load the workpiece. This chamber is connected by a rectangular flange to the main chamber, and a self constricted gate can be controlled by a hand arm from outside. The main chamber contains three magnetrons so the sputtering process can be done for three different materials without braking the vacuum.

The main geometrical and mechanical construction, the glue test and selection, the pumping and evacuation system design, the workpiece transportation and the sputtering magnetrons design are tedious tasks in the vacuum chamber design will be discussed in this chapter.

3.2. Design and Mechanical Load Of The Chamber

3.2.1. Design Constraints

As described before the two chambers are connected mainly by a rectangular gate, each chamber consists of rectangular aluminum plates treated as described in chapter one, for cleaning and the reduction of the outgassing rates. They are screwed together by aluminum screws and glued together for the required vacuum sealing.

In the design of the chamber the following constraints were taken into account:

1. Mechanical stability under vacuum and temperature.
2. Optimization of the chamber dimensions to minimize the inner surface area that influences the vacuum conditions and the chamber pumping down speed.
3. Sputtering of three different materials without braking the vacuum with the possibility of transportation of the workpiece between the three different targets location and

from and to the pre-vacuum chamber without changing the vacuum conditions or opening the vacuum chamber.

4. Simple construction of the vacuum chamber and more flexible in the constructional conception of the inner gate, transportation and movement of the workpiece with the possibility of rotation to the workpiece to simplify the sputtering of bigger parts, also in the uniformity of the coating.
5. Achievement of high vacuum conditions and low outgassing and leak rates.
6. Simple construction.
7. Capability of baking the chamber from outside.
8. Liquid nitrogen cold traps.

3.2.2. Mechanical Properties of the Vacuum Chamber

A finite element model was used to study the mechanical stress of the rectangular vacuum chamber under uniformly distributed atmospheric pressure. Fig. 3.1 shows the schematic sketch of the deformation of a plate for a rough estimation of the deformations. The results of the finite element calculation of the deformations for the vacuum chamber are shown in Fig. 3.2. The calculations show that the maximum deformation in the weak section of the chamber does not exceed 0.5 mm. The calculation has been done for the total chamber profile, loading is uniformly distributed and is 0.1 N/mm^2 which corresponds to the pressure of one atmosphere. The internal pressure of the chamber is approximated by to be zero. As it can be seen from fig.3.2 the plate model shows maximum deformation. The other critical point is the angle of deflection that occur between the two connected plates. Therefore the screws were positioned in a distance of $1/3$ of the thickness of the plate from outside to minimize the deflection angle and reduce any shear or bending force that arises.

As it can be seen from above the vacuum chamber shows stability under the distributed load. The results give a possibility to investigate the sealing for the chamber for vacuum tightness.

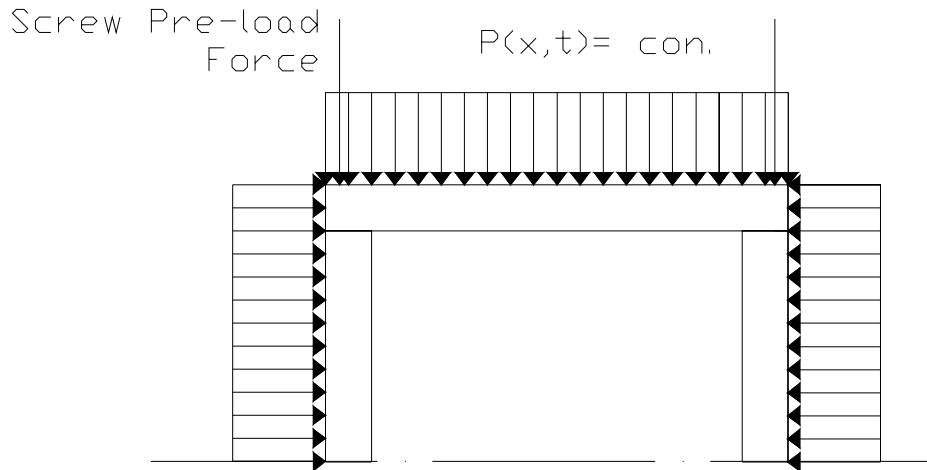


Fig. 3.1 Aluminum Plate Deformation Model

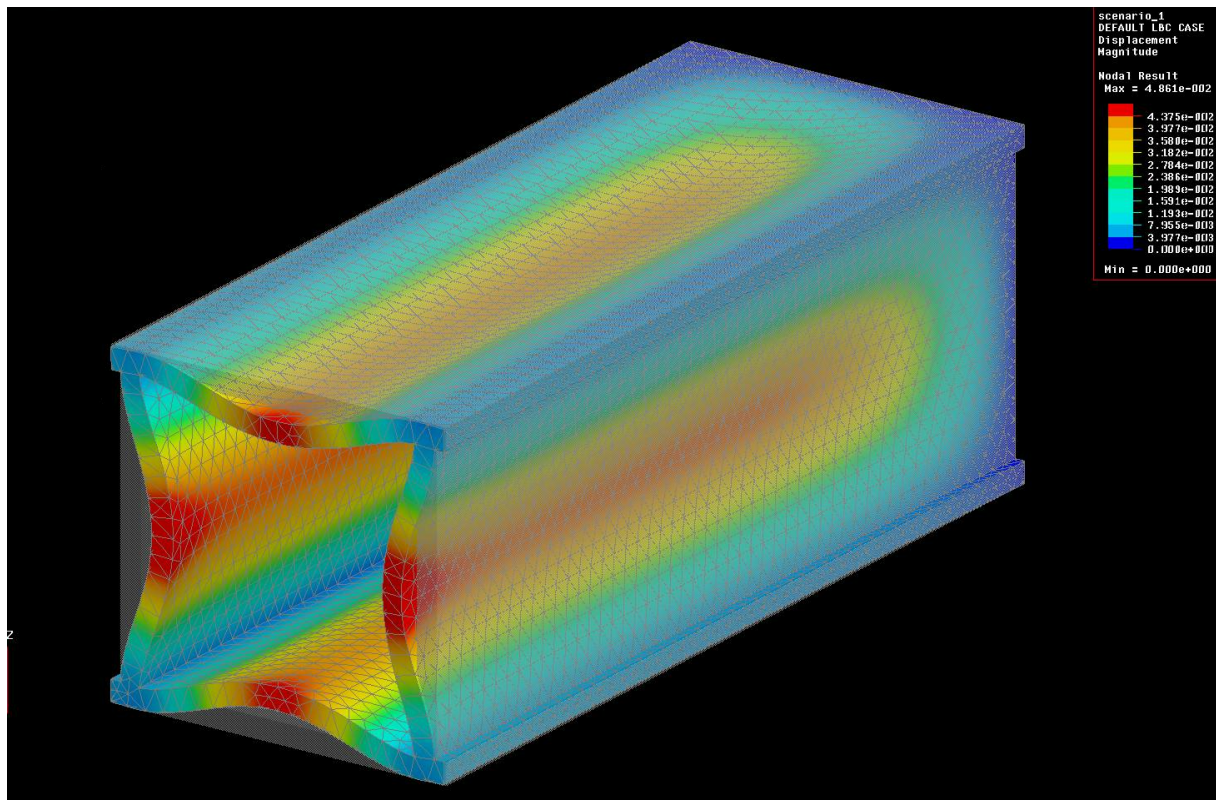


Fig. 3.2 Finite Element Deformation Model

3.3. Glue Selection and Tests

In the previous sections the finite element calculations for the deformation showed that the construction of the chamber could stand the mechanical loads. In this section a procedure for

3. Vacuum Chamber Design

the sealing of the chamber for vacuum application will be discussed. As a matter of fact welding the chamber from inside is the best choice for vacuum tight connections. Due to the special dimensions of the aluminum plates (25 mm thickness), and the dimension and shape of the vacuum chamber (1000×330×330) there was no possibility to weld the chamber together since the welding equipment need high current and also high temperature is produce during the welding process. For that reason the application of glue and adhesive material for the sealing of the chamber is used. Glue and adhesion material in general have a lot of characteristics and properties that make it suitable for sealing the chamber for vacuum tight [10],[24]. In general the selected glue should have the following properties.

1. Low viscosity that allows the bonding of small gaps with large areas.
2. Good vacuum characteristics, especially low outgassing rate and chemical and mechanical stability in the sense of low evaporating of gasses or other volatile material under vacuum and temperature.
3. Strong bonding and adhesion with aluminum and uniform distribution of stress in the bonding layer.
4. Low temperature for curing and high allowable operating temperature resistance especially for thin layers.

The first research was carried out to find a single component bonding glue, that should have low viscosity that should produce high capillary forces in the gap between the two aluminum plates. Therefore two aluminum plates (100×25×50) mm was fixed together with a gap of 20μm from one end sides between the two plates. The glue was applied to one side of the joints and the capillary force was able to block the gap between the two plates and suck the glue to the other side.

The above test procedure has been applied first to some single component glues, namely: Loctite product 480 (Cyanoacrylate adhesive), Loctite product 290 (anaerobic thread locking material), Loctite product 601 (single component anaerobic adhesive), Loctite product 603 (single component anaerobic adhesive), Figures, 3.3, 3.4, 3.5, 3.6 show photos of the (tested) sample plates with the various glues.



Fig. 3.3 Photo of The Aluminum Plates Bonded by the Loctite product 480 glue

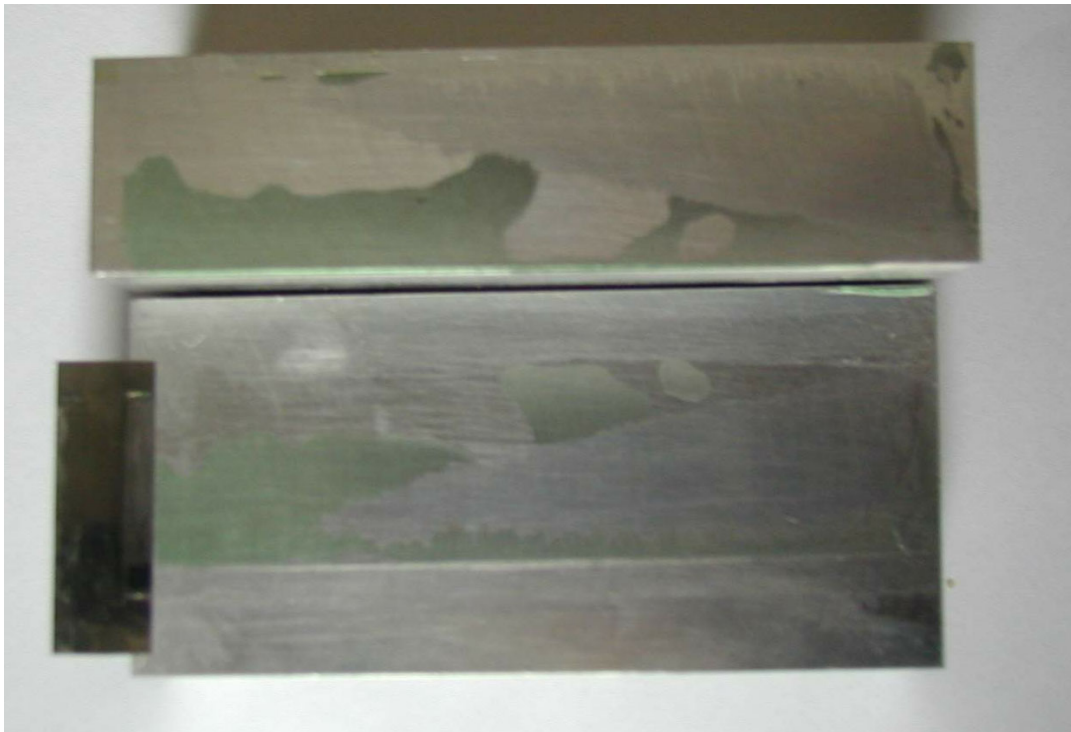


Fig. 3.4 Photo of The Aluminum Plates Bonded by the Loctite product 290 glue

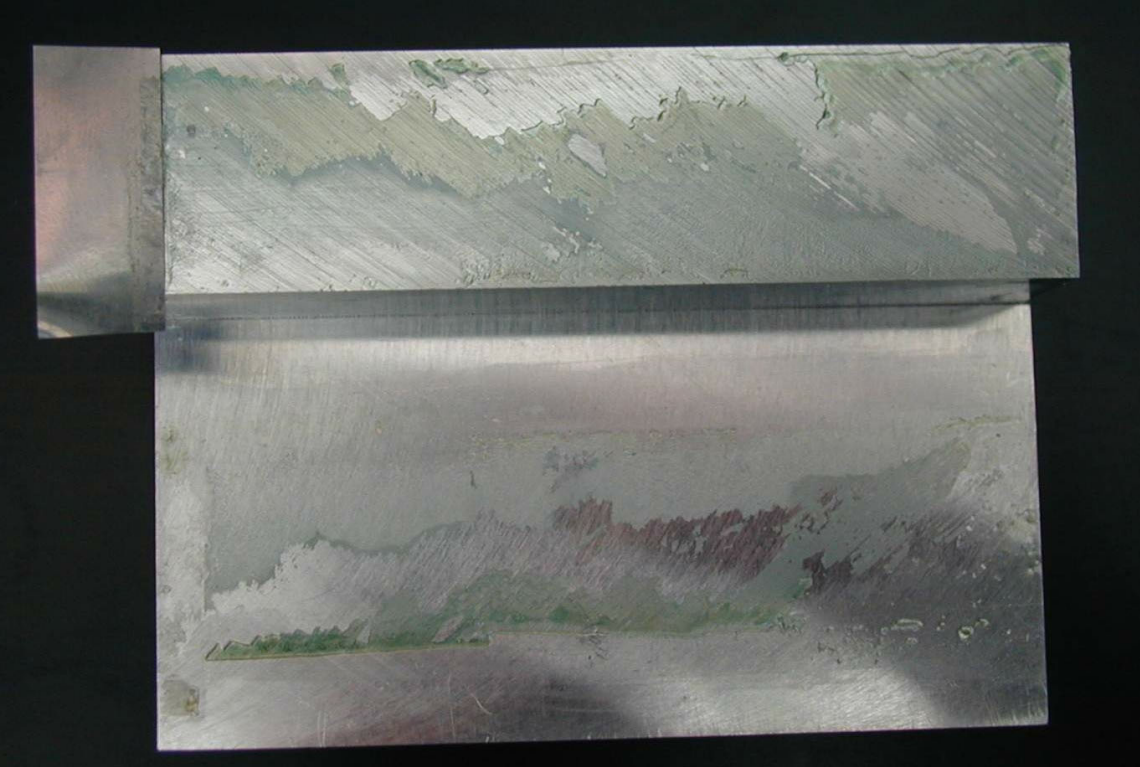


Fig. 3.5 Photo of The Aluminum Plates Bonded by the Loctite product 601 glue



Fig. 3.6 Photo of The Aluminum Plates Bonded by the Loctite product 603 glue

All of the above tested glues showed low viscosity with a sucking speed through the gap between the two aluminum plates faster than 0,5 m/s, and a uniform distribution of the glue in the gap area. In fig. 3.3, and fig. 3.5 both glues show a non uniform curing that left some of the glue not cured. Loctite 290 and 603 as shown in fig. 3.4 and fig. 3.6 show a better curing but not as sufficient as it is acceptable for vacuum applications. Another test was carried out to improve the curing of the last two glues by adding a surface activator (Loctite Activator 7649) to the surface of the aluminum plates. The goal is to promote the speed of cure. Fig. 3.7 and Fig. 3.8 show the results of the effect of that activator in the curing time of both glues. It is obvious that the activator is able to speed up the curing of both glues, but some non uniform cure and air bubble areas still exist which will effect the main object of the glue to seal the chamber. For this reason a search for another glue took place.

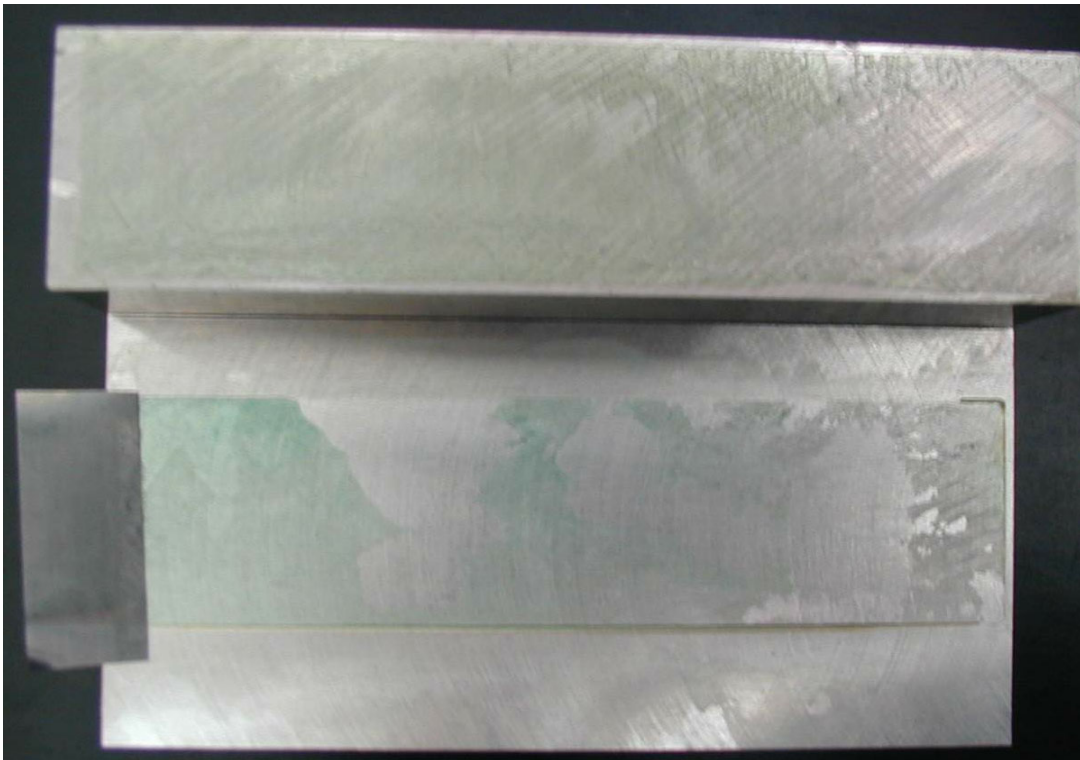


Fig. 3.7 Photo of The Aluminum Plates Bonded by the Loctite product 290 glue with the Loctite Activator 7649

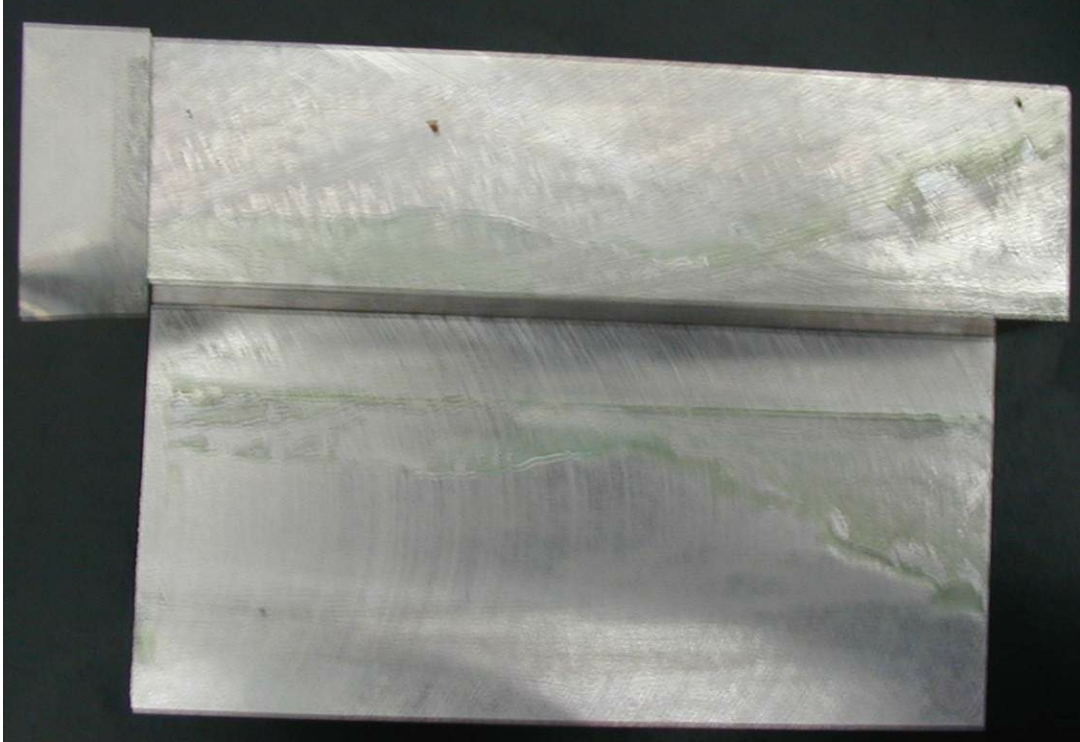


Fig. 3.8 Photo of The Aluminum Plates Bonded by the Loctite product 290 glue with the Loctite Activator 7649

Two component epoxy adhesives are used in a wide range of industrial applications for the bonding of aluminum parts [24-26]. Because of the high shear strength it can produce, and also for the high adhesion to aluminum surfaces it is a good choice. The properties of the epoxy in vacuum couldn't be found in the literature. Therefore three different types of epoxy namely Araldit LX 3505, Araldit LX 103, Araldit 2020 with low viscosity had to be tested in the same procedure as mentioned before for the sealing of the vacuum chamber.

Fig. 3.9 and Fig. 3.10 show the results from the two first epoxy glue, where both of them showed good curing, but poor uniformity of the bonding layer even if cured at room temperature (21 C°). Fig. 3.11 shows the Araldit 2020 epoxy. First a higher uniformity of the glue thickness in the gap between the two plates, and high capillary force can be observed. Furthermore it is able to produce a surface free from air bubbles, also if it is cured at room temperature.

Other tests were made with this epoxy to test its properties. The above tests have been repeated with the modification of leaving the samples for 5 minutes at room temperature. After curing at different temperatures (60 C°, 80 C°) for 3 hours, the epoxy showed good and uniform curing. A further test for the selection of glue is shown in Fig. 3.12. The outgassing rate test for (30×30×25) mm aluminum plate coated with a 20 μm layer of epoxy glue, was

carried out using the same outgassing test stand and test conditions described in section 2.5. It was cured at 60 C° for 3 hour. It can be seen that the epoxy showed low outgassing rate that made it suitable to be used in vacuum applications.

As a result from all the above tests with different glues, the epoxy Araldit 2020 was selected for filling the gaps between the aluminum plates in the designed vacuum chamber.

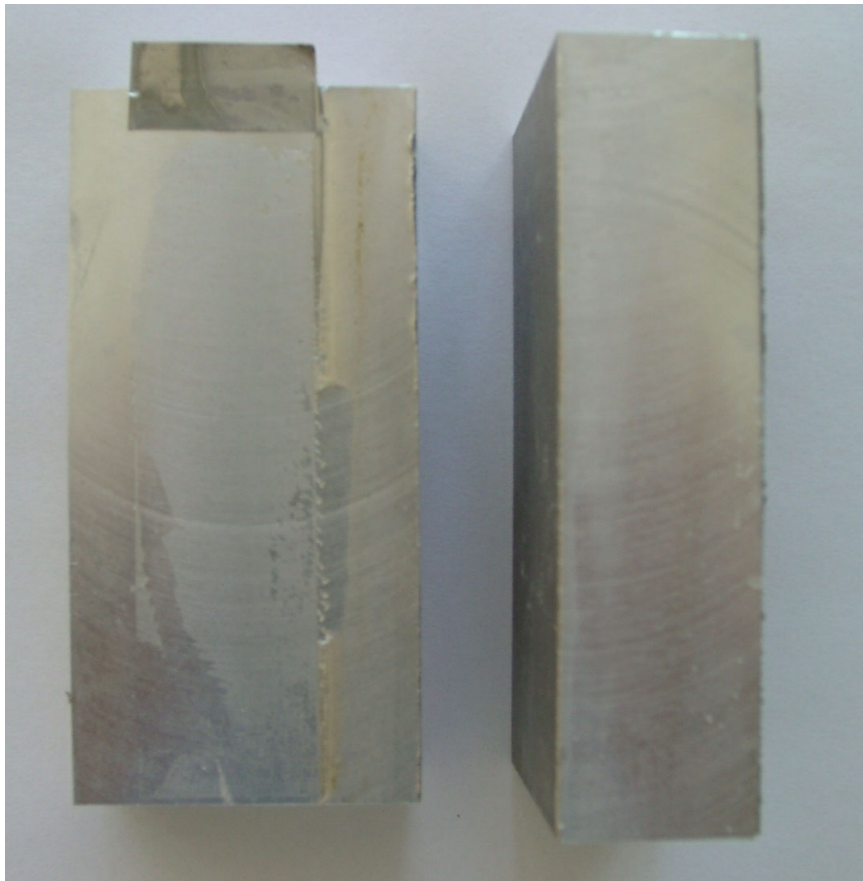


Fig. 3.9 Photo of the Aluminum plates bonded by the Araldit LX 3505 glue



Fig. 3.10 Photo of the aluminum plates bonded by the Araldit LX 3505 glue



Fig. 3.11 Photo of the aluminum plates bonded by the Araldit 2020 glue

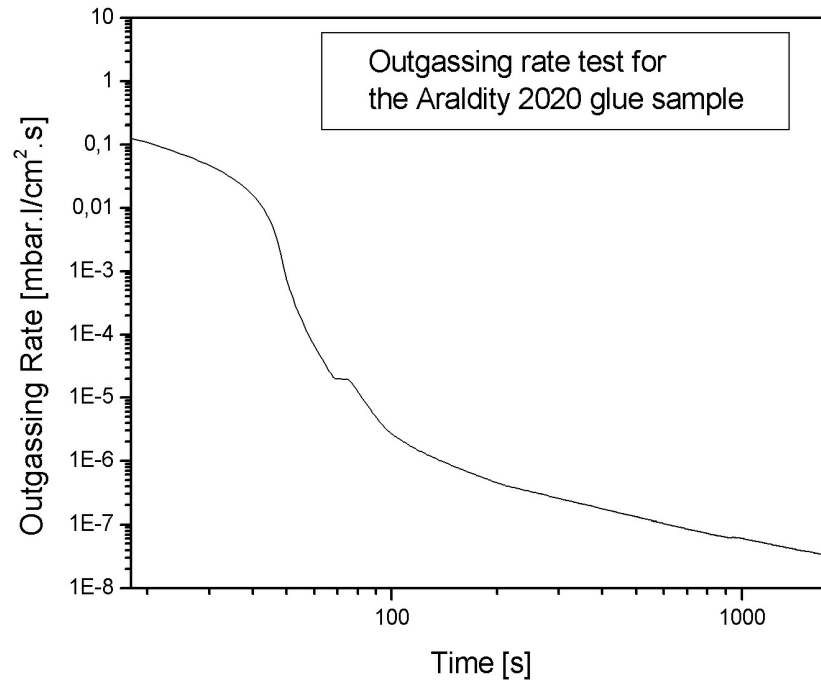


Fig. 3.12 Outgassing Rate for a 20µm thickness layer from the Araldit 2020 glue developed on a (30×30×25) mm aluminum plate sample, tested using the same outgassing test stand and conditions described in section 2.5

3.4. Workpiece Transportation System

Simple and easy movement of the workpiece not only between the two chambers but also between the different magnetron positions inside the main chamber was one of the hardest tasks in the construction and design of the vacuum chamber where the following conditions should be fulfilled:

1. Simple light weight construction, that is applicable to vacuum conditions, especially with low outgassing rates.
2. Movement of the workpiece between the two chambers through the inner gate without the need to change the vacuum conditions, especially for the electrical motor connections.
3. Simple assembly inside the chamber.
4. Simple clamping and fixing of the workpiece. Possibility of rotation of the workpiece to get uniform surface coatings for large parts.

The final design of the transportation system consists of two main cars connected together by an electrical coupling magnet, and a contact points matching box for the connection of electrical power and control signals to the motor in the second car which holds the workpiece.

The main job of the first car is to transport the second car between the different positions of the targets inside the main chamber and through the inner gate to the pre-vacuum chamber. The electrical and control signals for the motor in the second car are transmitted from the first car by the contact points of the matching box. By control of that motor it is possible to adjust the distance between the workpiece and the target, also to rotate the workpiece during the sputtering process to improve the uniformity of the deposited films in large surfaces.

In the pre-vacuum chamber the railway is designed to slide to a fixed railway by a step motor. So it is possible to slide it through the open inner gate to meet the fixed railway inside the main chamber. Then it is possible for the driving car to push the car holding the workpiece through that railway. The car drive back the sliding railway of the pre-vacuum chamber and so its possible again to close the inner gate. All of the three used motors were step motors that are controlled from the outside by a control card connected to a computer. The electrical connections to these motors were realized through a 16 pin feed through ceramic flange connected to one of the chamber flanges. Ball bearings where used as wheels in the used cars. These ball bearings are degreased and use nitride balls and steel rings

3.5. Assembly of the Chamber

The rectangular plates of the two chambers were cut to the required dimensions plus one millimeter as machining tolerance. The following steps were carried out for that plates:

1. The plates where annealed in an oven at 150 C°, then the oven was switched off. The plates cooled down slowly to relay the internal stresses.
2. The plates where machined to the right dimensions and shape. Afterwards they are cleaned with Acetone.
3. Pickling and anodizing process where done to the plates in the same conditions as described in chapter two.
4. The chamber was built to its rectangular shape and screws. The aluminum screws where fixed and pre-loaded with 90% of the required pre-load on each screw and 20µm step steel sheets were put between each two plates to fix the gap between each two plates.
5. The Araldit 2020 epoxy glue was applied to the four contact lines of the plates inside the chamber. After 20 minutes a hot air heater was inserted into the chamber, so the chamber reached a temperature of 60 C° for 12 hour.

6. A uniform thin layer of epoxy glue was applied to both end sides of the chamber. This was done by gluing each end side to a stainless steel plate wetted with water solvent soap. After removal of the stainless steel plates a highly polished surface for the O-ring sealing is resulting
7. The full pre-load force were applied to each screw in the chamber. Both chambers where connected together by screws through the connected flange, where a viton O-ring was fixed between both chambers.
8. The inner gate, the transportation system, the turbo molecular pump, the windows, and the door have been assembled.
9. From outside many electrical resistances are glued to the outer surface of both chambers for baking of the chamber to improve its pumping down characteristics. It should be mentioned here that the thin epoxy glue layer work as an insulation layer for the movement of heat between the connected plates. The aluminum screws showed a good conduction for the heat transformation. Heating is regulated by applied voltage and currents

Fig. 3.13 showed a computer model of the vacuum chamber and its main parts, the pre-vacuum chamber, the main chamber, the unbalanced sputtering magnetrons, the turbo molecular pump and the inner rectangular gate

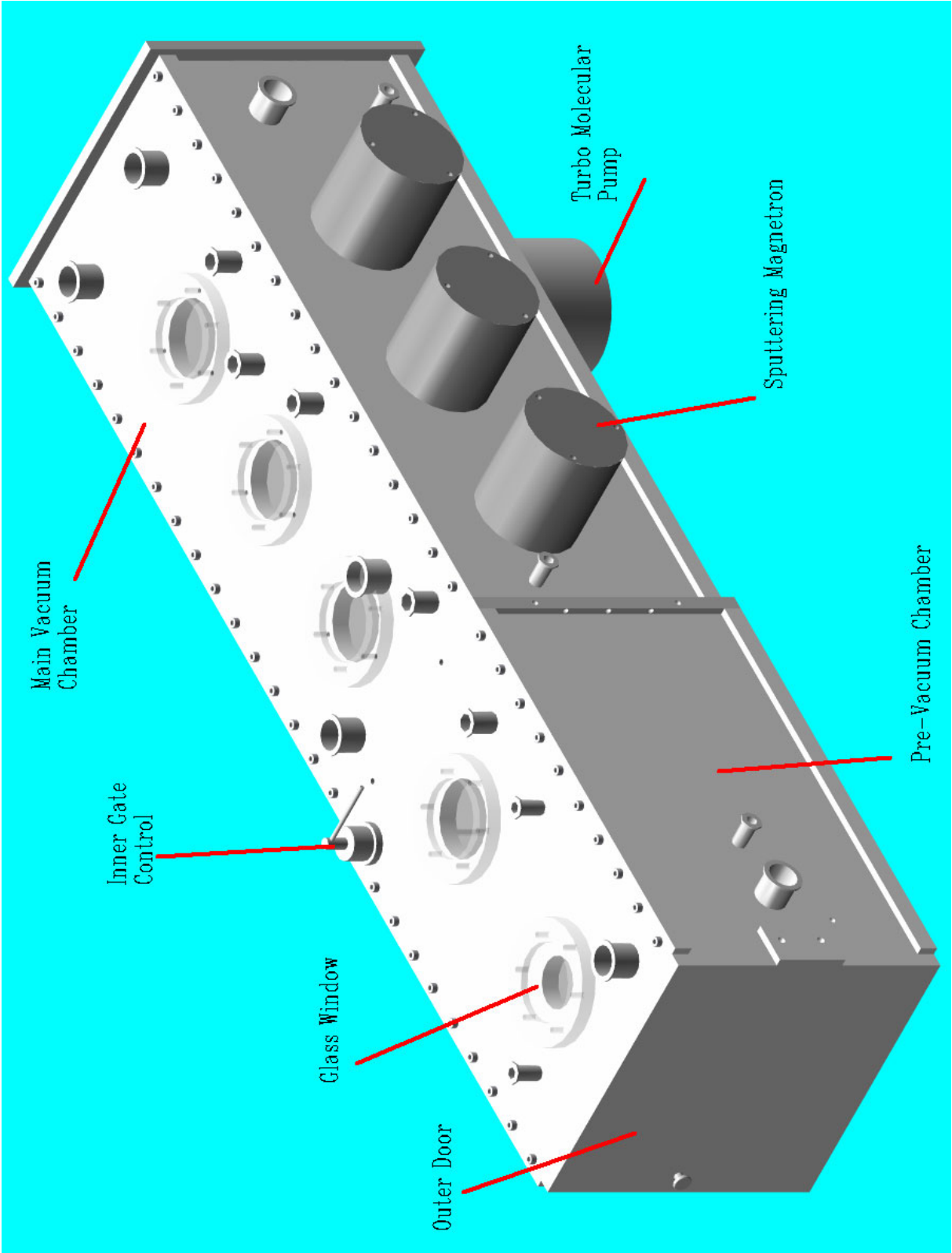


Fig. 3.13 The constructed vacuum chamber

3.6. Pumping System

The main chamber with 1.43 m² inner surface area was pumped down by a (450 l/s) turbo molecular pump connected directly to the base of the main chamber by a KF 180 flange sealed with a viton O-ring. The exit of the turbo molecular pump was connected to a (200 l/s) single stage rotary vane pump through a valve. The pre-vacuum chamber with 0,96 m² inner surface area was connected to a (300 l/s) single rotary vane pump through a valve.

Since the main residual gases inside the chamber is water vapor as proofed in chapter one, a simple liquid nitrogen trap was designed to freeze the water vapor inside the chamber and improve the pumping down of the chamber. Fig. 3.14 shows one of the used traps.

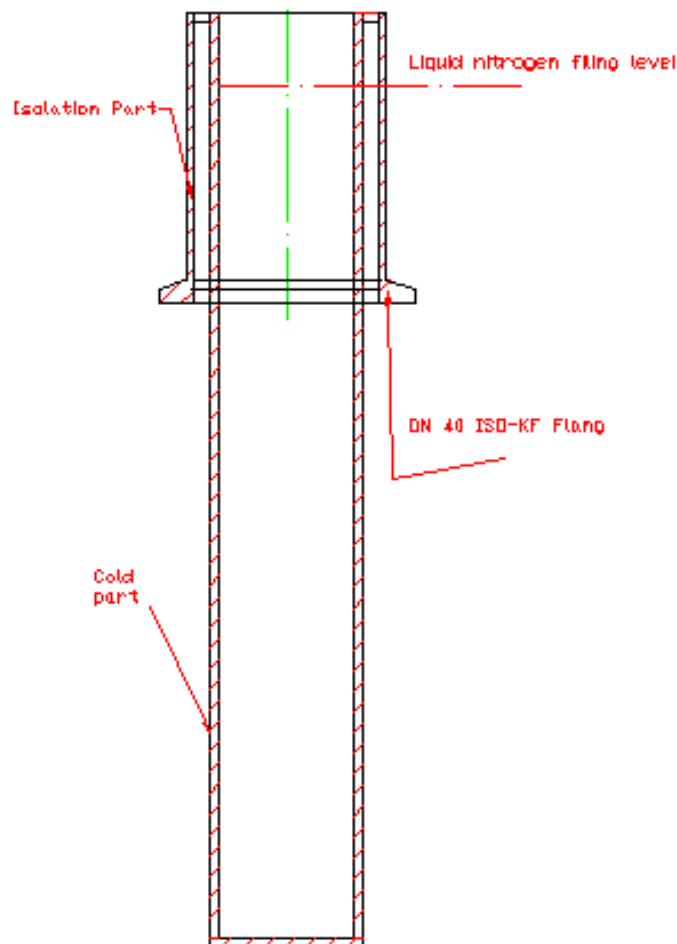


Fig. 3.14 Liquid Nitrogen trap (Stainless Steel)

3.7. DC-Sputtering Magnetron

DC sputtering magnetrons are one good choice for coating. A magnetic field, electrical power with high voltage, water cooling and vacuum sealing are accesspal. In recent years in our

3. Vacuum Chamber Design

department designed and constructed an unbalanced magnetron[27]. The same construction was taken and some modifications and changes in the design of some parts were done to improve its performance especially with respect of the water cooling system. Fig. 3.15 shows an evacuation curve for the main chamber versus time. From this curve it's clear that a good low pressure of range 1×10^{-6} mbar can be achieved within one hour of pumping down without baking of the chamber. This is usually accepted in the process of deposition thin film coating in sputtering process (PVD).

As a result from all the above work it was possible to construct a vacuum chamber that fulfill the main conditions and constraints mentioned before. Especially the short pumping down time and also the low outgassing and leak rates, make it now possible to deposit several thin film from different materials. This gives the possibility to carry out experiments under different test conditions. The rectangular shape and the design of the vacuum chamber make it possible for us to reduce the contamination that can reach the workpiece surface.

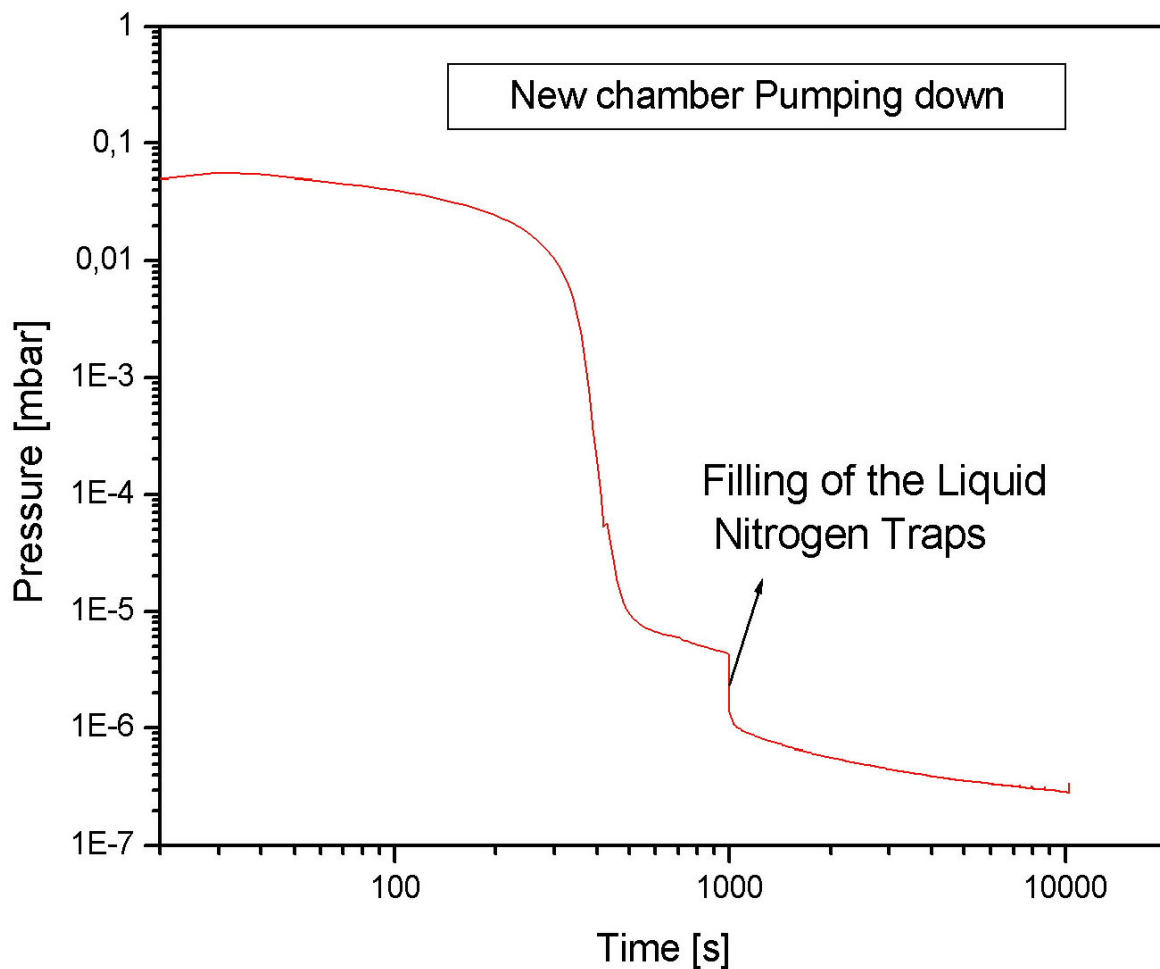


Fig. 3.15 Pumping down curve of the vacuum chamber

4. DEPOSITION OF NANOCOMPOSITE (TI, SI, AL)N COATINGS

4.1. Introduction to Sputtering Process

The deposition of hard coating materials using the PVD magnetron sputtering deposition has gained a high share within coating techniques due to its universal applicability. With this technology hard coatings for cutting tools, wear resistance, high friction contact surfaces, and many others mechanical applications are made.

Different methods and materials are used to produce this hard coatings now a days[28], such as single layer coating, multilayers coating, and the two phase nanocrystal amorphous coating like nc- $(Ti_{1-x} Al_x) N/a-Si_3N_4$ [29].

The constructed vacuum chamber and magnetrons were used in different experiments to sputter different thin layers of TiN, AlSiN with different thickness and composition. The hardness and the chemical composition of the coated samples were tested before and after annealing at 600 °C for one hour using the Vickers hardness test and the SNMS.

In this chapter the sputtering process types and mechanism's, hard coatings types and applications, multilayers coatings properties, used experiment procedure, and the samples tests and results are topics will be discussed.

4.2. Sputtering Process

4.2.1. Sputtering Mechanisms

Sputtering is an atomic process that use a glow discharge to generate a flux of ions incident on the target surface. These ions cause atoms, and occasionally clusters of atoms, to be knocked free from the target surface by momentum transfer. In the energy range most relevant to sputter deposition, the interaction and subsequent interactions, can be treated as a series of binary collisions. The sputtering process is very often compared to the break in a game of atomic billiards (see fig. 4.1) in which the cue ball (bombarding ion) strikes the nearly arranged pack (the atomic array of the target), scattering balls (target atoms) in all directions, including some back out of the target surface. In the real process, the inter atomic potential or function (the variation of inter atomic repulsion or attraction with separation distance) is rather different from the hard sphere billiard case. Ions are normally used as incident particles since they can easily be accelerated by an electrical field, where as neutrals pose a problem in

this respect. Furthermore, the ions are likely to be neutralized by the auger emission of an electron from the target as the ion approaches, so that the impacting species are actually mostly neutral. When an ion strikes the cathode (the target), along with the generation of heat and the removal of neutral (sputtered) atoms there is about a 5-10 % probability of secondary electron emission. Emitted secondary electrons are then accelerated back into the negative glow region [6]. In this region the electrons expend most of their energy creating additional ions and generating a cold cathode discharge.

The magnetic field is designed to prevent charge of the electrons from this region. The cooling system is designed to remove the heat from the target.

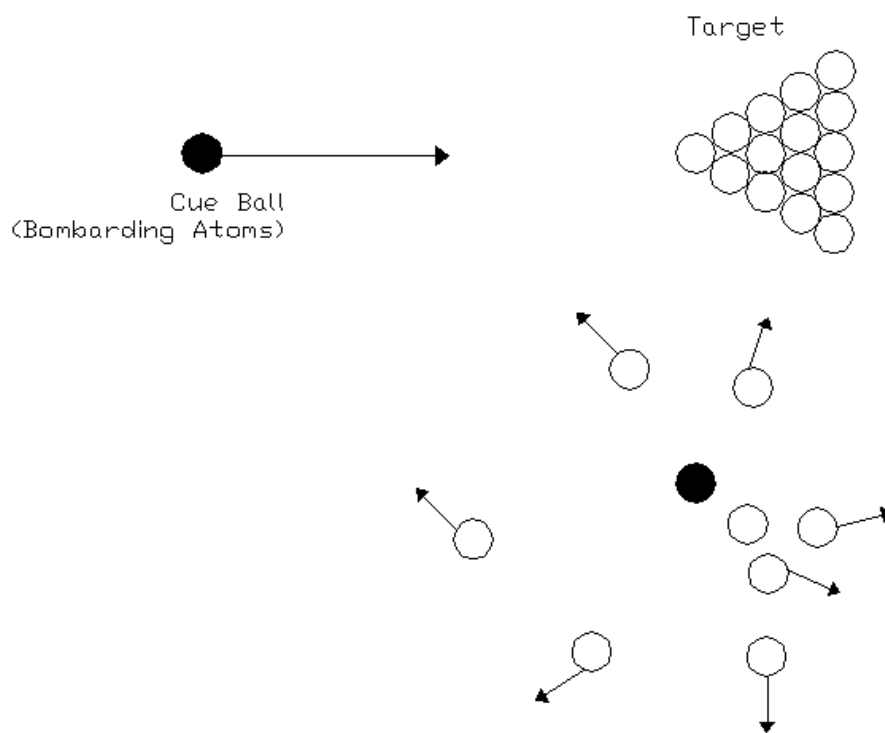


Fig. 4.1 sputtering the atomic billiards game [6]

4.2.2. Interactions of Ion Approached the Surface of a Target

When an ion approached the surface of a target one or all of the following phenomena may occur.(see fig. 4.2)

1. The ion impact setting a series of collisions between atoms of the target, leading to the ejection of one or less than one per collision of these atoms. This ejection process is known as sputtering. The sputtering yield is in the regent of 0.05-1 atom/collision
2. The ion will neutralized if reaching the target and rejected.

3. The impact of the ion may cause the target to eject an electron, usually referred to as a secondary electron
4. The ion may become buried into the target (ion implantation), this process will soon saturate
5. The ion impact may also be responsible for some structural rearrangements in the target materials.

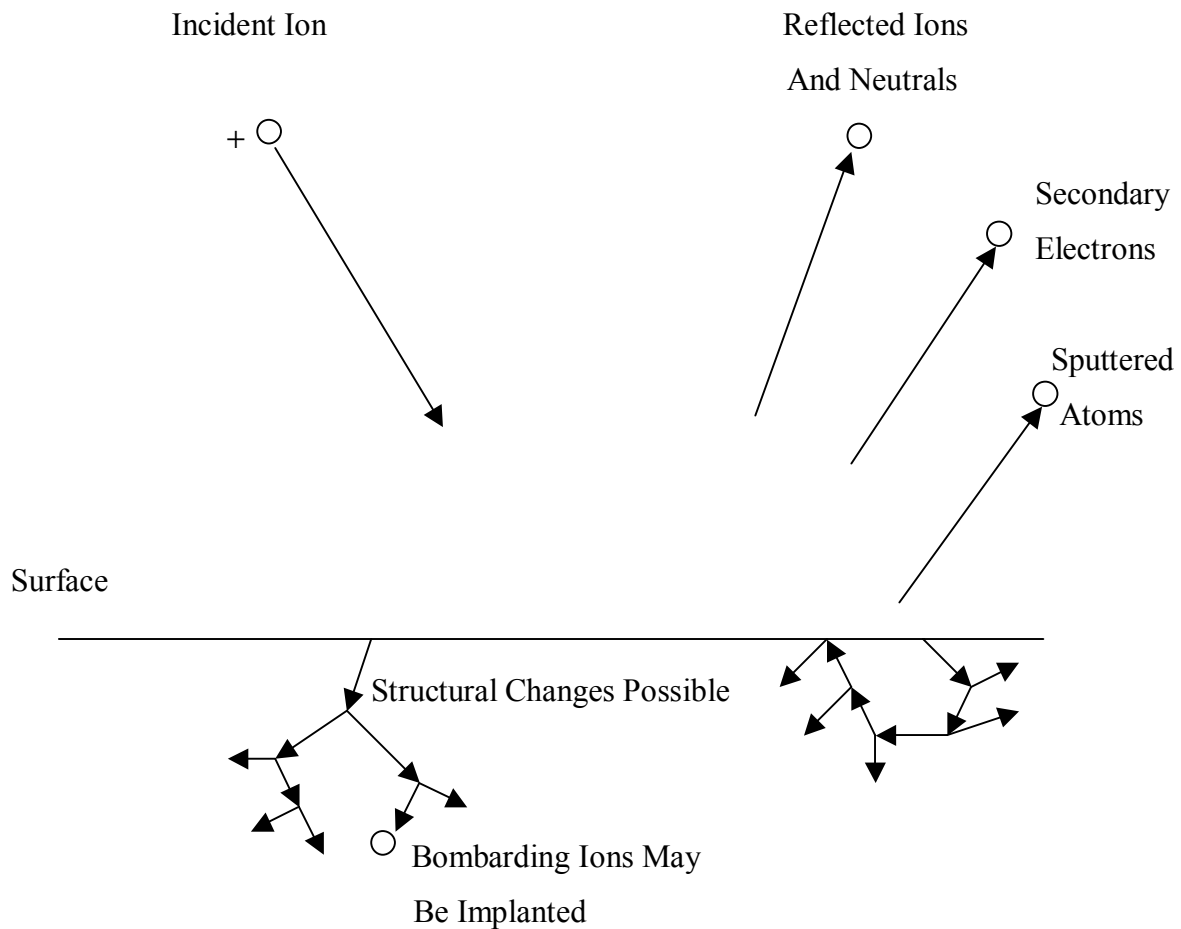


Fig. 4.2 Interactions of ions with surfaces [6]

4.2.3. Sputtering Advantages

Some of the unique characteristics of sputtering that are considered in evaluation of this coating method are the following [30]:

1. Thickness uniformity of the deposited coating
2. Deposition of refractory materials

3. Deposition of insulating films
4. Large area targets
5. No spitting, as in the thermal evaporation (problem of the ejection of particles from sources during evaporation)
6. No droplet formation, as in arc deposition.
7. Long life time of sputtering target compared with others evaporation methods
8. Simple of sputtering alloys and other complicated materials

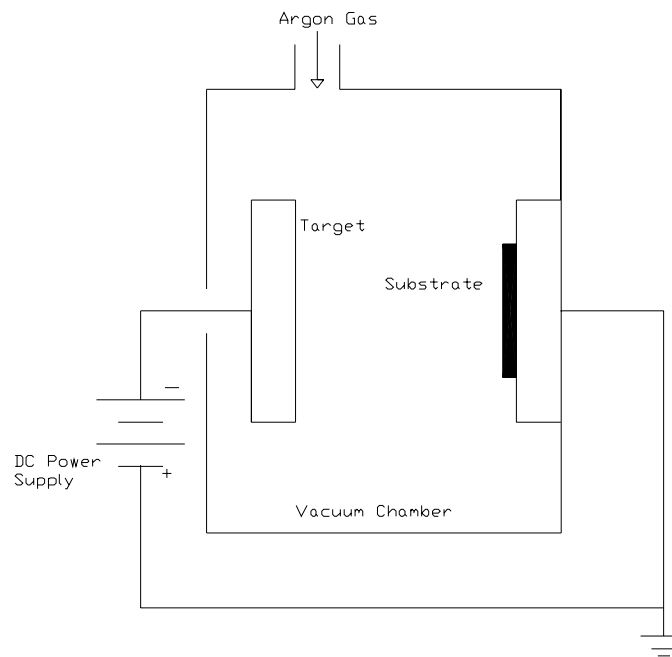


Fig. 4.3 Schematic of a DC-sputtering system [6]

4.2.4. Sputtering Techniques

In the last few years, a number of sputtering deposition techniques to deposit thin films of various materials have evolved. Fig. 4.3 shows a schematic of a DC sputtering system. The following section provides an overview of several common sputtered deposition techniques.

4.2.4.1. Non-Reactive Sputtering Processes

Sputtering is carried out using inert gas plasma. Usually Argon, which does not participate directly in the formation of compounds on either the target or substrates. Argon is most prevalent since its mass is high enough to ensure high sputtering yields, and its cost is lower than Xe or Kr. These inert gas ions are not incorporated into either the target or film as primary constituents, even in very small proportions inert gas incorporation can have deleterious effects on film properties. For example, in hard coatings Ar incorporation can

cause lattice expansions. The internal stress of the films increase. Additionally, inert gas ion bombardment of the substrate film couple can strongly influence the gas incorporation probability, as well as the growth mode, stoichiometry, and properties of deposited films.

4.2.4.2. Reactive Sputtering Processes

Reactive sputtering films can be deposited using a variety of techniques including: DC-diode, RF-diode, triode, magnetron, and modified RF. magnetron sputtering. There are basically two reactive sputtering modes: metallic cathode and compound-coated cathode. The other alternative, sputtering from a compound-coated cathode, is straightforward. However, the sputtering rates are usually much lower for compounds. In this process the elemental or alloy targets is sputtered in reactive gases like nitrogen to form nitride or oxygen to form oxides.

4.2.4.3. Diode Sputtering

Diode sputtering is the oldest sputtering technique. Diode plasma is formed when a relatively large potential (1000-5000 V) is applied between the cathode/anode pair in the presence of a sufficient gas concentration. A small fraction of these gas atoms become ionized, and these ions are then accelerated across the potential gradient of the cathode sheath and collide with the target. This causes sputtering of the surface. DC-diode sputtering can be used with a large variety of single and multi-component. A common example of DC-diode sputtering is the deposition of thin conductive films on samples for electron microscopy. While the greatest advantage of using DC-diode sputtering process is it's simplicity, its use is limited primarily by low deposition rates, high substrate heating and energy inefficiency.

4.2.4.4. RF Sputtering

The use of an oscillating power source to generate a sputtering plasma offers several advantages over DC method. It is possible to sputter using low AC frequencies such as 50 Hz. However, when the frequency is greater than about 500 kHz, the electrons in the negative glow region will have sufficient energy to be able to ionize the gas atoms directly and thus, the number of electrons required to sustain the discharge will be substantially reduced. Additionally, above 500 kHz it is no longer necessary for both electrodes to be conductive, since the current can be coupled also through capacitors. Above the low megahertz range, the ions due to their relatively large mass are no longer able to follow the oscillations of the

potential. As a result there is little ion accumulation during the part of the cycle in which the electrode is acting as a cathode.

There are two primary advantages of RF sputtering. First the ability to sputter insulating materials. Second the accessibility of lower operating pressures. Unfortunately, the deposition rates in RF sputtering are often limited by the poor thermal conductivity of insulating targets; thus in many instances it is preferable to deposit insulating films reactively from a metal source. Almost any material can be sputtered in an RF discharge, reactively or non-reactively. The applications of RF sputtering are quite varied and include deposition of metals, metallic alloys, oxides, nitrides and carbides.

4.2.4.5. Triode Sputtering

In addition to a cathode and anode pair, triode sputtering utilizes a third electrode to enhance ionization. This electrode may be a simple biased conductor or a thermo ionic electron source. With this additional electrode the discharge is no longer dependent solely on the generation of secondary electrons at the cathode to sustain the discharge, thus the discharge may be maintained at lower pressures, or at reduced discharge voltages. By varying the excitation of the electron source the discharge current can be varied independent of the discharge voltage, making high ion densities at the target and substrate possible using low discharge potentials. Triode discharges, both DC and RF, have been successfully used to deposit films of a great variety of materials for wear resistance, optical, semiconductor, and other coating applications. The primary advantages of triode sputtering are lower discharge pressures, lower discharge voltages, higher deposition rates and independent control of the plasma density.

4.2.4.6. Magnetron Sputtering

Magnetron sputtering differs from other sputtering techniques in that the majority of the plasma is confined to a region near the target surface by using strong magnetic fields to bend the trajectories of the secondary electrons ejected from the target surface into convoluted spiral-like patterns across the target surface. Using such arrangement well-confined plasma can be maintained very near the surface of the target, giving rise to an increase in the ionization probability and more than an order of magnitude increasing the plasma density in the region adjacent to the target.

There are several advantages of confining the plasma, which include:

1. Increased deposition rates (higher sputtering rates)

2. Reduced sputtering from the substrate and walls of the chamber
3. Reduced substrate heating during deposition
4. Reduced working gas pressure requirements
5. Producing high quality and low impurity films at reasonable deposition rates

Magnetron sputtering systems can be operated in any of the above described methods. The applications of magnetron sputtering are multiple, especially deposition of hard coatings, low frictions coatings, wear resistance, optical, and for many others applications it is used.

4.2.4.7. Unbalanced Magnetron Sputtering

Many studies have shown that, ion bombardment during deposition can produce changes in the nucleation behavior, morphology, composition, orientation and mechanical properties for a variety of thin films. Typically in magnetron sputtering, ions are extracted from the discharge surrounding the substrate by applying a negative potential of 300-700 V to the substrate. However, the current density incident on the films/substrate surface is generally quite low, (0.05-0.1 ions per deposited atom in conventional DC magnetrons). This is sufficient in many applications, it would be advantageous in some cases to increase this ratio. In the field of hard coatings. It is desirable to deposit films with a minimum of intra and inter granular voids, while inducing minimal damage within the crystalline lattice in order to maximize the corrosion and wear resistance of these films. To circumvent these limitations it would be preferable to increase the ion current density (the ions to deposited atoms ratio), and thus keeping the energy of the impinging ions low so no undesirable defects in the films appear. An unbalanced magnetron can provide this type of ion bombardment. The unbalanced magnetrons can be divided into three basic types shown in figure 4.4. A type I magnetron has a strong inner pole and weak outer pole type II is vice versa. The intermediate type is nearly balanced, in the case of conventional magnetrons. Using the type I geometry, the ion bombardment at the substrate is very low. This leads to ion deposited atom ratio as low as 0.25:1. In comparison, the type II geometry gives strongly enhanced ion bombardment, resulting in ion to deposited atom ratios of the order of 2:1 at low substrate bias potentials. The unbalanced magnetron has an additional benefit in that the ion energy and flux can be varied almost independently of one another, making it possible to investigate more comprehensively the interrelationship between the relevant process parameters and the resultant film microstructures [32].

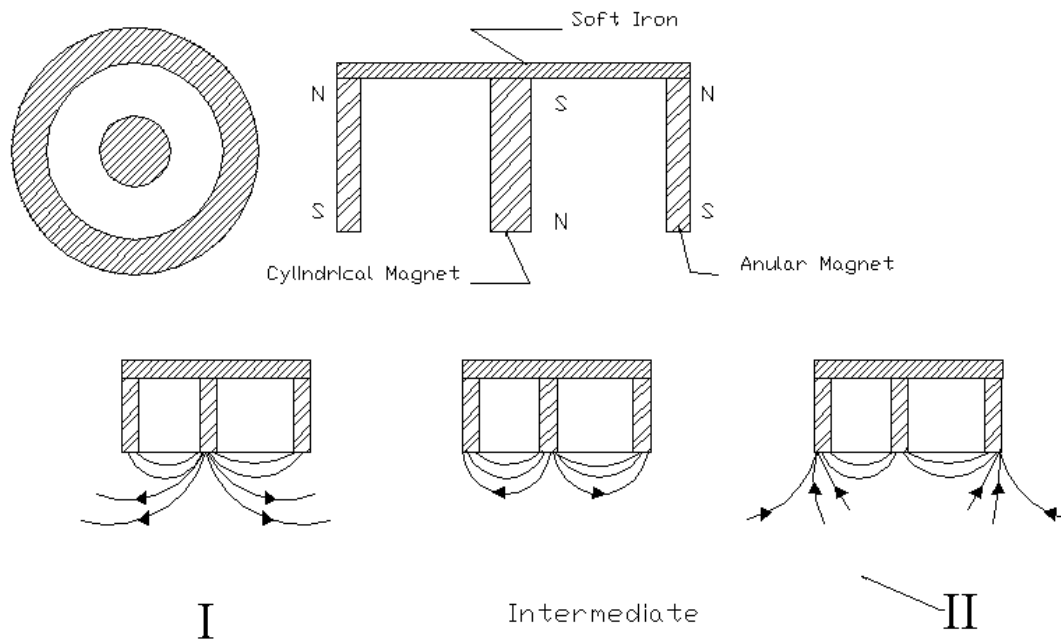


Fig. 4.4 Unbalanced magnetron design [31]

4.3. Deposition of Hard Coatings

Plasma vapour deposition (PVD) processes are often used to deposit coatings and thin films in order to reduce wear and friction of tools and machine parts. These techniques especially allow the deposition of a broad spectrum of materials, particularly covering the nitrides and carbides of the transition metals and some borides and oxides as well as carbon-containing coatings like diamond, diamond-like, metal-carbon and carbon-nitrogen coatings. On the basis of the binary compounds TiN and TiC [33], various strategies were developed to improve or adapt the hard coatings to a specific tribological problem. This was the first realized in multicomponent coatings by adding other metallic or non-metallic elements also with graded concentrations. Further developments were focused on the deposition of multilayer coatings and most recently on nanostructured coatings where in addition to hard components also soft and lubricating materials are deposited.

In this section the recent developments of tribological coatings give examples of their structure, properties and performances.

4.3.1. Types of Hard Coatings

4.3.1.1. Multicomponent Coatings

Adding different elements to a coating is one of the possibilities to adapt some of its properties to a value desired for specific applications. This allows modification of the basic physical properties such as hardness, lattice constant, thermal expansion coefficient, optical properties, grain size, texture, chemical reactivity, diffusion coefficient, elasticity, oxidation behavior, and internal stress, that alters the final performance. When alloying an additional element with an existing single phase coating the additional element can either be diluted in the matrix and a new single phase coating is produced or the additional element forms a second phase resulting in a two phase coating.

The most successful hard PVD coating is TiN [34]. It was one of the first ones developed due to the relative's ease with which it can be deposited. It is still the one that is usually tried first when a new application for PVD hard coating is tried. Work on improving TiN has usually involved adding another element to the compound to make a multicomponent compound with three or more constituent elements. Adding new elements changes the properties of the coating, such that the new coating can operate at higher temperature or can be more wear resistant. One modification is the (Ti, Al) N [35-36]. One of the main advantages of the (Ti, Al) N is the higher oxidation temperature than that of TiN. Aluminum forms a stable oxide layer at the surface of these films upon exposure to oxidizing conditions, thus protecting the underlying (Ti, Al) N. This feature has been successfully introduced as a protective coating on high-speed tools. Multicomponent coatings allow the deposition of graded layers with a continuous variation of the concentration of the components in order to fulfill specific requirements at the substrate interface or at the surface. Such gradients can be easily be obtained by a variation of the relative deposition rate or the reactive gas pressure.

4.3.1.2. Multilayer Coatings

A composite coating usually consists of two or more phases combined either as different layers (multilayer) or as a mixture of different phases (multiphase) [37]. The aim of a multicomponent coating is to combine desired properties from different components as well as the creation of new properties generated by the combination of suitable materials[38]. Since coatings are usually deposited by PVD process, multilayers can easily be obtained by using different material sources (magnetron, evaporator, etc.) in PVD deposition processes.

Dealing with multilayer coatings two cases have to be distinguished. Classical multiple layer coatings and nanoscale multilayer coatings. Classical multiple layer coatings consist of few different layers and have a total thickness of 1-8 μ m. These types of multilayer coatings are commercially available since a long time. They usually consist of one or more of TiAlN layers between layers of TiN, or others combinations. Additionally, multilayer coating of materials with different mechanical properties may show a better performance since crack propagation may be deflected or stopped at the interface or in the more ductile material [39]. The tribological behavior of the classical single layer coatings TiN and TiC could be improved by building multilayer structures. (TiC/TiN, TiN/TiC/BN, TiN/TiVC/AlN). Multilayer structures may exhibit a lower coefficient of friction as well as longer edge life when applied on cutting tools.

In nanoscale multilayer coating, the thickness of each single layer is in the nanometer range. Superlattice effects may additionally increase the hardness of the coating [28],[40]. The reason for this hardness enhancement is a hindering of the dislocation movement across a sharp interface, when the two materials have a large difference in their dislocation line energies. Since the dislocation line energy is proportional to the shear modulus, the main requirement for a hardness enhancement in these films is a difference in the elastic moduli of the two layer materials. A convincing model explaining the hardness enhancement of nanoscale multilayer films is given in [41]. The model takes dislocation movement across an interface, dislocation glide within individual layers as well as an interface with interface composition gradient into account. The calculations confirmed that a difference in the shear modulus is necessary a precondition for a hardness increase in nanoscale multilayers.

If each single layer is thinner than 3-5 nm the strain field around a dislocation is mainly outside the particular layer and the hardness increase induced by the periodical shear modulus variation will disappear in multilayer structure. Additionally depending on the deposition conditions and the thermal load applied, interdiffusion between the layer will decrease the amplitude of the shear modulus modulation and therefore also the hardness. The interface sharpness plays therefore a decisive role in the hardness enhancement of multilayers [42].

4.3.1.3. Nanocomposite Hard Coatings

Analogous to the nanoscale multilayer coatings presented above, it is possible to deposit isotropic nanocomposite coatings consisting of crystallites, embedded in an amorphous matrix, with grain sizes in the nanometer range [43-44]. Two different materials namely the

crystalline and the nanocomposite material form by a phase separation. A prerequisite for the phase separation is complete immiscibility of the two phases. In contrast to the multilayer structures, where any material combination can be deposited at any multilayer period, nanocomposites can only be obtained for certain material combinations. Additionally, the size of the crystallites cannot be independently controlled by the deposition process [45], because it is essentially determined both by the properties of the materials and by the deposition conditions (temperature, plasma conditions, elemental concentrations) [46-47]. In the last decade some nanocomposite thin films systems, have been deposited and investigated. Based on the concept of incorporating stable oxide forming elements (Al, Si, Cr, Zr) into TiN. Efforts have been undertaken to codeposit silicon and titanium nitride, in contrast to single phased hard materials, silicon cannot be substitutionally built in the lattice of TiN [46]. In accordance with the Ti-Si-N phase diagram, which does not present any stable ternary phase under equilibrium conditions, two phases TiN/ Si_3N_4 coatings are formed when silicon is added during deposition of TiN. In further experiments these coatings were identified as nanocomposite consisting of TiN crystallites (nc-TiN) surrounded by an amorphous Si_3N_4 (a- Si_3N_4) matrix [47]. Two main examples of such nanocomposite coatings are the nc-TiN/ (a- Si_3N_4), and the nc- $(\text{Ti}_{1-x}\text{Al}_x)\text{N}$ / (a- Si_3N_4) which is schematically illustrated in Fig. 4.5 with the $(\text{Ti}_{1-x}\text{Al}_x)\text{N}$ crystals embedded in an amorphous matrix of Si_3N_4 [48-49].

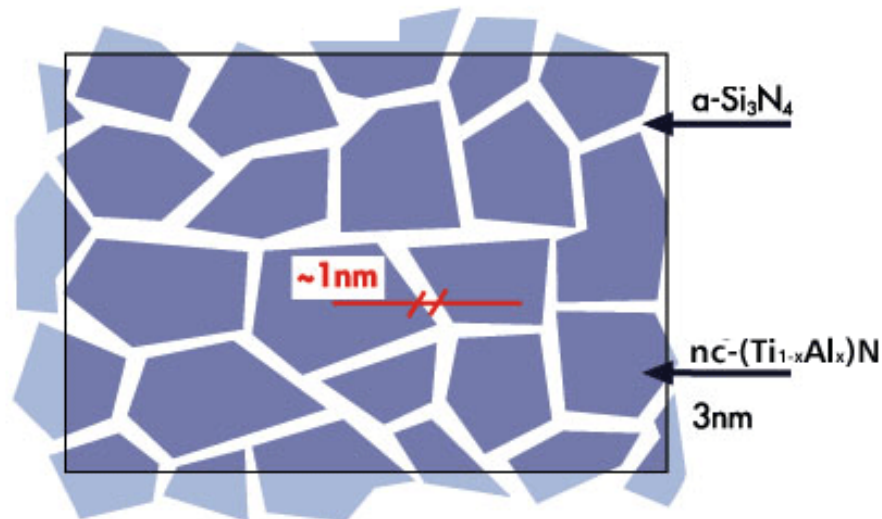


Fig. 4.5 Schematic representation of a nanocomposite consisting of a nanocrystalline phase embedded in an amorphous matrix [55]

Analogous to the situation in multilayer structures described above, a hardness increase can be expected in any two phase material, as long as they have sharp interfaces and a large difference in their shear modulus. One striking difference to the multilayers systems, is the fact that nanocrystalline / amorphous systems are isotropic [53]. In other words, the orientation and sequence of both phases is random. It is reasonable to assume that the shear modulus of these two phases are different (both materials differ in their structure and in their electronic properties). They will form barriers for dislocation movement. The sharp interfaces encountered in nanocomposite coatings are due to the immiscibility of the two phases. In order to achieve the sharp phase transition, a perfect encapsulation of the crystalline material by the second phase is necessary [48]. This is the case for superlattices with atomically sharp interfaces. For nanocrystalline isotropic materials such a close convergence of nanocrystals can be obtained by amorphous materials [53]. Due to their structural flexibility, they can adapt to the shape and orientation of the nanocrystals. Furthermore, incoherence of the crystallites can be accommodated by an amorphous material with its possibility to adopt any orientation within a few atomic distances. An additional improvement of the nanocomposite coatings as compared to TiN is their improved oxidation resistance [28]. A two-step oxidation process is likely to govern the oxidation in the regime between 600 °C and 1000°C. The first process, being dominant at low temperatures up to about 820 °C is characterized by the slow diffusion of oxygen through the Si₃N₄ barriers into the TiN nanocrystals. An increase of the Si₃N₄ fraction in the coatings means a thicker Si₃N₄ layer encapsulating the TiN grains, and hence a lower oxidation rate is observed. This is accompanied by the formation of an amorphous silica passivation layer, which further reduces the oxygen diffusion rate into TiN. Above 820 °C the oxidation is dominated by the recrystallization and growth of TiO₂ crystals, which leads to well faceted grains, caused by the discontinued protective a-SiO_x and a-Si₃N₄ layers to an accelerated oxidation.

4.4. Characteristics and Properties of Hard Coatings

4.4.1. Hardness

Hardness is a measure of a materials resistance to deformation by surface indentation. Hardening of a material is possible in two ways. First, the chemical bonding between the atoms is change by element addition. Second, the hardness of a material is also increased by hindering the dislocation movement by lattice distortions (grain boundaries, defects,

dislocations, precipitations) as known from classical metallurgy[32][50-55]. By coating of additional element, defects (solid-solution hardening) and grain boundaries may be introduced into the coating. This results into an increased hardness. However, hard coatings can be produced in such a way that they already have a very good defect and grain boundary density (small grain size). This is also why a deposited coating usually exhibits a higher hardness than a single crystal made of the same material. Additionally, the internal stress can favor delamination of the films. Hardness of thin films is mainly measured by Vickers hardness test. (See Fig. 4.6). The operating principles of the Vickers hardness test are similar to that for the Brinell test. The Vickers test uses a square-based diamond pyramid tip with a characteristic 136-degree angle the indenter. Since determining the diagonal of a square impression is easier than determining the diameter of a circular impression the hardness obtained by the Vickers test may be more accurate than the Brinell test. This test is applicable for measuring the hardness of very hard and thick materials such as coatings.

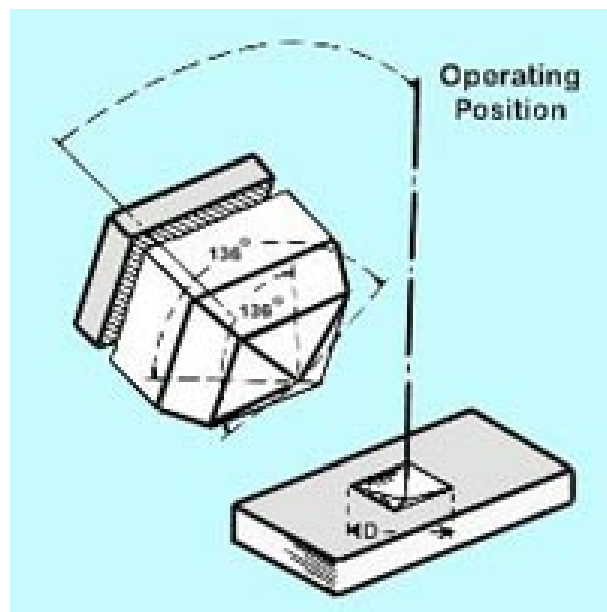


Fig. 4.6 Schematic representation of Vickers hardness test

4.4.2. High Temperature Oxidation

Surface oxidation at high temperature is an issue not only for cutting and drilling operations, but also for applications in hot environments. In the cutting process the cutting edge temperatures reached more than 600 °C [32][50-55], and even on planes exposed to severe friction. Efforts have been therefore under taken to improve the high temperature oxidation behavior of coating. For example the adding of oxidation resistance elements such as Al,

during the deposition process of TiN, lead to the development of a new single-phase materials derived from the TiN. The introduction of aluminum in TiN increases the oxidation resistance from approximately 550 °C to 800 °C and additionally an increased hardness is observed. The enhanced oxidation resistance is a consequence of the formation of an aluminum rich protective Al₂O₃ passive layer at the surface.

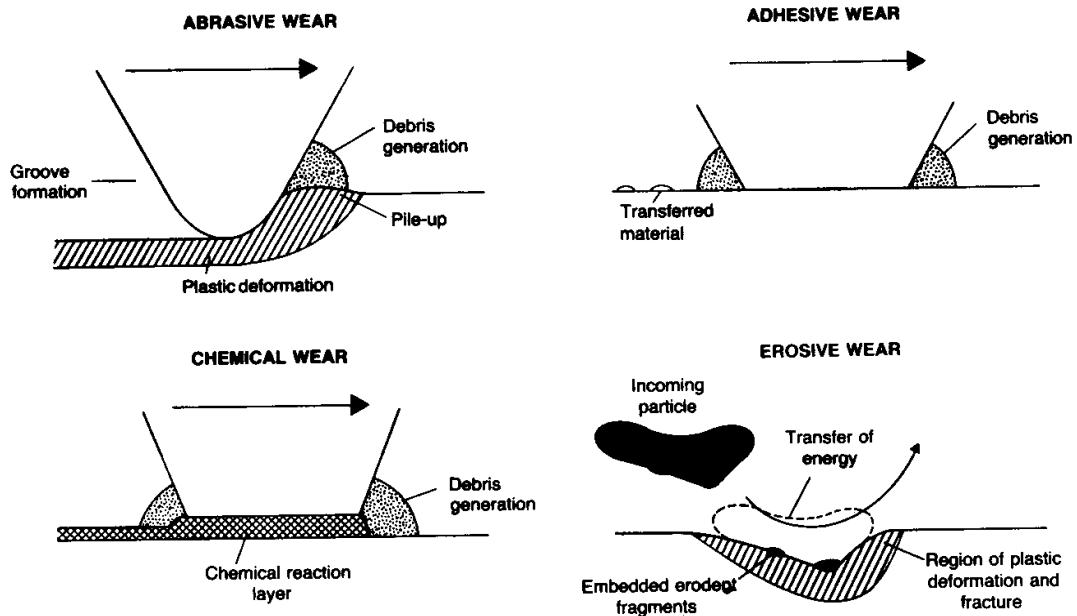
4.4.3. Friction and Wear

Adding different elements to the coating can influence the tribological behavior of a coating. A prediction of the influence of the elements added is usually not possible. The real response of a coating in a specific application has to be determined by conducting field tests. In tribological systems many properties and parameters (the different material properties of the friction counterparts, environment, test conditions) interact with each other in a nonlinear and locally different way, which prevents a theoretical prediction of the final tribological behavior[48],[57]. Additionally, when a coating is improved by alloying (sputtering of different materials) for certain tribological applications, it may perform worse under some other tribological conditions. Low coefficient of friction is the main subject for selection of wear resistance coatings. The most important wear mechanisms fall into four groups and these are illustrated in fig. 4.7:

1. Abrasive wear. Hard abrasive particles cut through a softer substrate material or coating substrate system.
2. Adhesive wear. The sliding counterface adhere to each other forming bonds (physical or chemical).
3. Chemical Wear. A chemical reaction between the two sliding counterfaces take place and lead to generation of weak phases, which can easily be removed.
4. Erosive wear. This occurs when a surface is subjected to repeated impacts of a stream of particles, which then result in the removal of materials.

4.4.4. Other Selected Properties of Coatings

There are more properties of the coated materials that can be influenced by changing the coating parameters and adding one or more elements to an existing coating; surface chemistry, electrical, magnetical, optical are interesting properties of coating that can find many industrial applications.



5. Fig. 4.7 Schematic representation of basic wear mechanisms [58]

4.5. Deposition of Nanocomposite (Ti, Si, Al)N Coatings

The nanocomposite coating materials have recently attracted increasing interest due to the possibility to combine high hardness, high oxidation resistance, stiffness, and low friction coefficient properties. The most studied systems up to now are the (Ti, Si) N and the (Ti, Si, Al) N system [28],[32],[46-50]. These films were characterized as being nanocomposites consisting of TiN or TiAlN embedded in an amorphous matrix of silicon nitride. The hardness of these composites depends on the crystalline and amorphous phases that all together must form strong materials with high cohesive energy at their interfaces. The usual mechanisms of deformation and mechanical failure are absent or hindered in such a material. Dislocations and other structural defects that may be formed during the deposition will become annihilated within the grain boundaries, so that even if formed under a high-applied stress, the dislocations within the nanocrystals cannot glide through the amorphous grain boundary matrix. The nanocomposite coating materials are normally prepared using the physical vapour deposition process (PVD) by deposition of the different materials (Ti, Si) in the (Ti, Si) N system or (Ti, Si, Al) in the (Ti, Si, Al) N system instantaneously to form the required structures of the nanocomposite coatings. This method was used in all the work done by many work groups producing the nanocomposite coatings. In this work the investigation of a (Ti, Si, Al) N system was done. The main point of investigation was to study the possibility of getting

the nanocomposite coating structures by deposition of multilayers films from TiN, AlSiN. One point is to understand the relation between the mechanical properties (hardness, Young's modulus), and the microstructure (nanocrystalline with individual phases). Particularly special attention will be given to the temperature effects on microstructural changes in annealing at 600 °C for the coatings. The surface hardness, elastic modulus, and the multilayer diffusions and compositions will be the test tools for the comparison between the different coated samples with and without annealing at 600 °C.

4.5.1. Experiment

The rectangular aluminum vacuum chamber designed in chapter three was used to deposit different (Ti, Si, Al) N coating layers to a non-polished ceramic (Al₂O₃) substrate to study the possibilities of achieving the nanocomposite coating structures using the deposition of multilayers coatings. The magnetrons were used with a RF power supply to sputter the different thin film layers from a high purity Ti target and different AlSi alloy targets with different percentages of silicon (7.6, 9.9, 12.5)% in the aluminum silicon alloy targets. The depositions were carried out in a N₂ reactive gas atmosphere. A Ti adhesion layer of approximately 0.15 μm was deposited onto these samples before deposition of the different coating layers. Further detailed information regarding some deposition parameters are presented in Table I.

Table I. Basic deposition parameters and conditions for the (Ti, Si, Al) N coatings

Basic pressure	8x10 ⁻⁷ mbar
Deposition pressure	1x10 ⁻² mbar
Target to substrate distance	60 mm
Target surface area	37 cm ²
Power of the Ti target [RF frequency]	400 W
Power of the AlSi target [RF frequency]	400 W
Substrate bias	0 V
Film thickness	0.9-1 μm

Different combinations of coatings were deposited starting with an Ti adhesion layer, and then a TiN layer followed by another AlSiN layer. The procedure was repeated until the required coating thickness was achieved. Then a thin TiN layer was deposited as an over-

layer. By changing the TiN layer thickness and using different AlSi targets it was possible to get 5 different multilayer-coated samples. The samples were not only made with different layer thicknesses, but also with different amount of silicon, titanium and aluminum which makes it possible to study composition effects of the three different materials in the coated samples. In each test two samples were coated. One was tested without annealing; the other one was annealed in a Krysal 18 gas (18% CO₂ in argon) atmosphere at 600 °C. The samples were introduced into a horizontal furnace, then being subjected to a thermal cycle consisting of a heating time of two hours up to the annealing temperature, one hour being held at that temperature (600 °C), followed by slow cooling to room temperature. The secondary neutral particle mass spectrometry (SNMS) was used to analyze and study the chemical composition of the different samples with and without annealing. It is clear that a complete diffusion between the different thin layers can be measured, which indicate that a multilayer system does not anymore exist. The atomic force microscope (AFM) (which is equipped with a Vickers diamond indentation) was used to evaluate the tribological properties and measure the surface hardness. A series of hardness tests for the different samples with a maximum load of 700μN were performed, where the indentation depth did not exceed 15 % of the coating thickness. To study the microstructure of the deposited coating further samples were deposited on tungsten carbide substrates. The (XRD) was used to study the structure of this samples after annealing were it was clear that a two phase system can be found.

4.5.2. Results and Discussion

4.5.2.1. Chemical and Structural Analysis

Table II presents some experimental details as well as some results such as thickness of the titanium layer, thickness of the AlSi layer, fractions of the silicon on the aluminum silicon alloy targets and the Young's modulus of deposited (Ti, Al, Si) N coated samples.

Table II. Experimental details, TiN layer thickness, AlSiN layer thickness, Number of TiN layers, Number of AlSiN layers, Si % and some results of the deposited (Ti, Al, Si) N coatings

Sample Name	Ti layer thickness (nm)	AlSi layer thickness (nm)	Si % in the AlSi layer	Annealed at (600°C)	Hardness (Gpa)	Young's Modulus (Gpa)	Number of Ti. layers	Number of AlSi layers
Sample A	50	35	7.6	No	22.4	269	11	10
Sample A1	50	35	7.6	Yes	23.6	295	11	10
Sample B	25	12	7.6	No	21.2	260	21	20
Sample B1	25	12	7.6	Yes	21.6	276	21	20
Sample C	50	40	9.9	No	24.5	302	11	10
Sample C1	50	40	9.9	Yes	24.9	306	11	10
Sample D	25	12	9.9	No	31	302	21	20
Sample D1	25	12	9.9	Yes	33	309	21	20
Sample E	25	12	12.5	No	23	294	21	20
Sample E1	25	12	12.5	Yes	24	290	21	20
Sample 1	25	12	9.9	Yes	27	306	21	20
Sample 2	25	12	9.9	Yes	25	319	21	20

As described before the main investigation object of this study is to test the possibility of producing nanocomposite coating structures by deposition of thin multilayers. Fig. 4.8 shows the secondary neutral particle mass spectrometry (SNMS) test results of sample A. From this

figure its clear that the three deposited elements (Ti, Al, Si) exist in each layer of the test sample coatings. This gives an indication that a complete diffusion between the different layers took place. This indicates that there are stability driving force other than the (thermodynamic forces (thermal heating)) is responsible of that diffusion, since the deposition was done at low substrates temperature. The high magnetic flux of the used unbalanced magnetrons and the high used sputtering power were able to produce a high ion-to-atom flux which give high mobility to the coated atoms. The interaction between the high mobility and the ion-to-atom flux were sufficient to enhance the diffusion between the different deposited thin layers [32]. The Titanium intensity in the sample shows constant values in the different layers except some variations in the first two layers. The intensity of aluminum is increasing in the first two layers, then vary around a constant value in the other layers except the last titanium adhesive layer. The fraction of silicon stays constant, and that result does not match with the procedure was followed, where different low silicon content in an aluminum silicon alloy targets where used. Because of the background of the (SNMS) test system with a chamber made of glass (SiO_2), it is possible that some layers of the glass chamber were sputtered and enhanced the silicon fractions in the (SNMS) measurement. As a result we could not have good estimates of the silicon in the different deposited layers. The N_2 intensity also shows constant values during the test. It decreases as the titanium adhesion layer is reached. Annealing at $600\text{ }^\circ\text{C}$, sample A1 (see fig. 4.9) does not show a big effect on the diffusion between the different layers. It was mainly required to increase the hardness of the coating by the segregation of the nanocrystalline/amorphous phase structure through the forming of the amorphous phase. This effect couldn't be detected by the (SNMS). Fig. 4.10 shows the results of sample B, while fig. 4.11 shows the results after annealing. It is clear also that a complete diffusion between the different layers was detected. Fig. 4.12 shows the results of sample C, where lower percentages of titanium were sputtered. On the other hand higher AlSi percentages was sputtered. The first three layers exhibit the characteristics of multilayers with low diffusion between the different layers. The other layers have higher diffusion. In this sample thicker layers of the different materials were deposited (see table II). The annealing of this sample is able to enhance the diffusion between the first three layers as it can be seen in fig. 4.13. Figures 4.14, 4.16 show more or less that the same conclusion as above can be drawn for sample D and E. The same results can be also found for the annealed samples D1, E1 (see fig. 4.15, 4.17).

4. Deposition of Nanocomposite (Ti, Si, Al) N Coatings

As a result of the (SNMS) tests we were able to see that the procedure to deposit the coatings is able to enhance the diffusion between the different coating materials in the different layers. But the question should be answered what type of coating we deposit?. For that, four samples were tested using the x-ray diffraction (XRD). Fig. 4.18, and fig. 4.19 show the x-ray diffraction (XRD) diagram obtained from sample 1 and sample 2, which was deposited on a tungsten carbide substrate while the diagrams for sample C1 and D1 are in figures 4.20 and 4.21 respectively. Two distinct phases were observed in all figures. The typical TiN Fcc structures can be detected, while other unknown peaks were also detected. This peaks are due to the low deposition temperature and the selected deposition conditions (no substrate bias voltages). The possibility for not only an amorphous phase of (SiN_x) to occur but also of forming an AlN amorphous phase cannot also be excluded [32],[45]. The tested samples also exhibit an asymmetric broad peak where both phases are not markedly distinguished. Corresponding to the peak centroid of an intermediate lattice parameter, this behavior evidences that a solid solution of both phases is available too.

As result from the (SNMS) and the (XRD) we can see that we were able to deposit a two phase nanocrystals/amorphous coating with a TiN as a nanocrystaleic phase. Different types of amorphous structures may have taken place; mainly the (SiN_x). But amorphous AlN or a Ti-Si-N phase may also have been assumed.

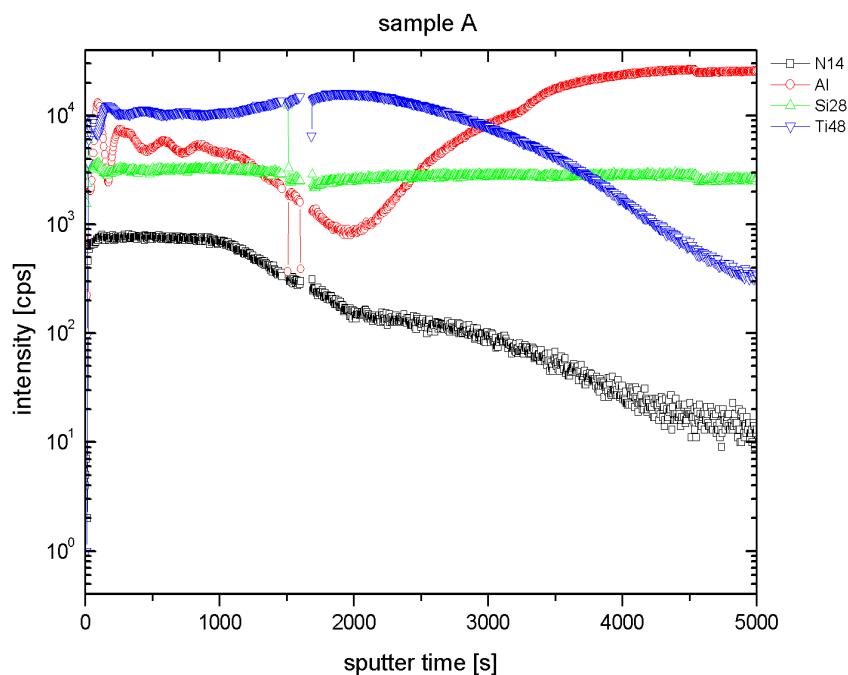


Fig.4.8 The SNMS spectrometry of sample A [(Ti, Al, Si)N] films on a ceramic substrate, thickness of the film $\approx 1 \mu\text{m}$

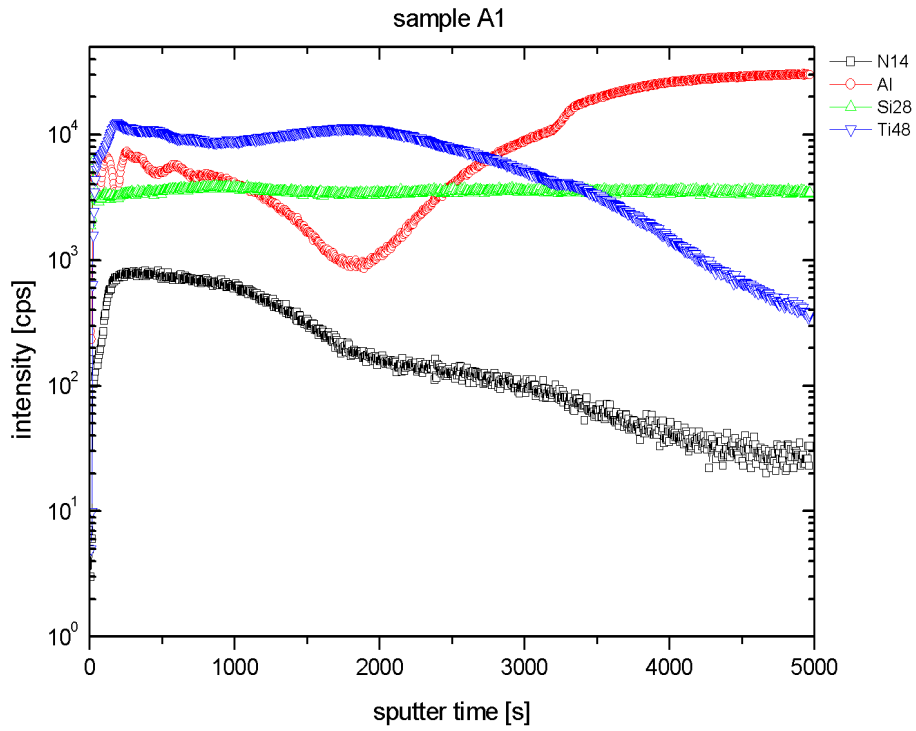


Fig.4.9 The SNMS spectrometry of sample A1 [(Ti, Al, Si)N films on a ceramic substrate, thickness of the film $\approx 1 \mu\text{m}$]

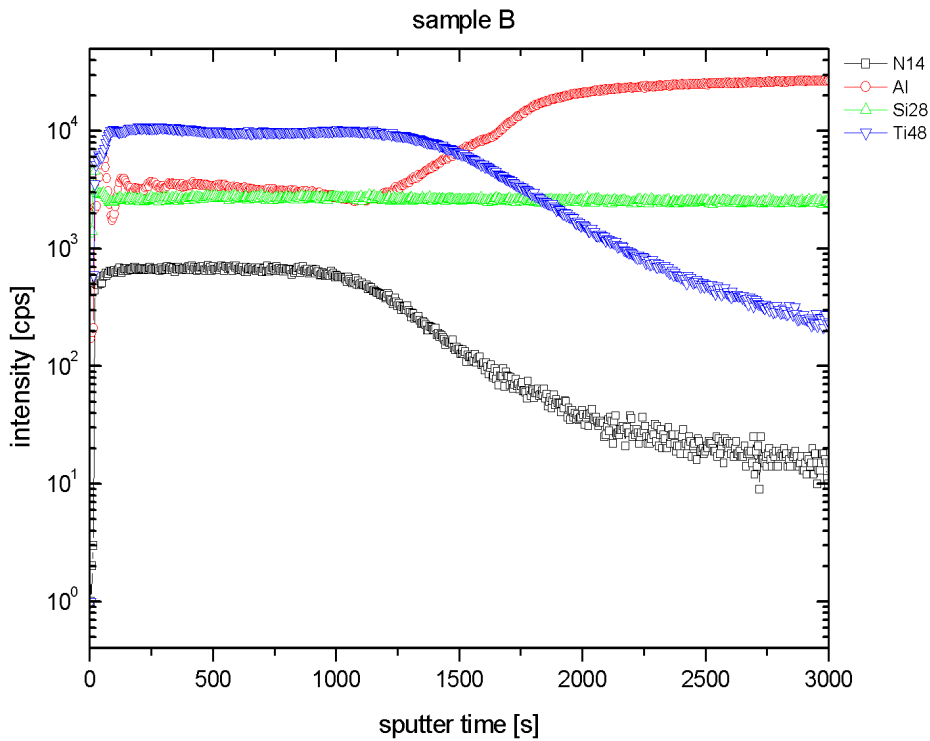


Fig.4.10 The SNMS spectrometry of sample B [(Ti, Al, Si)N films on a ceramic substrate, thickness of the film $\approx 0.9 \mu\text{m}$]

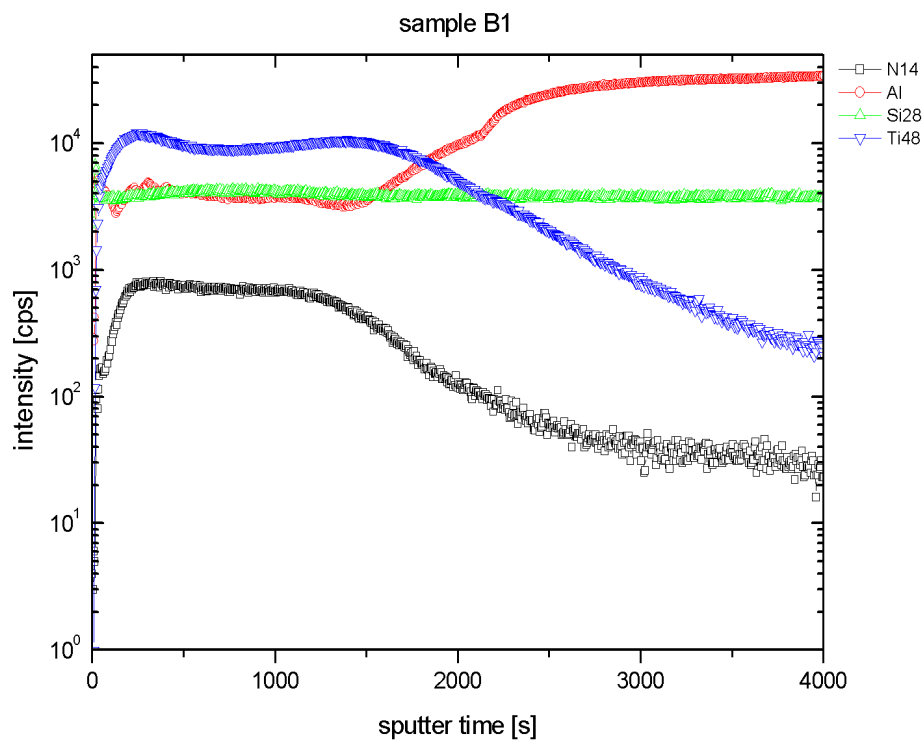


Fig.4.11 The SNMS spectrometry of sample B1 [(Ti, Al, Si)N films on a ceramic substrate, thickness of the film $\approx 0.9 \mu\text{m}$]

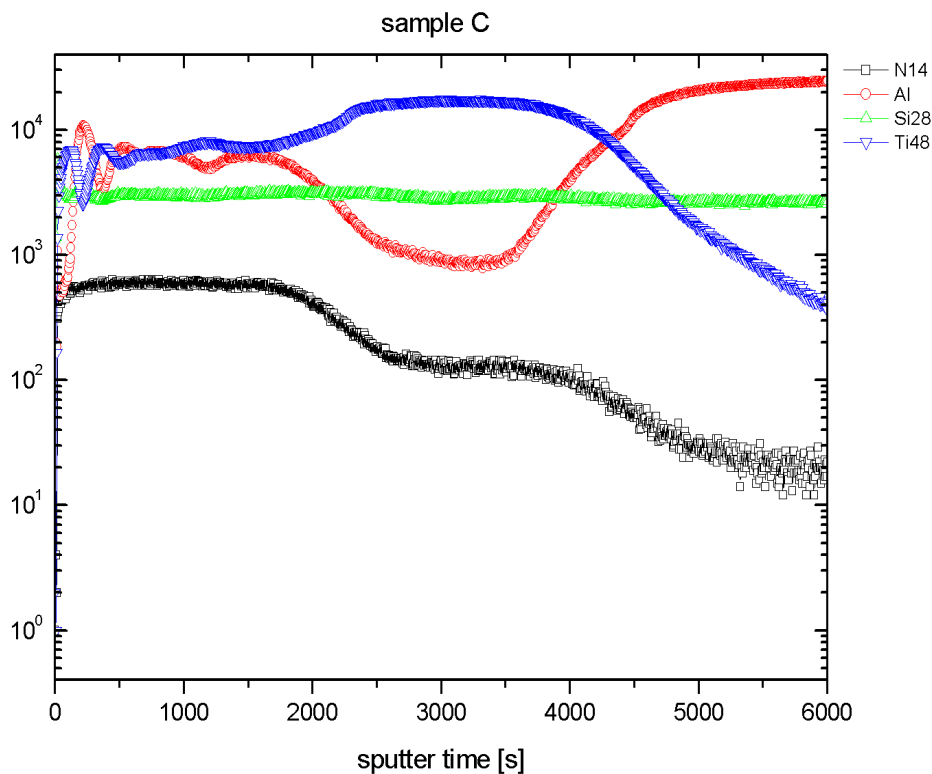


Fig.4.12 The SNMS spectrometry of sample C [(Ti, Al, Si)N films on a ceramic substrate, thickness of the film $\approx 1 \mu\text{m}$]

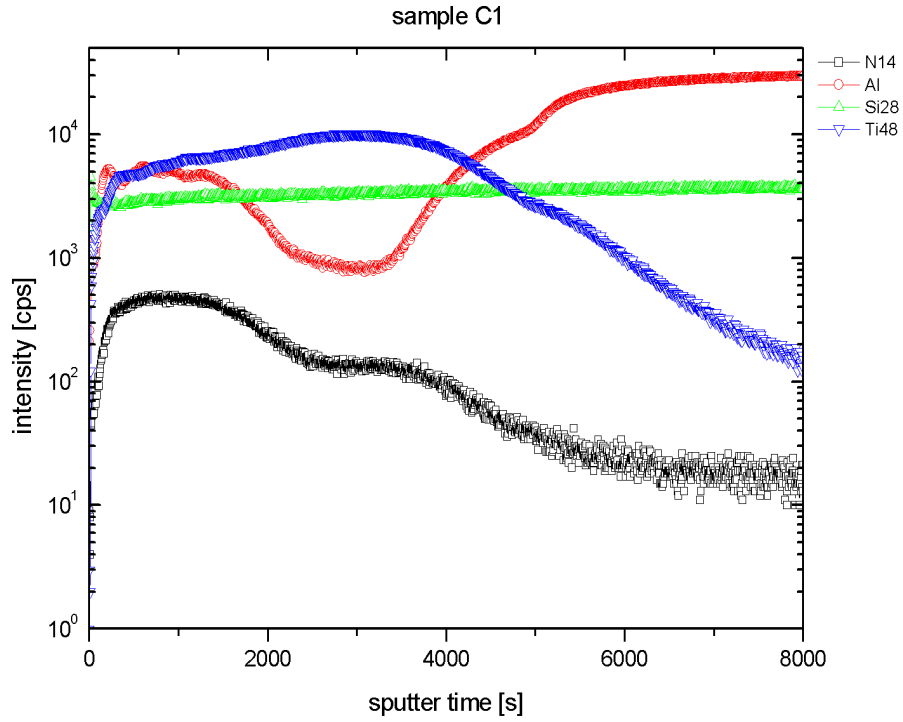


Fig.4.13 The SNMS spectrometry of sample C1 [(Ti, Al, Si)N films on a ceramic substrate, thickness of the film $\approx 1 \mu\text{m}$]

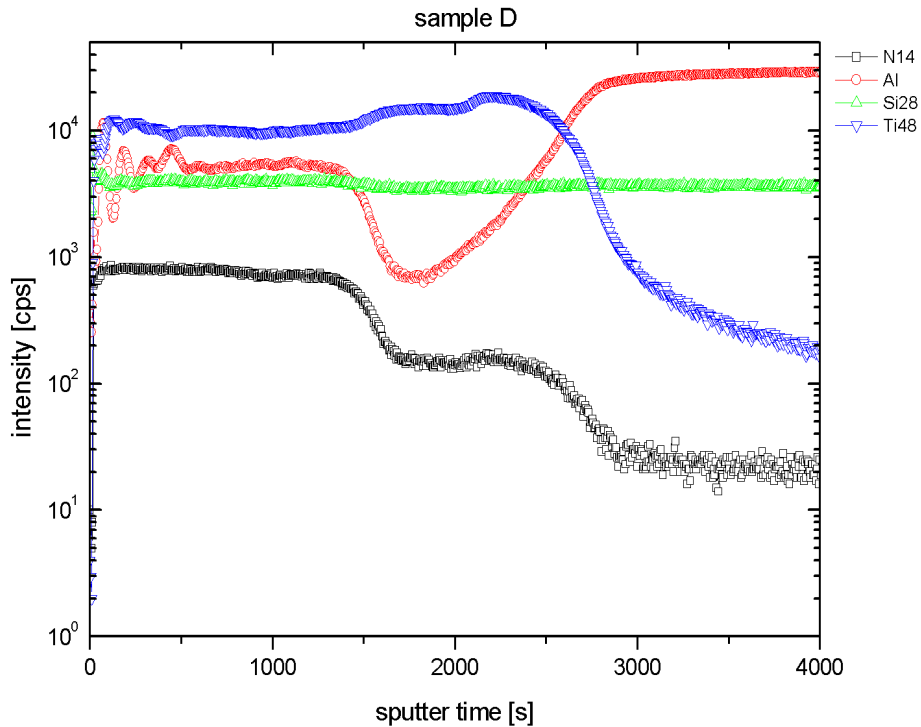


Fig.4.14 The SNMS spectrometry of sample D [(Ti, Al, Si)N films on a ceramic substrate, thickness of the film $\approx 0.9 \mu\text{m}$]

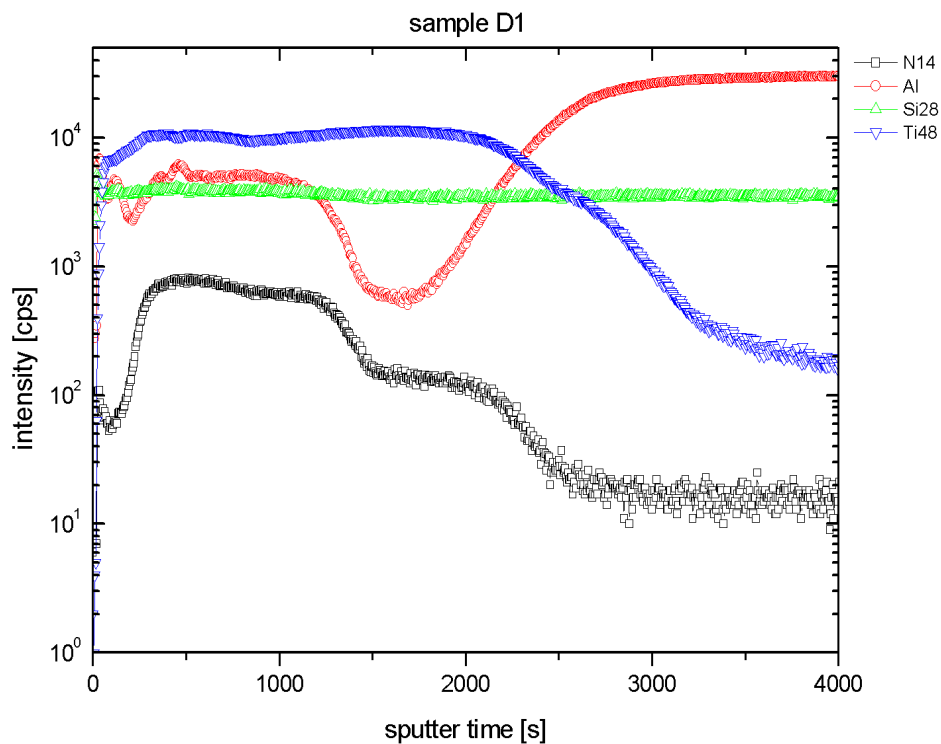


Fig.4.15 The SNMS spectrometry of sample D1 [(Ti, Al, Si)N films on a ceramic substrate, thickness of the film $\approx 0.9 \mu\text{m}$]

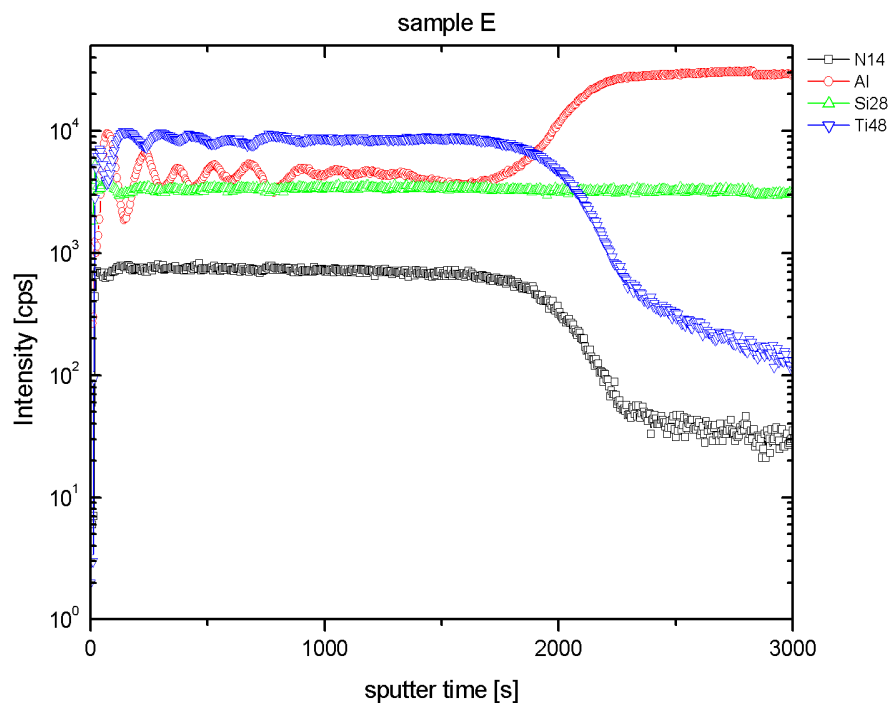


Fig.4.16 The SNMS spectrometry of sample E [(Ti, Al, Si)N films on a ceramic substrate, thickness of the film $\approx 0.9 \mu\text{m}$]

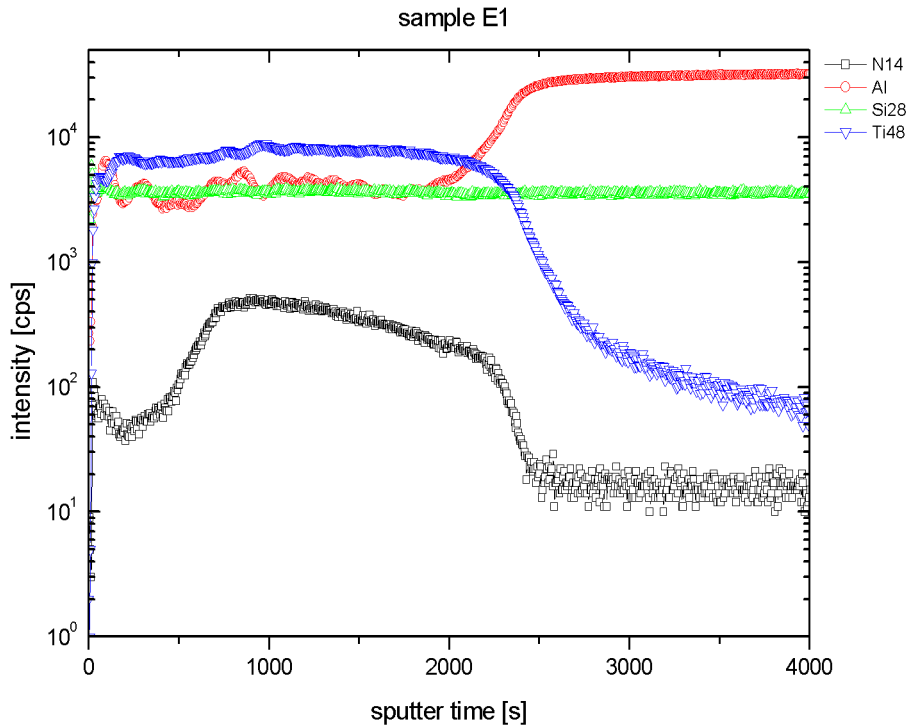


Fig.4.17 The SNMS spectrometry of sample E1 [(Ti, Al, Si)N films on a ceramic substrate, thickness of the film $\approx 0.9 \mu\text{m}$]

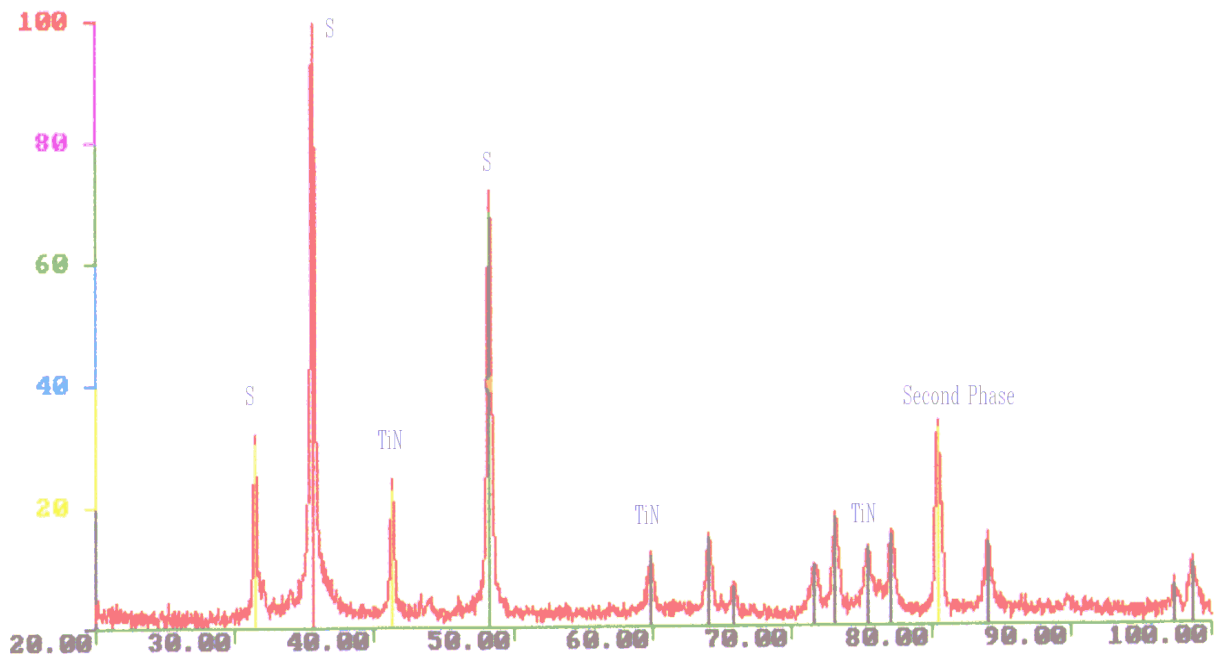


Fig. 4.18 The XRD diffraction patterns of sample 1 [(Ti, Al, Si)N films on a tungsten carbide substrate, thickness of the film $\approx 0.9 \mu\text{m}$], the peaks from the substrate are labeled with S

4. Deposition of Nanocomposite (Ti, Si, Al) N Coatings

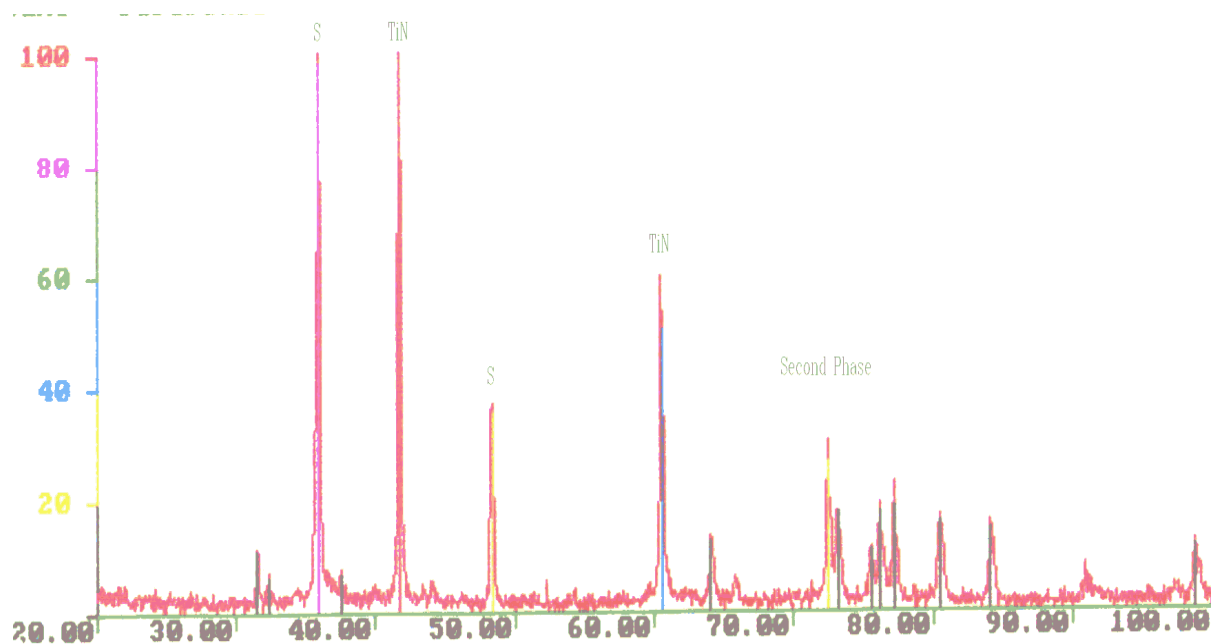


Fig. 4.19 The XRD diffraction patterns of sample 2 [(Ti, Al, Si)N films on a tungsten carbide substrate, thickness of the film $\approx 0.9 \mu\text{m}$], the peaks from the substrate are labeled with S

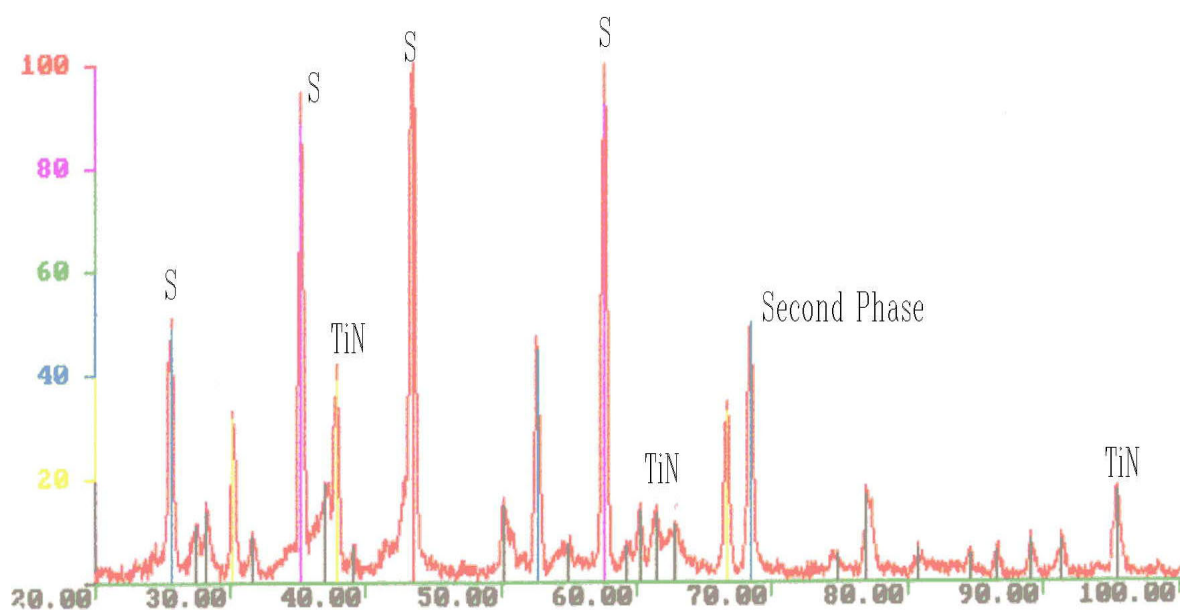


Fig. 4.20 The XRD diffraction patterns of sample C1 [(Ti, Al, Si)N films on a ceramic substrate, thickness of the film $\approx 1 \mu\text{m}$], the peaks from the substrate are labeled with S

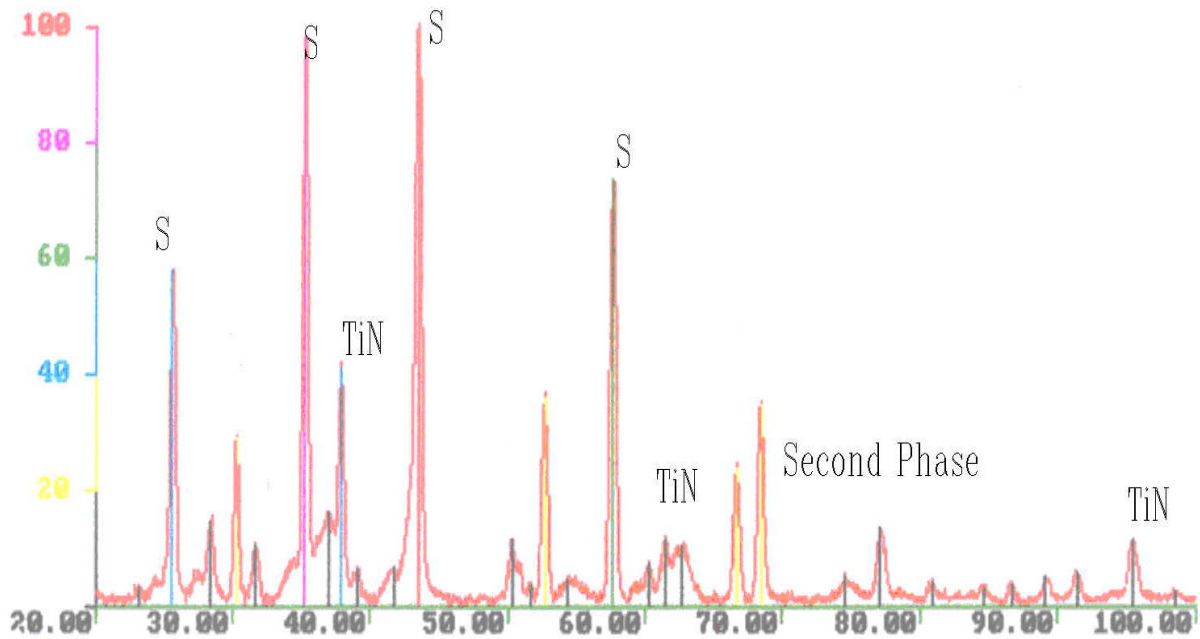


Fig. 4.21 The XRD diffraction patterns of sample D1 [(Ti, Al, Si)N films on a ceramic substrate, thickness of the film $\approx 0.9 \mu\text{m}$], the peaks from the substrate are labeled with S

4.5.2.2. Mechanical Properties Analysis

Because of the high surface roughness of the non-polished ceramics (Al_2O_3) substrate, the (AFM) profiles of all the test samples show rough coating surfaces (see fig. 4.22, 4.23, 4.24, 4.25, 4.26, 4.27, 4.28, 4.29, 4.30, 4.31, 4.32, 4.33). This surface roughness does not only influence the estimation of the coefficient of friction, it also influences the accuracy of the Vickers hardness measurement for the hardness and Young's modulus determination. Table II shows the hardness and Young's modulus values for the different coating samples. The sample D1 has the highest surface hardness (33 GPa) and Young's modulus (309 GPa). The other samples nearly show an equivalent measured value. The hardness indentation depth did not exceed 15% of the coating thickness and from the (SNMS) test figures it is obvious that the over-layer of the coated samples shows a multilayer structure. For that, the measured hardness values don't represent accurately the actual nanocomposite coating below the over-layers.

The annealing process at 600°C for the samples were able to increase the surface hardness of the samples in different magnitudes. This could be due to the different fractions of the composition of the coating materials. Especially the silicon is responsible for the forming of

4. Deposition of Nanocomposite (Ti, Si, Al) N Coatings

the amorphous phase which decreases the nanocrystalline particles size. As a result the hardness is increased.

The measured hardness values show lower values compared to the ones achieved by other groups. This may be because of the low substrate temperature and using no bias voltages during the deposition process. By increasing the substrate temperature hardness is expected to increase, since the cooperation between the surface mobility induced by the enhanced ion-to-atom arrival rate ratio and the corresponding expected effect from increasing the substrate temperature are enough to ensure an enhancement in the nanocrystals/amorphous phase segregations. For that further studies should be done to understand the influence of each condition on the deposition process.

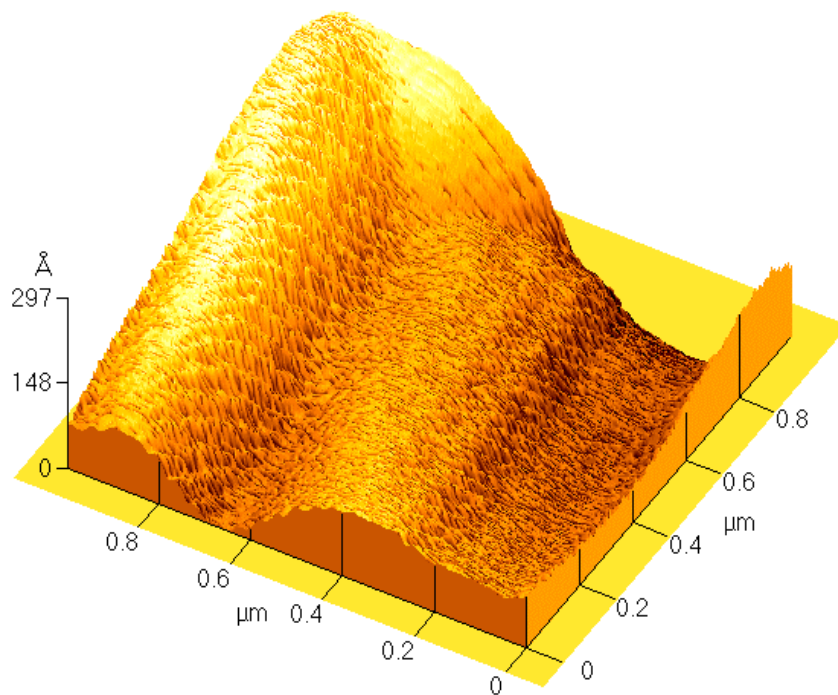


Fig. 4.22 AFM scan profile of sample A [(Ti, Al, Si)N films on a ceramic substrate, thickness of the film $\approx 1 \mu\text{m}$]

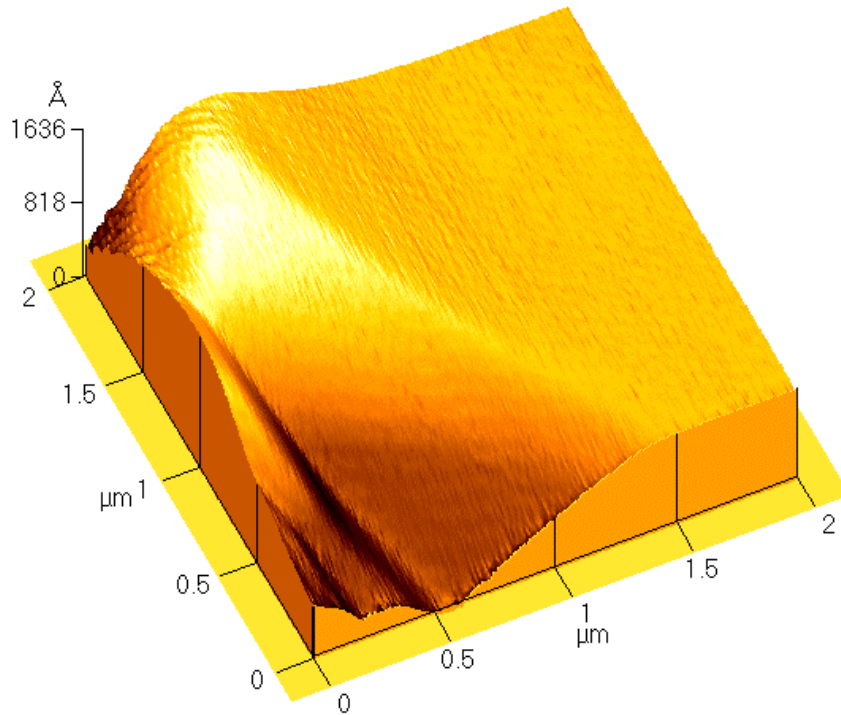


Fig. 4.23 AFM scan profile of sample A1 [(Ti, Al, Si)N films on a ceramic substrate, thickness of the film $\approx 1 \mu\text{m}$]

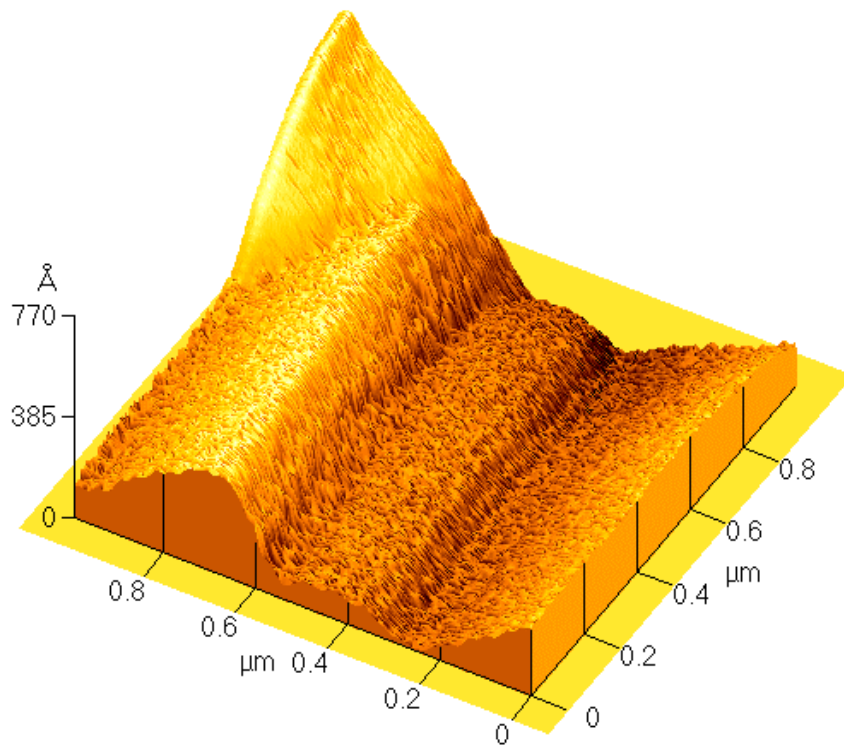


Fig. 4.24 AFM scan profile of sample B [(Ti, Al, Si)N films on a ceramic substrate, thickness of the film $\approx 0.9 \mu\text{m}$]

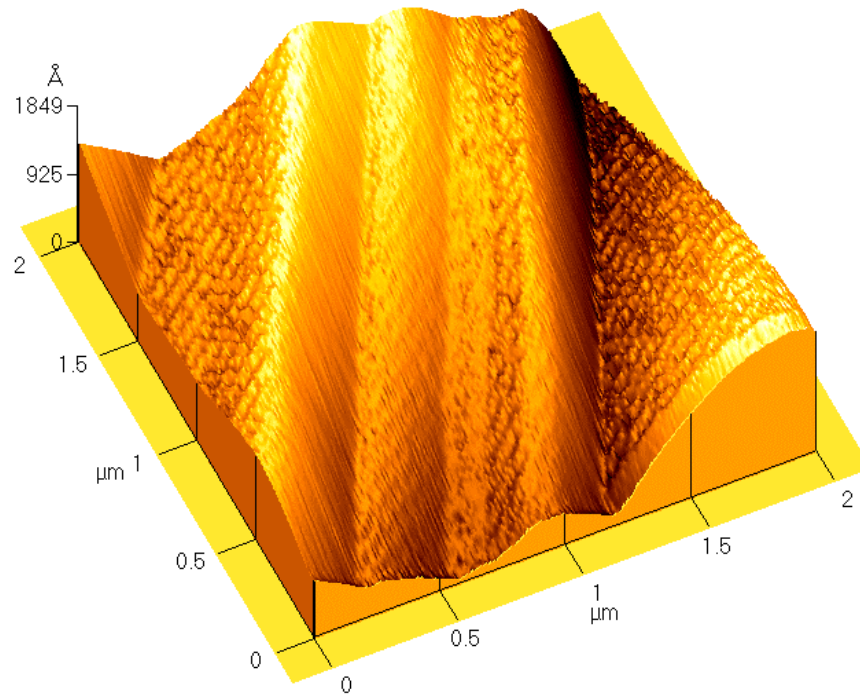


Fig. 4.25 AFM scan profile of sample B1 [(Ti, Al, Si)N films on a ceramic substrate, thickness of the film $\approx 0.9 \mu\text{m}$]

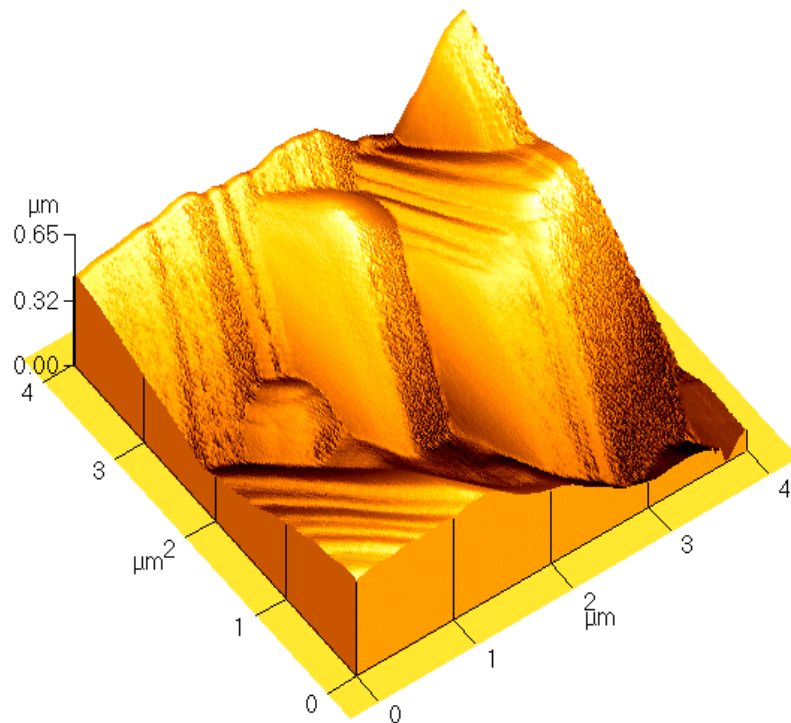


Fig. 4.26 AFM scan profile of sample C [(Ti, Al, Si)N films on a ceramic substrate, thickness of the film $\approx 1 \mu\text{m}$]

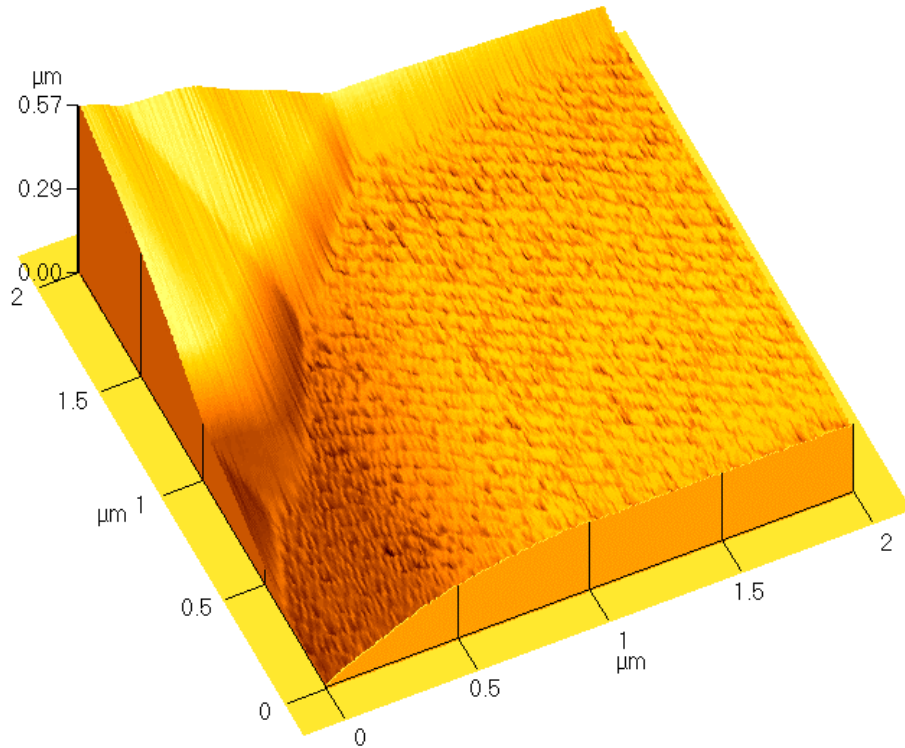


Fig. 4.27 AFM scan profile of sample C1 [(Ti, Al, Si)N films on a ceramic substrate, thickness of the film $\approx 1 \mu\text{m}$]

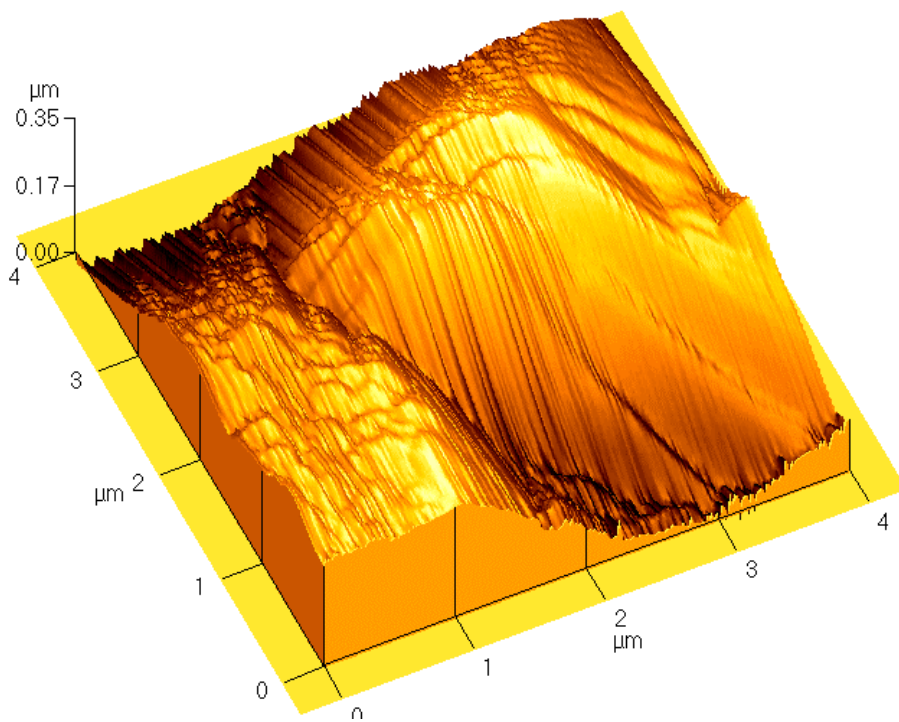


Fig. 4.28 AFM scan profile of sample D [(Ti, Al, Si)N films on a ceramic substrate, thickness of the film $\approx 0.9 \mu\text{m}$]

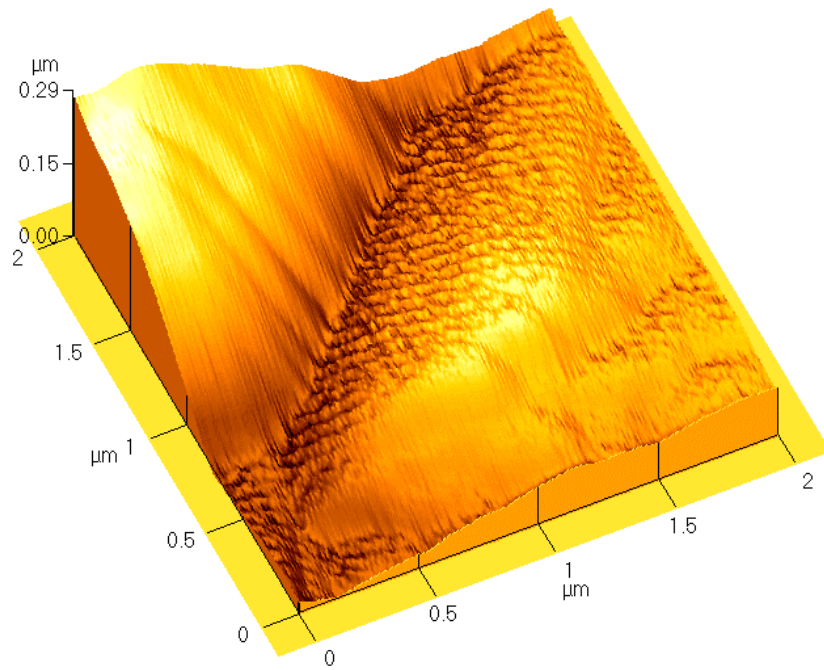


Fig. 4.29 AFM scan profile of sample D1 [(Ti, Al, Si)N films on a ceramic substrate, thickness of the film $\approx 0.9 \mu\text{m}$]

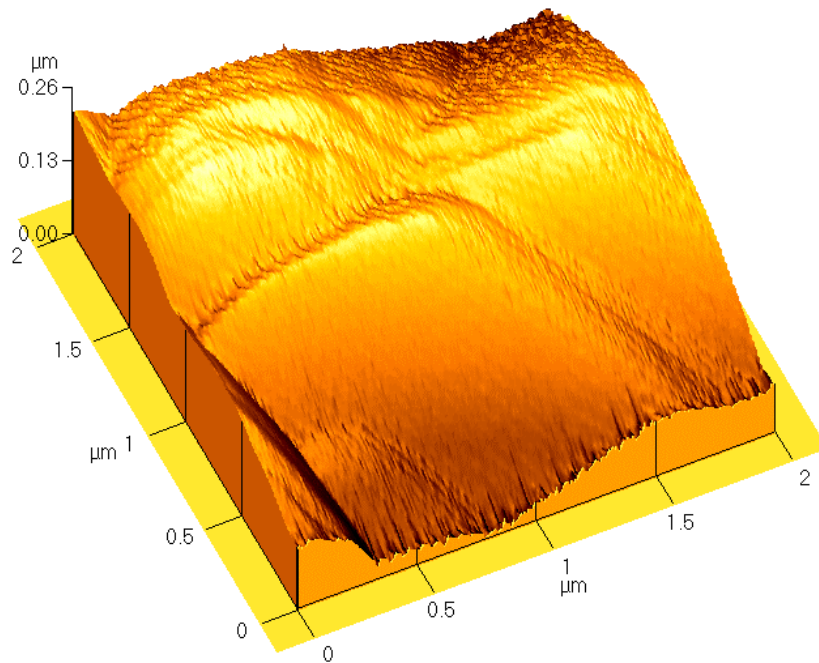


Fig. 4.30 AFM scan profile of sample E [(Ti, Al, Si)N films on a ceramic substrate, thickness of the film $\approx 0.9 \mu\text{m}$]

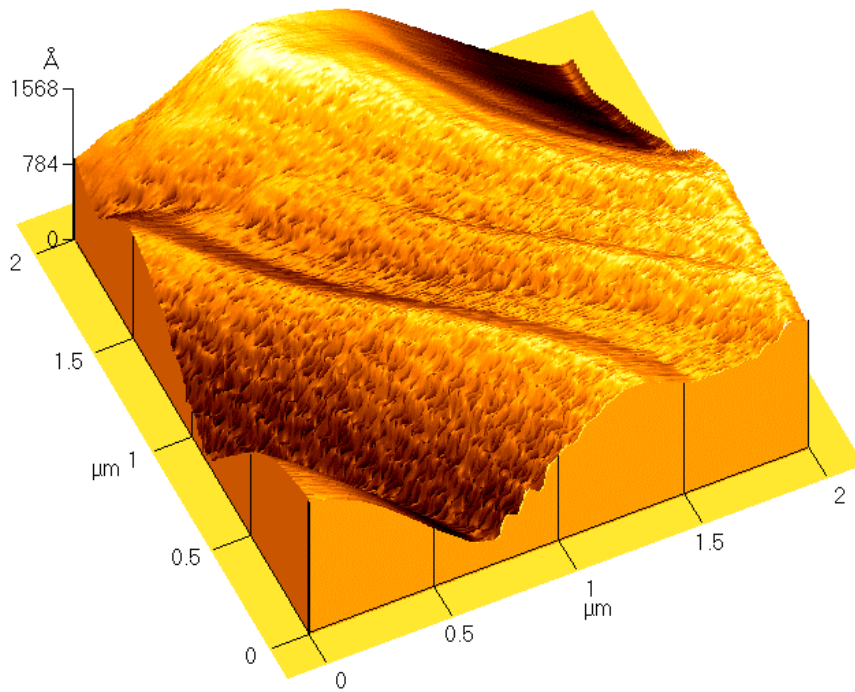


Fig. 4.31 AFM scan profile of sample E1 [(Ti, Al, Si)N films on a ceramic substrate, thickness of the film $\approx 0.9 \mu\text{m}$]

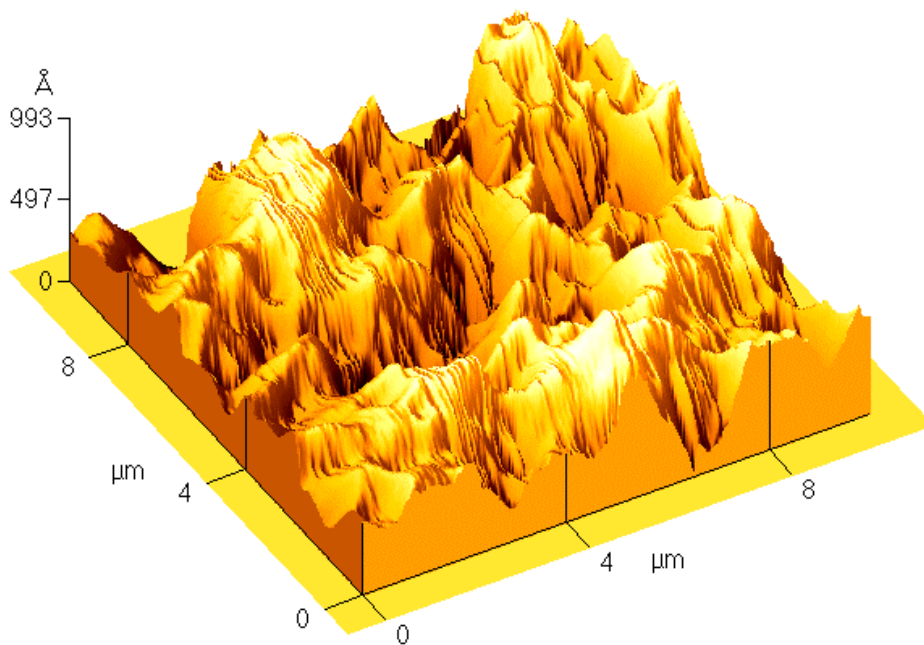


Fig. 4.32 AFM scan profile of sample 1 [(Ti, Al, Si)N films on a tungsten carbide substrate, thickness of the film $\approx 0.9 \mu\text{m}$]

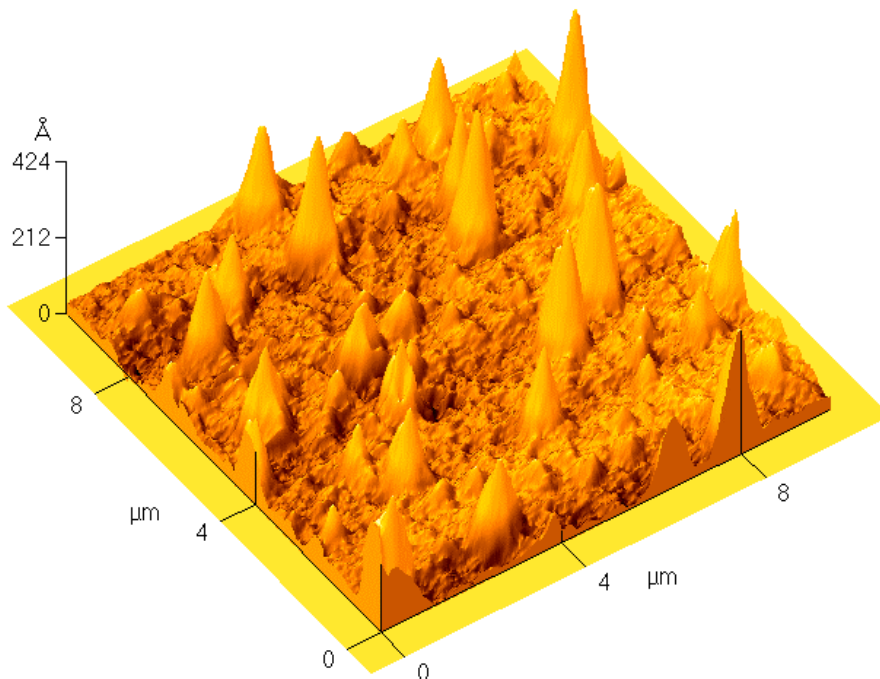


Fig. 4.33 AFM scan profile of sample 2 [(Ti, Al, Si)N films on a tungsten carbide substrate, thickness of the film $\approx 0.9 \mu\text{m}$]

4.5.3. Conclusions

The present work demonstrates that nanostructured thin film within the (Ti, Al, Si) N system can be prepared by reactive magnetron sputtering of multi thin film layers of TiN, AlSiN. The (SNMS) spectrometry of the test samples shows that a complete diffusion between the different deposited thin film layers in each sample take place, even at low substrate deposition temperature. Because of the high magnetic flux of the unbalanced magnetrons and the high sputtering power it is possible to produce a high ion-to-atom flux which give high mobility to the coated atoms. The interactions between the high mobility of the coated atoms and the ion-to-atom flux were sufficient to enhance the diffusion between the different deposited thin film layers. Increasing the temperature of the substrate doesn't only expected to enhance the diffusion, but also enhances the segregations of the two phases in the nanocomposite coatings structures. As a result the mechanical properties are enhanced. Furthermore, it was shown from the XRD diagrams for this system that the structure of the formed mixture consist of two phases. One phase is noted as TiN bulk and another detected unknown amorphous phase, which could be SiN_x or an amorphous AlN phase or a combination phase of Ti-Al-Si-N. The measured values of hardness and Young's modulus show higher values than the TiN coating

which have a hardness value between [20-22] (GPa). But lower values than expected compared with hardness values of nanocomposite coatings achieved by other working groups. They are influenced by the high surface roughness of the substrate. It can be seen that the first over-layer of the coating samples is rather comparable to multilayer structure characteristics than to a nanocomposite structure.

5. CONCLUSION

5.1. Outgassing Rate Test

- The throughput outgassing rate test method was used in the comparisons between the two aluminum materials (A2017 and A5353) samples short time period (one hour) outgassing rates. Both samples show low outgassing rates with the different surface treatment tests.
- The machining of the surface of material A (A2017) with ethanol as coolant fluid was able to reduce its outgassing rate a factor of 6 compared with a non-machined sample surface of the same material.
- The reduction of the surface porous oxide layer on the top of the aluminum surface by the pickling process with HNO₃ acid, and the protection of it by producing another passive non-porous oxides layer using anodizing process (30 V, Boric acid) will protect the surface for longer time and will minimize the outgassing rates even under humid atmosphere.
- The pickled and anodized aluminum sample show a lower outgassing rate in the short time period (one hour) test compared with the results of stainless steel samples. This will give the application of aluminum in the construction of vacuum systems a big forward push.
- The residual gas analyzer (RGA) test shows that more than 85% of the gases inside the test chamber were water vapor (H₂O) and the rests are (N₂, H₂, CO), so liquid nitrogen water vapor trap can enhance the chamber pumping down process.

5.2. The Vacuum Chamber Construction

- A rectangular aluminum vacuum chamber with three unbalanced sputtering magnetrons for the deposition of thin film coatings from different materials was constructed.
- The chamber consists mainly of two chambers, the pre-vacuum chamber to load the workpiece, and the main vacuum chamber where the sputtering deposition of the thin film coatings take place. The workpiece is moving on a car traveling on a railway between the two chambers through a self constructed rectangular gate controlled

manually from outside the chamber and between the different sputtering magnetrons inside the main chamber.

- Different types of glue were tested for the vacuum sealing of the chamber. The epoxy Araldit 2020 was not only able to develop uniform thin layer in the gap between the aluminum plates, but also, low outgassing rates which make it suitable for the vacuum use.
- The constructed chamber shows low outgassing and leak rates. It is possible to reach the range of 1×10^{-6} mbar within one hour of pumping down.
- An existing unbalanced magnetron was enhanced in its cooling and assembling properties and was used in the sputtering deposition process of the thin films .

5.3. Deposition of Nanocomposite (Ti, Si, Al)N Coatings

- Multilayer thin film coating was deposited to demonstrate that nanostructured thin film within the (Ti, Al, Si) N system could be prepared by reactive magnetron sputtering of multi thin film layers of TiN, AlSiN.
- The (SNMS) spectrometry of the test samples show that a complete diffusion between the different deposited thin film coating layers in each sample takes place, even at low substrate deposition temperature.
- The high magnetic flux of the unbalanced magnetrons and the high sputtering power were able to produce a high ion-to-atom flux, which give high mobility to the coated atoms. The interactions between the high mobility of the coated atoms and the ion-to-atom flux were sufficient to enhance the diffusion between the different deposited thin layers.
- Increasing the substrate temperature doesn't only enhance the diffusion, but also enhances the segregations of the two phases in the nanocomposite coating structures.
- It was shown from the XRD patterns for this system that the structure of the formed mixture consists of two phases. One phase is noted as TiN bulk and another detected unknown amorphous phase, which can be SiN_x or AlN or a combination of Ti-Al-Si-N.
- The measured values of hardness and Young's modulus show lower values than expected. They are influenced by the high surface roughness of the substrate. Also the

5. Conclusion

fact that the first over-layer of the coating samples is rather comparable to a multilayer structure characteristics than to a nanocomposite structure.

6. SUMMARY

In this work the investigation of a (Ti, Al, Si) N system was done. The main point of investigation was to study the possibility of getting the nanocomposite coatings structures by deposition of multilayer films from TiN, AlSiN, . This tries to understand the relation between the mechanical properties (hardness, Young's modulus), and the microstructure (nanocrystalline with individual phases). Particularly special attention was given to the temperature effects on microstructural changes in annealing at 600 °C for the coatings. The surface hardness, elastic modulus, and the multilayers diffusion and compositions were the test tools for the comparison between the different coated samples with and without annealing at 600 °C.

To achieve this object a rectangular aluminum vacuum chamber with three unbalanced sputtering magnetrons for the deposition of thin film coatings from different materials was constructed. The chamber consists mainly of two chambers, the pre-vacuum chamber to load the workpiece, and the main vacuum chamber where the sputtering deposition of the thin film coatings take place. The workpiece is moving on a car travel on a railway between the two chambers to the position of the magnetrons by step motors. The chambers are divided by a self constructed rectangular gate controlled manually from outside the chamber. The chamber was sealed for vacuum use using glue and screws. Therefore, different types of glue were tested not only for its ability to develop an uniform thin layer in the gap between the aluminum plates to seal the chamber for vacuum use, but also low outgassing rates which made it suitable for vacuum use. An epoxy was able to fulfill this tasks.

The evacuation characteristics of the constructed chamber was improved by minimizing the inner surface outgassing rate. Therefore, the throughput outgassing rate test method was used in the comparisons between the selected two aluminum materials (A2017 and A5353) samples short time period (one hour) outgassing rates. Different machining methods and treatments for the inner surface of the vacuum chamber were tested. The machining of the surface of material A (A2017) with ethanol as coolant fluid was able to reduce its outgassing rate a factor of 6 compared with a non-machined sample surface of the same material. The reduction of the surface porous oxide layer on the top of the aluminum surface by the pickling process with HNO₃ acid, and the protection of it by producing another passive non-porous oxides layer using anodizing process will protect the surface for longer time and will minimize the outgassing rates even under humid atmosphere. The residual gas analyzer (RGA)

6. Summary

test shows that more than 85% of the gases inside the test chamber were water vapour (H₂O) and the rests are (N₂, H₂, CO), so liquid nitrogen water vapor trap can enhance the chamber pumping down process. As a result it was possible to construct a chamber that can be pumped down using a turbo molecular pump (450 L/s) to the range of 1×10^{-6} mbar within one hour of evacuations where the chamber volume is 160 Liters and the inner surface area is 1.6 m². This is a good base pressure for the process of sputtering deposition of hard thin film coatings.

Multilayer thin film coating was deposited to demonstrate that nanostructured thin film within the (Ti, Al, Si) N system could be prepared by reactive magnetron sputtering of multi thin film layers of TiN, AlSiN. The (SNMS) spectrometry of the test samples show that a complete diffusion between the different deposited thin film coating layers in each sample takes place, even at low substrate deposition temperature. The high magnetic flux of the unbalanced magnetrons and the high sputtering power were able to produce a high ion-to-atom flux, which give high mobility to the coated atoms. The interactions between the high mobility of the coated atoms and the ion-to-atom flux were sufficient to enhance the diffusion between the different deposited thin layers. It was shown from the XRD patterns for this system that the structure of the formed mixture consists of two phases. One phase is noted as TiN bulk and another detected unknown amorphous phase, which can be SiN_x or AlN or a combination of Ti-Al-Si-N.

As a result we were able to deposit a nanocomposite coatings by the deposition of multilayers from TiN, AlSiN thin film coatings using the constructed vacuum chamber

7. REFERENCES

- [1] O'Hanlon, F.: A User's Guide to Vacuum Technology, John Wiley & Sons Chichester, Second Edition, 1989.
- [2] Marquardt, N.: Introduction to the Principles of Vacuum Physics. In: CERN Accelerator School, Vacuum Technology Conference, Snekersten, Denmark, 28 May – 3 June (1999), pp.1.
- [3] de Segoria, J.: Physics of Outgassing. In: CERN Accelerator School, Vacuum Technology Conference, Snekersten, Denmark, 28 May – 3 June (1999), pp.99.
- [4] Jousten, K.: Thermal Outgassing. In: CERN Accelerator School, Vacuum Technology Conference, Snekersten, Denmark, 28 May – 3 June (1999), pp.111.
- [5] Rohde, S., Muenz, W.: Sputter Deposition, Advanced Surface Coatings: a Hand Book of Surface Engineering, London, Blackie, 1991.
- [6] Chapman, B.: Glow Discharge Processes, New York, John Wiley & Sons, 1980.
- [7] Holland, F.: Vacuum Deposition of Thin Films, London, Chapman and Hall, 1970.
- [8] Hornbogen, E.: Levels of Structure Related to Man-Made Engineering Artifacts, Acta-Metall, Volume 32(1984), pp 615.
- [9] Mueller, K.: Computer Simulation of Thin Film Deposition, J. Appl. Phys. Volume 58 (1989), pp 2573.
- [10] Gruber, W.: High-Tech Industrial Adhesives, Landsberg/Lech, Verlag Modern-Industries, 2001.
- [11] Dylla, H., Manos, D., LaMarche, P.: Correlation of Outgassing of Stainless Steel and Aluminum with Various Surface Treatments, J. Vac. Sci. Technol. A 11(5), Sep/Oct 1993, pp 2623.
- [12] Ishimaru, H.: Ultimate Pressure of the Order of 10^{-13} Torr in an Aluminum Alloy Vacuum Chamber, J. Vac. Sci. Technol. A 7(3), May/June 1989, pp 2439.
- [13] Suemitsu, M., Shimoyamada, H., Matsuzaki, N., Miyamoto, N.: Photoemission Studies and Outgassing-Rate Measurements on Aluminum Alloy Surfaces Lathed with Various Alcohols, J. Vac. Sci. Technol. A 10(1), Jan/Feb 1992, pp 188.
- [14] Suemitsu, M., Shimoyamada, H., N., Miyamoto: Ultrahigh-Vacuum Compatible Mirror-Polished Aluminum Alloy Surface: Observation of Surface-Roughness-Correlated Outgassing Rates, J. Vac. Sci. Technol. A 10(3), May/June 1992, pp 570.

7. References

- [15] Chen, J., Narushima, K., Ishimaru, H.: Thermal Outgassing from Aluminum Alloy Vacuum Chambers, *J. Vac. Sci. Technol. A* 3(6), Nov/Dec 1985, pp 2188.
- [16] Ota, N.: Outgassing from Aluminum Surface Layer Induced by Synchrotron Radiation, *J. Vac. Sci. Technol. A* 14(4), Jul/Aug 1996, pp 2641.
- [17] Suemitsu, A., Kaneko, T., Miyamoto, N.: Aluminum Alloy Ultrahigh Vacuum Chamber for Molecular Beam Epitaxy, *J. Vac. Sci. Technol. A* 5(1), Jan/Feb1987, pp. 37.
- [18] Tajiri, K., Saito, Y., Yamanaka, Y., Kabeya, Z.: Pit-Free Electropolishing of Aluminum and its Application for Process Chamber, *J. Vac. Sci. Technol. A* 16(3), May/Jun 1998, pp 1196.
- [19] Jitschin, W., Ronzheimer, M., Khodabakhshi, s.: Gas Flow Measurement by Mean of Orifices and Venture Tubes, *Vacuum* 53 (1999), pp 181.
- [20] Ichimura, S., Kokubun, K., Hirata, M., Tsukahara, S., Saito, K., Ikeda, Y.: Measurement of outgassing characteristics from a vacuum chamber fabricated for pressure calibration in UHV/XHV region, *Vacuum* 53 (1999), pp 291.
- [22] Cavaleiro, A., Vieira, M., Ramos, F., Dias, J.: The ultimate vacuum pressure and the charactersits of sputtered coatings, *Thin Solid Films*, 290-291 (1996), pp 238.
- [23] Danby, G., Jackson, L.: Description of new vacuum chamber correction concept, Submitted to the 1989 Particle Accelerator Conferance, Chicago il, March 20-23, 1989.
- [24] Engelmann, G., Genet, M., Wahl, W.: Vacuum chambers in composite materials, *J. Vac. Sci. Technol. A* 5(4), Jul/Aug 1987, pp 2337.
- [25] Brockmann, W., Brémont, M.: Comparison of the degradation mechanisms of zinc-coated steel, cold-rolled steel, and aluminum/ epoxy bonded joints, *Adgesion*, Vol. 58 (1996).
- [26] Brockmann, W., Emrich, S., Neeb, T.: Wie wirksam sind mechanische Vorbehandlungen von Metallen, *Adhäsion Kleben U. Dichten*, Vol. 41 (1997) Heft12.
- [27] Mayer, R.: Optimierung eines DC- Sputtermagnetrons. Dissertation D386, University of Kaiserslautern, 1997.
- [28] Hauert, R., Patscheider, J.: From alloying to nanocomposites-improved performance of hard coatings, *Advanced Engineering Materials*, Vol. 2. No. 5 (2000), pp 247.

- [29] Carvalho, S., Rebouta, L., Cavaleiro, A., Rocha, L., Gomes, J., Alves, E.: Micro structure and mechanical properties of nanocomposite (Ti, Al, Si)N coatings, *Thin Solid Films*, 398-299 (2001), pp 391.
- [30] Stuart, R.: *Vacuum technology, thin film, and sputtering. An introduction*, Orland, Academic Press, 1983.
- [31] Rossnagel, S.: Use of plasm in deposition technologies, *Advanced Surface Coatings: A Hand Book of Surface Engineering*, London, Blackie, 1991.
- [32] Ribeiro, E., Malczyk, A., Carvalho, S., Rebouta, L., Fernandes, L., Alves, E.: Miranda, A.: Effects of ion bombardment on properties of d.c. sputtered superhard (Ti, Al, Si)N nanocomposite coatings, *Surface and Coatings Technology*, 151-152 (2002), pp 515.
- [33] Karamis, M., Sert, H.: The role of PVD TiN coating in wear behaviour of aluminum extrusion die, *Wear*, Vol. 217 (1998), pp 46.
- [34] Zlatanovi'c, M., Popobi'c, N., Bogdanov, Z., Celo'sevac, R., Kunosic'c, A., Gonici'c, B.: Microstructural modification of TiN deposited by magnitron ion plating: Influence of magnetic field configuration, *Thin Solid Films*, 317 (1998), pp 463.
- [35] Wang, S., Chang, S, Wong, K., Li, Y., Ho, W.: Improvement of the interfacial integrity of (Ti, Al)N hard coatings deposited on high speed steel cutting tools, *Surface and Coatings Technology*, 120-121 (1999), pp 388.
- [36] Zeng, X.: Multilayered (Ti, Al) ceramic coating for high-speed machining applications, *J. Vac. Sci. Technol. A* 9(4), Jul/Aug 2001, pp 1919.
- [37] Sproul, W.: Multilayer, multicomponent, and multiphase physical vapor deposition coatings for enhanced performance, *J. Vac. Sci. Technol. A* 12(4), Jul/Aug 1994, pp 1595.
- [38] Zima, L.: Possibilities of new materials with PVD and MTCVD coating and their cutting properties, In: *Sborník konference DF PM'99*, 19-22 Sept., 1999, Piešťany, Slovakia.
- [39] Chu, X., Barnett, S.: Model of superlattice yields stress and hardness enhancements, *J. Appl. Phys.* 77 (9), 1 May 1995, pp 4403.
- [40] Fayeulle, S., Misra, A., Kung, H., Nastasi, M.: Thermal annealing, irradiation, and stress in multilayers, *Nuclear Instruments and Methods in Physics Research*, B 148(1999), pp 227.

- [41] Chen, Y., Lee, K., Chiou, W., Chung, Y., Keer, L.: synthesis and structure of smooth, superhard TiN/SiN_x multilayer coatings with an equiaxed microstructure, *Surface and Coating Technology*, 146-147 (2001), pp 209.
- [42] Patscheider, J., Zehnder, T., Diserens, M.: Structure-performance relations in nanocomposite coatings, *Surface and Coating Technology*, 146-147 (2001), pp 201.
- [43] Holubar, P., Jilek, M., Sima, M.: Present and possible future applications of superhard nanocomposite coatings, *Surface and Coating Technology*, 133-134 (2000), pp 145.
- [44] Vaz, F., Rebouta, L., Goudeau, Ph., Girardeau, T., Pacaud, J., Rivière, J., Traverse, A.: Structural transitions in hard Si-based TiN coatings: the effect of bias voltage and temperature, *Surface and Coating Technology*, 146-147 (2001), pp 274.
- [45] Niederhofer, A., Nesládek, P., Maennling, H., Moto, K., Vepřek, S., Jílek, M.: Structural properties, internal stress and thermal stability of nc- TiN/a- Si₃N₄, nc TiN/TiSi_x and nc-(Ti_{1-y} Al_ySi_x)N superhard nanocomposite coatings reaching the hardness of diamond, *Surface and Coating Technology*, 120-121 (1999), pp 173.
- [46] Maennling, H., Patil, D., Moto, K., Vepřek, S., Jílek, M.: Thermal stability of superhard nanocomposite coatings consisting of immiscible nitrides, *Surface and Coating Technology*, 146-147 (2001), pp 263.
- [47] Vepřek, S., Reiprich, S.: A concept for the design of novel superhard coatings, *Thin Solid Films*, 268 (1995), pp 64.
- [48] Vepřek, S.: The search for novel, superhard materials, *J. Vac. Sci. Technol. A* 17(5), Sep/Oct 1999, pp 2401.
- [49] Musil, J.: Hard and superhard nanocomposite coatings, *Surface and Coating Technology*, 125 (2000), pp 322.
- [50] Vepřek, S., Argon, A.: Mechanical properties of superhard nanocomposites, *Surface and Coating Technology*, 146-147 (2001), pp 175.
- [51] Niederhofer, A., Nesládek, P., Maennling, H., Moto, K., Vepřek, S., Dollinger, G., Bergmaier, A.: Composition, nanostructure and origin of the ultrahardness in nc-TiN/a- Si₃N₄/a- and nc-TiSi₂ nanocomposites with HV = 80 to ≥ 105 Gpa, *Surface and Coating Technology*, 133-134 (2000), pp 152.
- [52] Vepřek, S.: New development in superhard coatings: the superhard nanocrystalline – amorphous composites, *Thin Solid Films*, 317 (1998), pp 449.
- [53] Vepřek, S., Reiprich, S., Shizhi, Li.: Superhard nanocrystalline composite materials: the TiN/ Si₃N₄ system, *J. Appl. Phys. Lett.* 66 (20), 15 May 1995, pp 2640.

- [54] Vepřek, S.: Electronic and mechanical properties of nanocrystalline composites when approaching molecular size, *Thin Solid Films*, 297 (1997), pp 145.
- [55] Technical information for the nanocomposite from the SHM company.
- [56] Jehn, H.: Multicomponent and multiphases hard coatings for tribological applications, *Surface and Coating Technology*, 131 (2000), pp 433.
- [58] Bull, S., Rickerby, D.: Evaluation of coatings, *Advanced Surface Coatings: a Hand Book of Surface Engineering*, London, Blackie, 1991.

CURRICULUM VITAE

PERSONAL DATA

Name	Khaleel N. Abu Shgair
Date of Birth	01.06.1972
Place of Birth	Kuferelma, Jordan.

EDUCATION

9/78 - 7/87	Elementary and Middle School at Kuferelma High School, Jordan.
9/87 - 7/90	Secondary School at Dairabuesaid Secondary School, General Secondary Education Certificate, in June 1990.
9/1990 - 6/1995	B.Sc. in Mechanical Engineering (Production Engineering), Jordan University of Science and Technology, Irbid, Jordan.
9/1995 - 6/1998	M. Sc. in Mechanical Engineering, Jordan University of Science and Technology, Irbid, Jordan.

WORKING EXPERIENCE

6/1994 - 10/1994	Practical Training, Jordan Seaport, Aqaba, Jordan.
10/1995 - 10/1996	Training Engineer, Vocational Training Corporation, Jordan.
9/1995 - 6/1998	Research Assistance, Department of Mechanical Engineering, Jordan University of Science and Technology, Irbid, Jordan.
7/1999 - present	Research Assistance, Department of Precision Engineering, University of Kaiserslautern, Germany.